

AD-A041 378

TEXAS UNIV AT AUSTIN APPLIED RESEARCH LABS
A SENSITIVITY STUDY OF UNDERWATER SOUND PROPAGATION LOSS AND BO--ETC(U)
FEB 77 K E HAWKER, K C FOCKE, A L ANDERSON N00039-77-C-0003
ARL-TR-77-17 NL

UNCLASSIFIED

1 OF 2
ADA
041378



ADA041378

12

J

APPLIED
RESEARCH
LABORATORIES
THE UNIVERSITY OF TEXAS
AT AUSTIN

ARL - TR - 77 - 17
28 February 1977

Copy No. 14

A SENSITIVITY STUDY OF UNDERWATER SOUND
PROPAGATION LOSS AND BOTTOM LOSS

Kenneth E. Hawker
Karl C. Focke
Aubrey L. Anderson

NAVAL ELECTRONIC SYSTEMS COMMAND
Contract N00039 - 77 - C - 0003



DDC FILE COPY

APPROVED FOR PUBLIC
RELEASE, DISTRIBUTION
UNLIMITED

UNCLASSIFIED

SECURITY CLASSIFICATION OF THIS PAGE (When Data Entered)

REPORT DOCUMENTATION PAGE		READ INSTRUCTIONS BEFORE COMPLETING FORM
1. REPORT NUMBER	2. GOVT ACCESSION NO.	3. RECIPIENT'S CATALOG NUMBER
4. TITLE (and Subtitle)		5. TYPE OF REPORT & PERIOD COVERED
A SENSITIVITY STUDY OF UNDERWATER SOUND PROPAGATION LOSS AND BOTTOM LOSS.		technical report.
7. AUTHOR(s)		6. PERFORMING ORG. REPORT NUMBER
Kenneth E. Hawker, Karl C. Focke Aubrey L. Anderson		ARL-TR-77-17
		8. CONTRACT OR GRANT NUMBER(s)
		N00039-77-C-0003
9. PERFORMING ORGANIZATION NAME AND ADDRESS		10. PROGRAM ELEMENT, PROJECT, TASK AREA & WORK UNIT NUMBERS
Applied Research Laboratories The University of Texas at Austin Austin, Texas 78712		
11. CONTROLLING OFFICE NAME AND ADDRESS		12. REPORT DATE
Naval Electronic Systems Command Department of the Navy Washington, DC 20360		28 February 1977
		13. NUMBER OF PAGES
		122
14. MONITORING AGENCY NAME & ADDRESS (if different from Controlling Office)		15. SECURITY CLASS. (of this report)
12-129p.		UNCLASSIFIED
		15a. DECLASSIFICATION/DOWNGRADING SCHEDULE
16. DISTRIBUTION STATEMENT (of this Report)		
Approved for public release; distribution unlimited.		
17. DISTRIBUTION STATEMENT (of the abstract entered in Block 20, if different from Report)		
18. SUPPLEMENTARY NOTES		
19. KEY WORDS (Continue on reverse side if necessary and identify by block number)		
Propagation Models Geoacoustical Subbottom Models Critical Angle Hidden Depth Stoneley Waves		
20. ABSTRACT (Continue on reverse side if necessary and identify by block number)		
This report describes the techniques used and results obtained in a model study of the sensitivity of propagation loss to variations in bottom loss and bottom loss to variations in the geoacoustical models of the subbottom. The propagation loss sensitivity study was carried out, using both ray and wave propagation models, for a variety of source-receiver depth combinations and with various sound speed profile types. The bottom loss sensitivity study was carried out using a model developed by Applied Research Laboratories (ARL).		

DD FORM 1 JAN 73 1473

EDITION OF 1 NOV 65 IS OBSOLETE

UNCLASSIFIED

SECURITY CLASSIFICATION OF THIS PAGE (When Data Entered)


404 434

UNCLASSIFIED

SECURITY CLASSIFICATION OF THIS PAGE(When Data Entered)

20. Abstract (Cont'd)

The University of Texas at Austin, and is concentrated on addressing questions of hidden depths, substrate effects, and sound speed and density profile effects.



Classified references, Page 115:
Document should remain for Unlimited
Distribution per Mr. J. Sinsky, NESO/
Code 320

UNCLASSIFIED

SECURITY CLASSIFICATION OF THIS PAGE(When Data Entered)

ARL - TR - 77 - 17
28 February 1977

**A SENSITIVITY STUDY OF UNDERWATER SOUND
PROPAGATION LOSS AND BOTTOM LOSS**

Kenneth E. Hawker
Karl C. Focke
Aubrey L. Anderson

NAVAL ELECTRONIC SYSTEMS COMMAND
Contract N00039 - 77 - C - 0003

ACCESSION SLIP	
PTS	DATE RECEIVED <input checked="" type="checkbox"/>
DOC	DATE SHIPPED <input type="checkbox"/>
UNANNOUNCED JUSTIFICATION	
DISTRIBUTION AND ACTIVITY CODES	
DATE	APPROVED FOR SPECIAL
A	

APPLIED RESEARCH LABORATORIES
THE UNIVERSITY OF TEXAS AT AUSTIN
AUSTIN, TEXAS 78712

APPROVED FOR PUBLIC
RELEASE; DISTRIBUTION
UNLIMITED.

ABSTRACT

This report describes the techniques used and results obtained in a model study of the sensitivity of propagation loss to variations in bottom loss and bottom loss to variations in the geoacoustical models of the subbottom. The propagation loss sensitivity study was carried out, using both ray and wave propagation models, for a variety of source-receiver depth combinations and with various sound speed profile types. The bottom loss sensitivity study was carried out using a model developed by Applied Research Laboratories (ARL), The University of Texas at Austin, and is concentrated on addressing questions of hidden depths, substrate effects, and sound speed and density profile effects.

TABLE OF CONTENTS

	<u>Page</u>
ABSTRACT	iii
I. INTRODUCTION	1
II. SENSITIVITY OF PROPAGATION LOSS TO VARIATIONS IN BOTTOM LOSS	7
A. Introduction	7
B. The Use of Range Averaged Intensity in a Sensitivity Study	9
C. Sensitivity in the Case of a Mid-Pacific Profile	10
1. General Characteristics	10
2. Critical Angle Dependence	19
3. Source Depth Dependence	23
4. Bottom Depth Dependence	30
D. Considerations of Additional Profiles	35
1. Source Depth Dependence	46
2. Bottom Depth Dependence	54
E. Conclusions	58
III. BOTTOM LOSS SENSITIVITY	59
A. Introduction	59
B. The Hidden Depth Problem	62
C. Bottom Loss Sensitivity Problems Above the Hidden Depth	87
1. Variations in Sediment Type	89
2. Substrate Effects	92
3. Sound Speed Profile Effect	96
4. Effects of a Continuously Variable Density	102
ACKNOWLEDGMENTS	113
REFERENCES	115

I. INTRODUCTION

Mathematical models are useful tools for predicting underwater sound propagation and ambient noise fields. Both the sound fields and the model predictions exhibit sensitivity to environmental variations and source/receiver geometries. To the extent that the model predictions exhibit the same response as the sound fields to environmental or geometrical variations, they are useful for sensitivity studies. For such sensitivity studies, one model input parameter is varied in a systematic manner while all other model input parameters remain fixed. The resulting variations in an output parameter of interest then describe the sensitivity of the model predictions to the input parameter variations.

Bottom interaction is a complex and often significant feature of underwater sound propagation and ambient noise fields. While significant progress has been demonstrated in recent years in predicting the waterborne component of underwater sound fields, the bottom interacting component remains as a complex challenge. This is especially true at low frequencies when sound energy can propagate to long ranges with significant bottom interaction. Topographic variations, subbottom penetration of energy with occasional manifestations of focusing or sediment layer interaction, slope enhancement, and seamount blockage or diffraction all serve to further complicate bottom interaction predictions.

A complex problem, such as bottom interaction of underwater sound, is often best approached by a systematic examination of separate features of the problem. As an understanding of the separate features is developed, the complications of simultaneous action of the different features can be treated. The present study has separately examined the sensitivity

of underwater sound propagation loss to bottom loss variations, and the sensitivity of bottom loss to sediment geophysical parameter variations. Results of these studies are described in the following two chapters.

The results reported here are a summary of work on these problems covering the period November 1975 to June 1976 under Contract N00039-76-C-0081. These studies are still in progress and more recent results will be documented in other reports to be issued under this contract.

Chapter II considers the problems of the sensitivity of computed propagation loss to variations in bottom loss. The bulk of these calculations was carried out using the FACT model, although the parabolic equal model was given considerable use. In both cases the variations in bottom loss were restricted to changes in critical angle of a simple phenomenological bottom loss type.

No attempt was made to incorporate, in catalog fashion, sound speed profiles from all the oceans of the world. Rather, extensive use was made of profiles typical of the mid-Pacific, North Pacific, and Indian Ocean regions. These regions are not only of considerable practical interest but also their profiles typify classes including a wide variety of physical effects. In particular, these profiles deal with the distinction between severe bottom limited cases and situations where propagation with little bottom interaction is possible.

In addition to studies involving sensitivity to bottom loss (critical angle) changes, consideration is also given to the effects of differing water depths and various source depths.

Although it would be possible to examine changes in propagation loss as a function of depth at fixed discrete ranges, the presence of

convergence and shadow zones makes such an approach complex and offers little practical insight into the systematic effects of real concern. To eliminate the problem of dealing with the full two-dimensional field (cylindrical symmetry is assumed), a range averaged propagation loss is used. This average, described in detail in the text, tends to smooth the lateral variations and weight the influence of shadow zone and convergence zone regions in a useful way.

The most important results obtained in this propagation loss sensitivity study are itemized below.

1. In the domain between the source depth and source conjugate depth, the range averaged propagation loss displays a regular and uniform dependence on critical angle changes.
2. Within this regular domain the amount of bottom influence on average propagation loss is a function of source and bottom depths.
3. Outside this domain of regularity, as the receiver approaches either the surface or the bottom, the influence of the bottom increases.
4. In the near bottom region, extending to 400 to 700 m above the bottom, the average propagation loss displays significant fine structure.

The second phase of this study concerns the problem of determining the sensitivity of bottom interaction to variations in the makeup of the subbottom. There are several possible approaches to this problem, that is, it is possible to construct various measures of the sensitivity. The most obvious of these measures includes using the computed bottom loss itself, examining changes in normal modes and eigenvalues, and using the propagation loss in a way that would combine the two aspects of this sensitivity study.

The results reported here are based on the first of these possibilities, use of computed bottom loss as a measure of the effects of variations in subbottom structure and composition. This method was chosen because of its intuitive simplicity, the direct application of results to a further propagation loss sensitivity study, and the availability of a sophisticated general purpose bottom loss model at ARL.

The problem of dealing with a multitude of parameters that arose in the propagation loss sensitivity study is even more significant in the bottom loss study. For this reason the study reported here focuses on a small number of specific effects and processes. In this way an encyclopedic approach is avoided and attention can be directed toward some physical processes of importance.

The bottom loss sensitivity study is centered on two central issues: (1) determination of the depth in the sediment to which any knowledge of subbottom structure is necessary (the hidden depth problem) and (2) the effects of variations in certain acoustic parameters in the region above the hidden depth. The first of these is in some sense the most important and far reaching since it determines the range over which the second must be investigated.

The most important conclusions obtained in this bottom loss sensitivity study are the following.

1. The depth in the sediment column to which detailed knowledge is necessary, called the hidden depth, is closely related to the ray turning depth, although it is not identical with it except in the high frequency limit.

- a. The precise definition of the hidden depth (the tolerance for "hiddenness") is not important; the hidden depth is a natural and physically meaningful quantity.

- b. The hidden depth is strongly influenced by the sound speed gradient through its (first order) effect on turning depth and its (second order) effect on the distance below the turning depth to the hidden depth.

- c. The hidden depth lies below the turning depth a distance which is frequency dependent according to a one-third power law.

2. In the low grazing angle regime, the solid aspects of a rock substrate are generally very small except for a narrow angular regime where Stoneley waves can cause a large increase in loss.

3. In the high grazing angle regime, rock substrate effects are dominated by shear and compressional critical angles.

4. For sediments of the silt-clay types, the sound speed gradient above the hidden depth exerts a strong influence on bottom loss over the low grazing angle regime.

5. The effects of sediment type variation are most usefully studied using the empirical porosity parameterization techniques developed principally by Hamilton at Naval Undersea Center (NUC).

II. SENSITIVITY OF PROPAGATION LOSS TO VARIATIONS IN BOTTOM LOSS

A. Introduction

For present purposes the bottom interaction problem can be defined by the questions of what influence the bottom has on long range acoustic propagation and how much information about the (sub)bottom is required in order to adequately predict these effects. Even in this restricted form the problem thus posed is a complex and detailed one involving the influence of many competing processes and a multitude of parameters. This complexity has led to the necessity for separating the problem into simpler components, a procedure dictated more by pragmatic computational considerations than by the physics of the problem.

Although it has certainly been appreciated for some time that the bottom can exert considerable influence on propagation loss for some configurations and little influence in others, no systematic attempt has been made previously to delineate these regimes. The beginnings of this present study are discussed in an earlier report,¹ but all the results given here are new.

The propagation loss sensitivity study described in this chapter was designed to isolate regions in the water column of extreme bottom sensitivity from those of minimal sensitivity. This isolation can be thought of as determining what acoustic energy has significantly interacted with the bottom and what the resultant effect on propagation loss was. This separation could therefore be carried out using very simple phenomenological bottom loss types and the deviation from them.

Throughout the study reported in this chapter, variations in bottom loss were restricted to changes in critical angle by using a bottom loss displaying zero loss below the critical angle and an essentially infinite loss above. The use of such a bottom loss description enables the propagation loss sensitivity study to be uncoupled from the bottom loss sensitivity study.

Two propagation models were used in this investigation: FACT, a ray trace model reported by Spofford² and by Baker and Spofford³ and a parabolic equation model reported by Brock.⁴ The nature of the ARL implementation of these models is described by Hawker, Foreman, and Focke.⁵ FACT defines the bottom in terms of a plane wave reflection coefficient applied at the water-sediment interface. The parabolic equation model simulates a critical angle effect by introducing a thin layer below the water column having a sound speed gradient and zero attenuation. This layer, in turn, overlies a homogeneous attenuating layer.

Various specialized terms used throughout the chapter are defined here. The depth at which the sound speed is the same as that at the source depth is referred to as the source conjugate depth. The depth at which the sound speed is the same as that at the surface is called the critical depth. The distance between the critical depth and the bottom (if the bottom lies below critical depth) is called the depth excess.

The work reported here was carried out using three profile types: Mid-Pacific, North Pacific, and Indian Ocean. Since the intent of this study was to carry out a thorough and systematic sensitivity study for several important profile types and not to survey the effects of profiles from the world's oceans, this selection of profiles was deemed adequate.

B. The Use of Range Averaged Intensity in a Sensitivity Study

A sensitivity study is designed to measure the influence of a given input parameter on the total output. This study is directed toward determining the effects of bottom loss variations on the total propagation loss. The energy contributions from the waterborne paths dominate the intensity calculations within the convergence zones, limiting the major bottom influence to the shadow zones.

The propagation loss sensitivity to bottom loss will be range dependent. This range dependence is a function of the remaining input parameters. Sensitivity measured at designated ranges would, therefore, be of very limited value. Measurements of the sensitivity within both the convergence zones and the shadow zones would be very convenient. Acquiring these results for a large number of model runs would not be practical because the location and widths of these zones will vary from case to case.

An average propagation loss calculated over a large range interval (covering several convergence zones) will provide a measure of the total propagation loss sensitivity to bottom loss for that range interval. The range interval between 100 and 200 nm was used when computing the averages. Propagation within this range interval will not involve the direct paths of the rays. There is only a nominal 3 dB increase in loss because of the increase in range across the interval; the run time for the parabolic equation model is not excessive out to 200 nm. Two forms of averaging have been considered. The first form involves averaging the propagation loss in decibels. This method represents an average measurement of the propagation loss and emphasizes the higher loss values. The method that was finally used calculates the propagation loss for the average intensity over the range interval. This method represents a physically meaningful average propagation loss.

For a given source depth, the average propagation loss was computed at designated receiver depths. The averages were then fitted with a curve and presented as a function of receiver depth.

Two of these curves will be presented (Figs. II-4 and II-5) along with their corresponding maximum, minimum, and median propagation loss, both for a highly reflecting bottom and for a totally absorbing bottom. In both cases the average propagation loss is within 3 dB of the median propagation loss even though the differences between the maximum and minimum propagation losses vary greatly between the two cases. Therefore, these averages do present a reasonable representation of the propagation losses within the range interval.

The use of similar average propagation loss versus depth curves has been presented in the literature. In a study of the intensity of field near the bottom, Gordon⁶ uses an average propagation loss defined by the random phase mode sum to investigate the depth dependence of propagation loss.

Tappert,⁷ in a discussion of the parabolic equation method and its uses, calculates the average propagation loss as a function of depth. He presents a series of curves for two source depths and various frequencies. He points out the surface image interference and the near bottom field anomalies.

C. Sensitivity in the Case of a Mid-Pacific Profile

1. General Characteristics

Variations in the bottom loss were limited to changes in the critical angle, using values of 0°, 1°, 5°, 10°, 15°, and 20°. The loss was 0 dB below the critical angle and 50 dB above it. Increases in the critical angle will result in additional energy and will indicate the importance of the higher angular bottom interactions.

Figures II-1, II-2, and II-3 demonstrate the effects of changes in the critical angle on propagation loss curves as computed by FACT. These curves are for a mid-Pacific profile with the bottom set at critical depth and a source depth of 152 m (500 ft). The receiver depths are 1200 m (between source depth and its conjugate depth), 2500 m (the source conjugate depth), and 3350 m (between source conjugate and the bottom). The mid-Pacific profile is shown in Fig. II-4.

Beyond 150 nm the 1200 m receiver and the 2500 m receiver lose the very deep shadow zones. The bottom refracting rays spread apart with increasing range and beyond 150 nm they are present at all ranges for these two receivers. This ray spreading also results in the rise of intensity in the shadow zones for the 3350 m receiver.

Caustics formed below the source conjugate depth result in the strong convergence zone structure of the 2500 m and 3350 m receivers. The propagation loss in these convergence zones is independent of the bottom loss. Regions outside these convergence zones do, however, show influence of the bottom.

As the critical angle decreases, the propagation loss in the shadow zones increases. The total increase in propagation loss is a nominal 5 dB for the 1200 m receiver and 6 to 8 dB for the 2500 m receiver and is greater than 10 dB for the 3350 m receiver. This increase appears to be linear with critical angle beyond 150 nm for the 2500 m receiver. For the 3350 m receiver, this increase is greatest between 5° and 10° . This leads to 0° , 10° , and 5° grouped together and 10° , 15° , and 20° grouped together.

A detailed study of propagation loss sensitivity using these propagation loss curves would require a step by step description of the sensitivity. The study could also require a separation of the effects

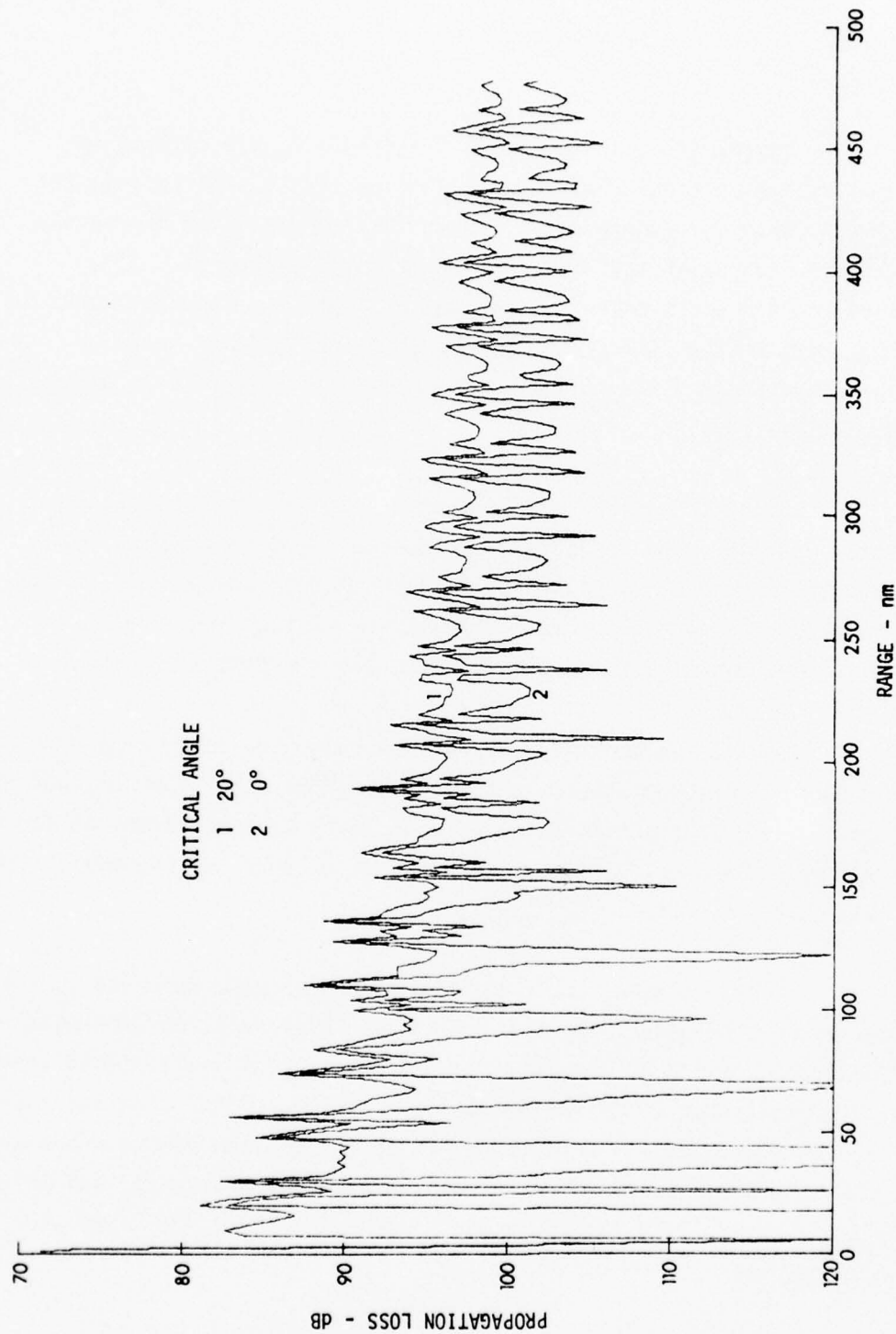


FIGURE II-1
PROPAGATION LOSS FOR VARIOUS BOTTOM LOSS CRITICAL ANGLES

SOURCE DEPTH: 152 m, RECEIVER DEPTH: 1200 m, BOTTOM DEPTH: 3952 m, MODEL: FACT

ARL - UT
AS-76-558
KCF - DR
4-21-76

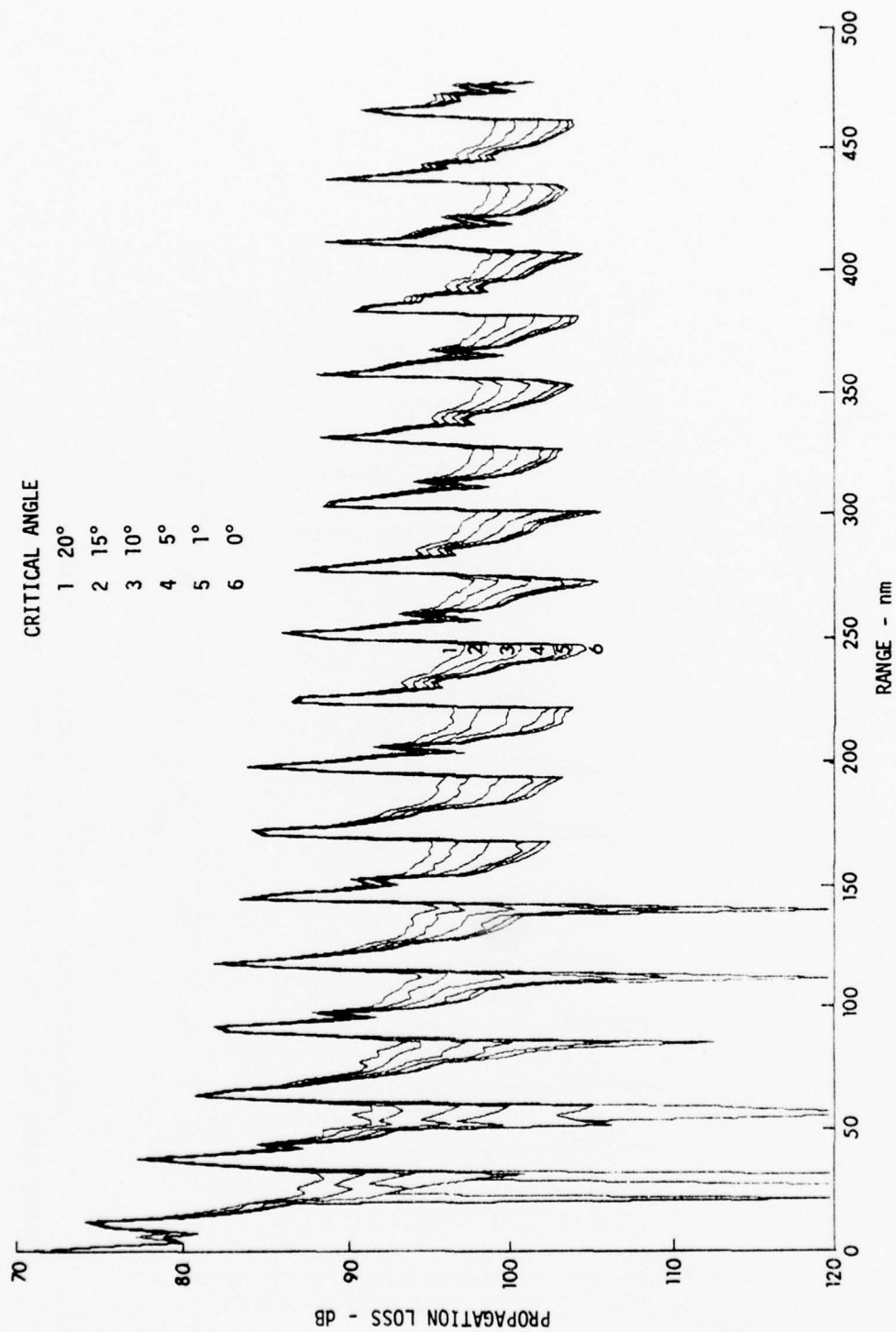
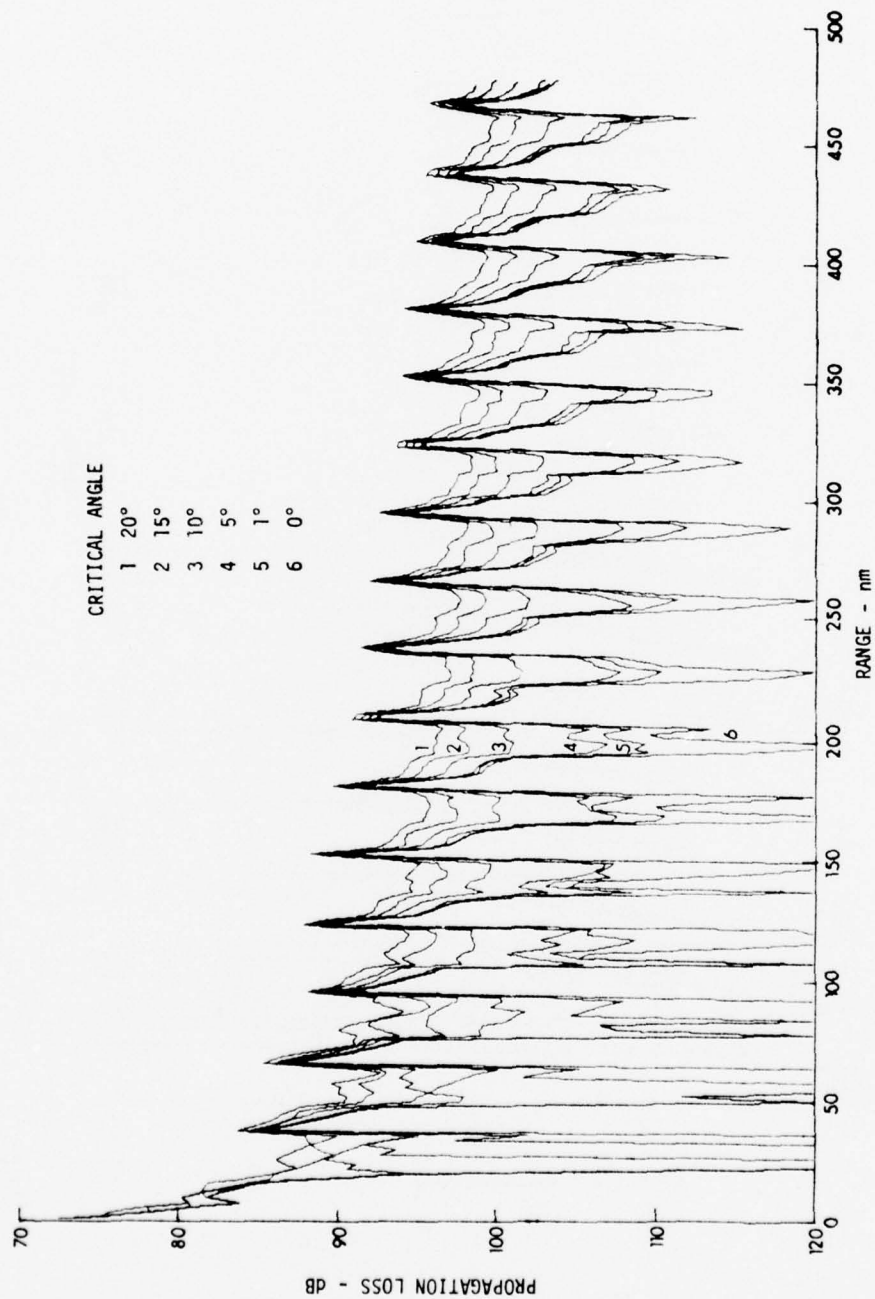


FIGURE II-2
PROPAGATION LOSS FOR VARIOUS BOTTOM LOSS CRITICAL ANGLES

SOURCE DEPTH: 152 m, RECEIVER DEPTH: 2500 m, BOTTOM DEPTH: 3952 m, MODEL: FACT

ARL - UT
AS-76-559
KCF - DR
4-21-76



ARL - UT
A5-76-560
KCF - DR
4-21-76

FIGURE II-3
PROPAGATION LOSS FOR VARIOUS BOTTOM LOSS CRITICAL ANGLES
SOURCE DEPTH: 152 m, RECEIVER DEPTH: 3350 m, BOTTOM DEPTH: 3952 m, MODEL: FACT

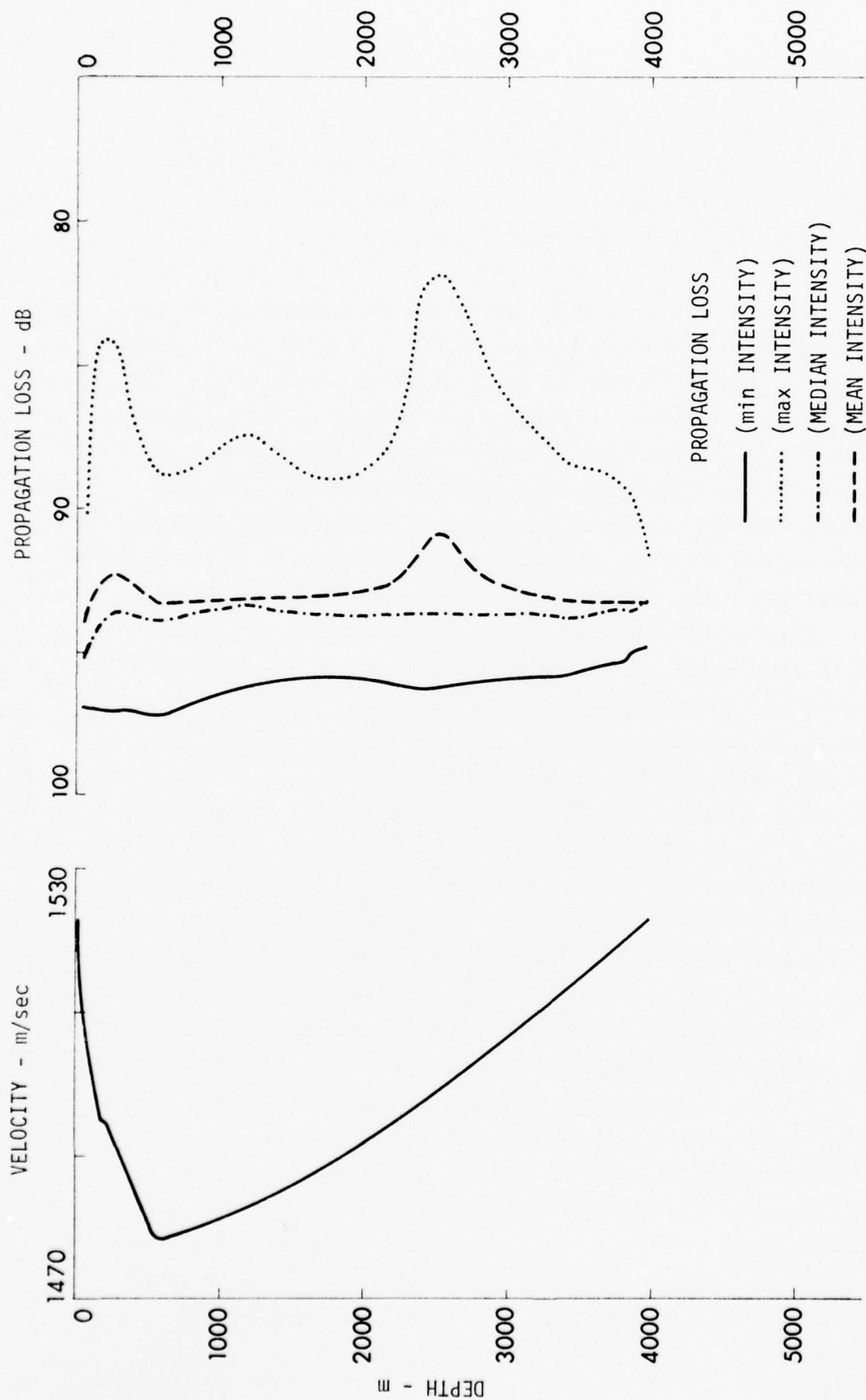


FIGURE II-4
CHARACTERISTICS OF THE PROPAGATION LOSSES
BETWEEN 100 nm AND 200 nm
MID-PACIFIC PROFILE

SOURCE DEPTH: 152 m, BOTTOM DEPTH: 3952 m, CRITICAL ANGLE: 20°, MODEL: FACT

ARL - UT
AS-76-552
KCF - DR
4-19-76

within shadow zones and convergence zones as well as a definition of the distinction between these two zones. Instead, the propagation losses of the average intensities within the 100 to 200 nm range interval were calculated for the sensitivity study.

A better understanding of the curves resulting from the use of the average values can be obtained from Figs. II-4 and II-5. These figures present characteristics of the propagation losses within the 100 to 200 nm range interval. To facilitate correlation of propagation loss features with profile changes, the mid-Pacific profile used for these calculations is shown accompanying the propagation loss plot. This practice will be followed throughout this chapter. The peaks in the maximum intensity curves occur at the source depth and its conjugate depth. They result from very narrow convergence zones as evidenced by the large separation between the median and these intensity maxima. These narrow convergence zone peaks influence the mean by creating the minima in the propagation loss of the average versus depth curves while leaving the median virtually unchanged. At other depths in the water column, the propagation losses are more uniformly distributed about the median value. This produces a mean value that is generally within 1 dB of the median value. The propagation losses for the average intensities will therefore represent the general propagation losses within the range interval with an indication of the strength of the convergence zones at the source depth and its conjugate depth.

These propagation loss versus depth curves will be more useful with an understanding of what a change in the average value represents in terms of changes in the propagation loss versus range curves. The average propagation losses for the curves in Figs. II-1, II-2, and II-3 are presented in Table I. The two curves for the 1200 m receiver (Fig. II-1) are represented by averages which differ by 3.6 dB. For the 2500 m receiver the average propagation losses exhibit a linear relationship with the critical angle, approximately a 0.7 dB increase for a 5° decrease in critical angle. For the 3350 m receiver the

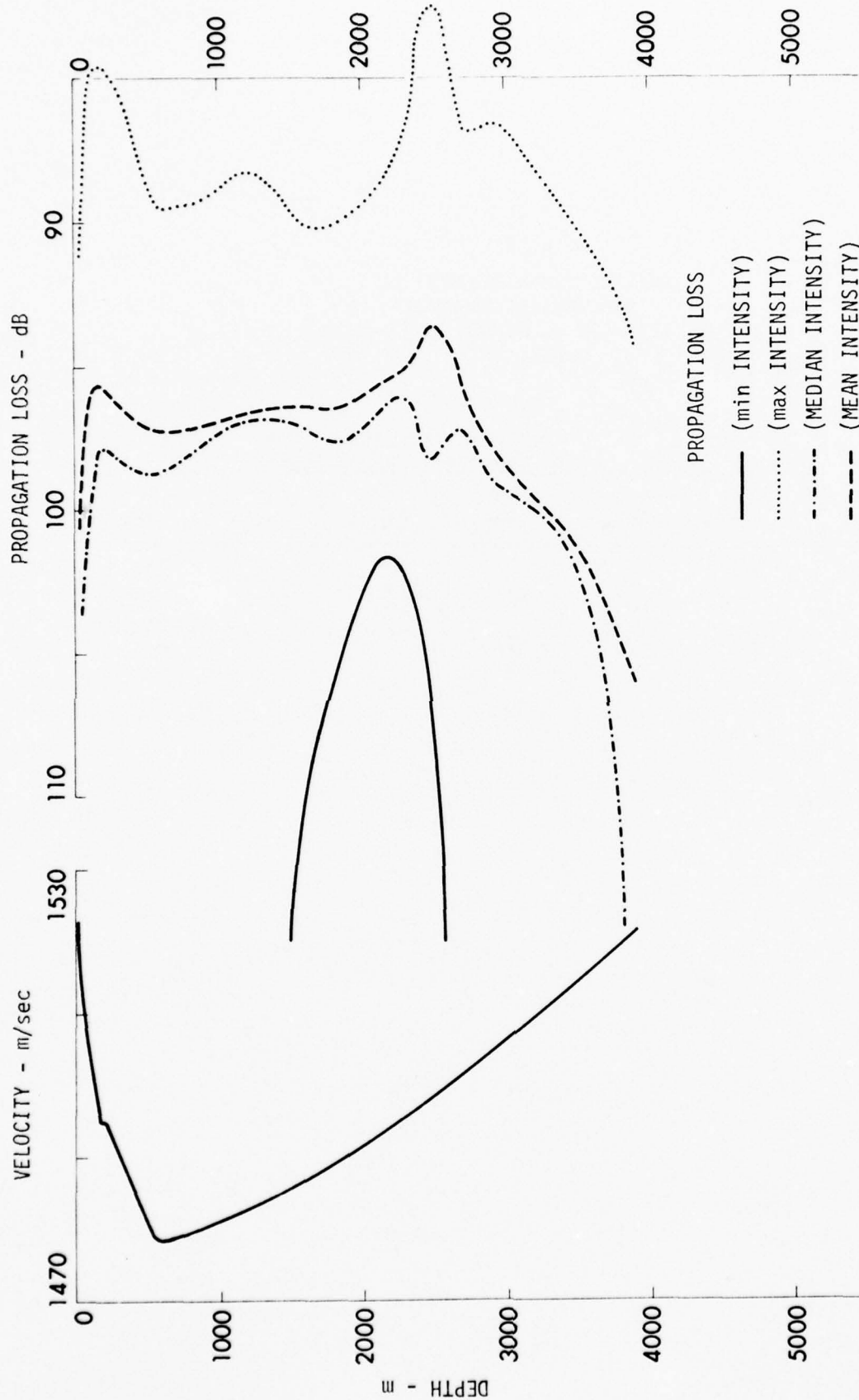


FIGURE II-5
CHARACTERISTICS OF THE PROPAGATION LOSSES
BETWEEN 100 nm AND 200 nm
MID-PACIFIC PROFILE

SOURCE DEPTH: 152 m, BOTTOM DEPTH: 3952 m, CRITICAL ANGLE: 0°, MODEL: FACT

TABLE I
 AVERAGE PROPAGATION LOSS:
 MID-PACIFIC PROFILE
 SOURCE DEPTH 152 m, BOTTOM DEPTH 3952 m
 MODEL: FACT

Receiver Depth (m)	Average propagation loss for various critical angles					
	0 (deg)	1 (deg)	5 (deg)	10 (deg)	15 (deg)	20 (deg)
1200	96.8					93.2
2500	93.6	93.4	93.1	92.4	91.6	90.9
3350	100.4	99.1	98.2	96.0	94.2	93.2

largest changes in the averages occur at the lower angles. The 0° to 1° change in critical angle results in the largest change in the propagation loss per 1° .

Figures II-6 and II-7 present the average propagation losses for two range intervals, 100 to 200 nm and 400 to 480 nm. The two sets of curves are seen to have similar shapes and separation between individual curves. The only major difference between the two sets is a 5 dB displacement, which results strictly from the change in the average range. The averages from the 100 to 200 nm range interval, therefore, are expected to be representative for all ranges.

2. Critical Angle Dependence

The average propagation losses for a 152 m (500 ft) source using the mid-Pacific profile are shown in Fig. II-6 for various bottom loss critical angles. The propagation loss increases with increasing critical angle. There is a local minimum in the propagation loss at the source depth and its conjugate depth for all critical angles. Maximum propagation losses generally occur at the surface and at the bottom.

The water column appears to be divided into three regions: above the source depth, between the source depth and the source conjugate depth, and below the source conjugate depth. For all bottom types the propagation loss increases as the receiver approaches the surface in the first region and the bottom in the third region. In the second region the maximum loss occurs at the axis depth and decreases as the receiver approaches either the source or its conjugate depth.

The differences between propagation losses for the 0° critical angle and the losses for the other bottom types are presented in Fig. II-8. These curves present the intensity contributions due to the various bottom interactions. As the critical angle increases, the influences of the bottom also increases. In both regions 1 and 3, the

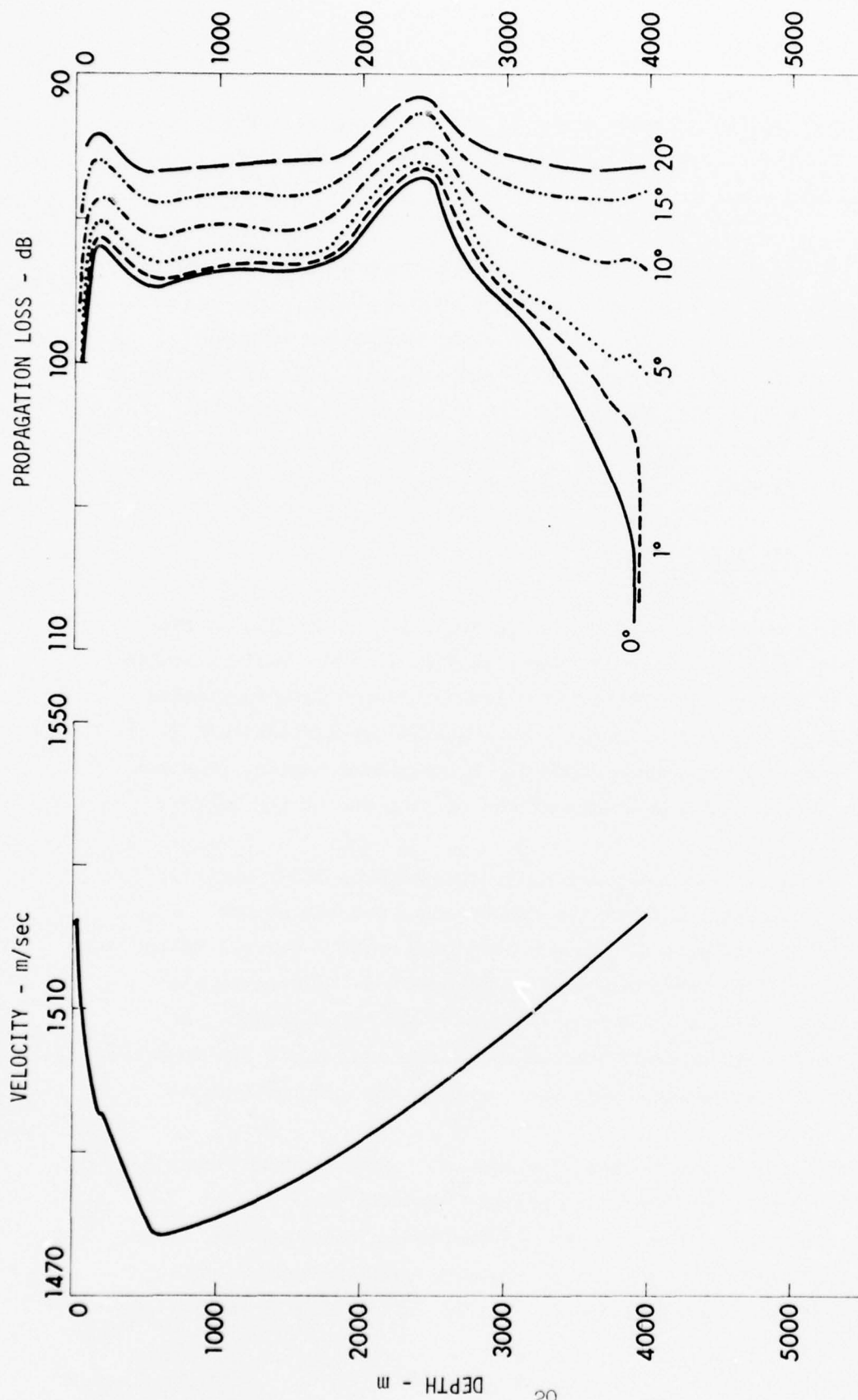


FIGURE II-6
AVERAGE PROPAGATION LOSS
Range Interval: 100-200 nm

MID-PACIFIC PROFILE

SOURCE DEPTH: 152 m, BOTTOM DEPTH: 3952 m, MODEL: FACT

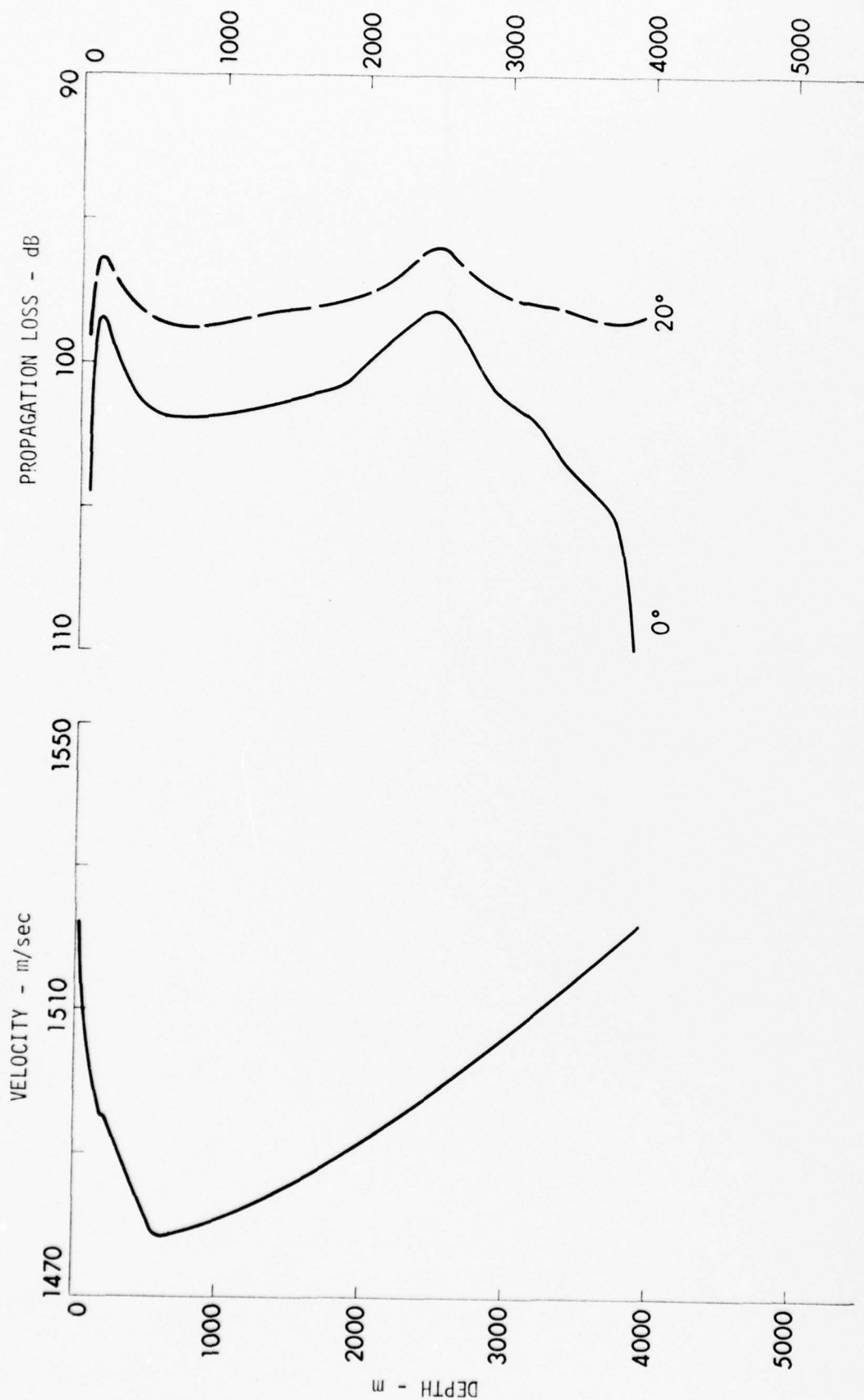


FIGURE II-7
 AVERAGE PROPAGATION LOSS
 Range Interval: 400-480 nm
 MID-PACIFIC PROFILE (2)
 SOURCE DEPTH: 152 m, BOTTOM DEPTH: 3952 m

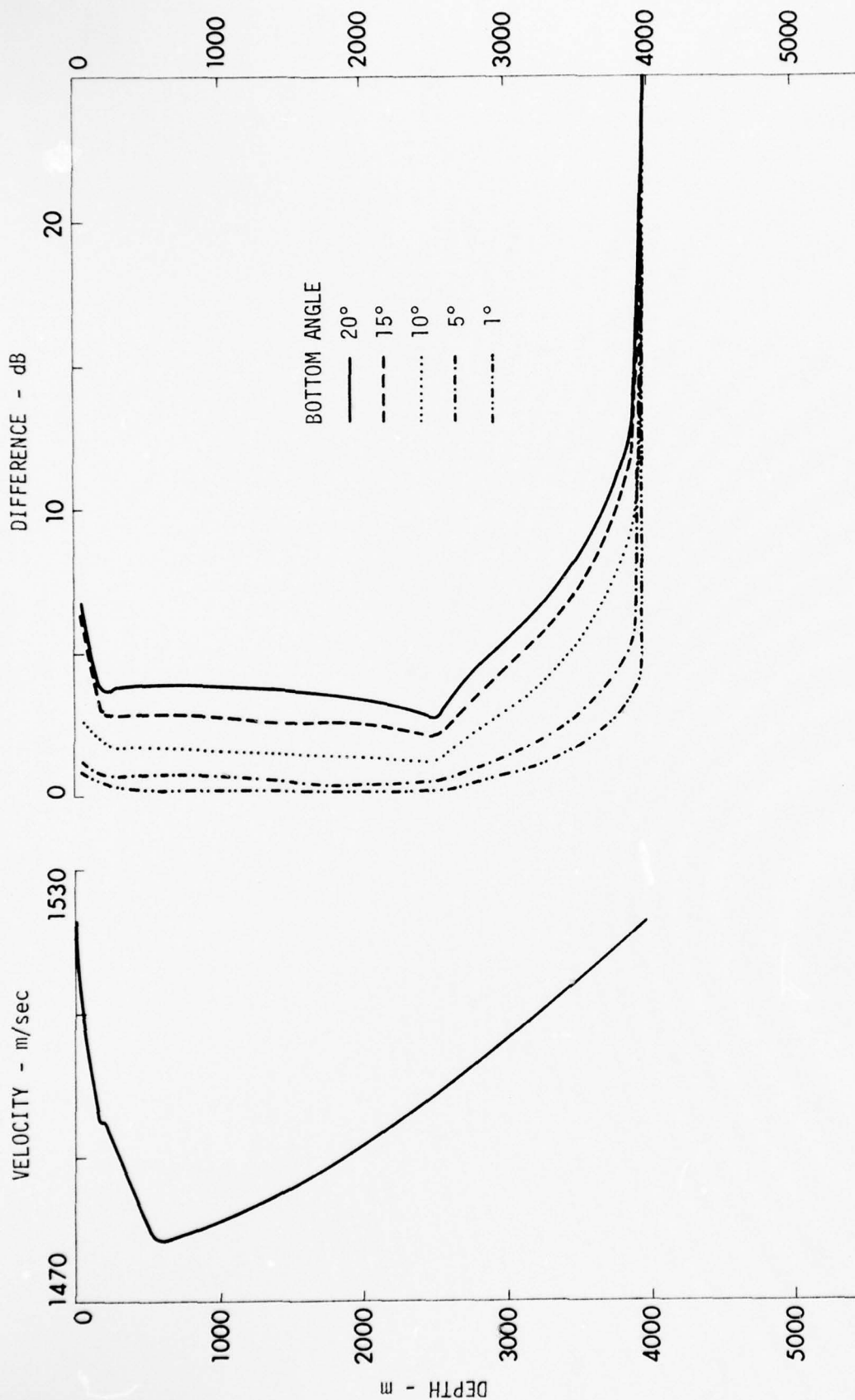


FIGURE II-8
 Δ - DIFFERENCE BETWEEN ABSORBING BOTTOM CASE
 AND THE PARTIALLY REFLECTING BOTTOM CASES

SOURCE DEPTH: 152 m (500 ft), BOTTOM DEPTH: 3952 m, MODEL: FACT

ARL - UT
 AS-76-553
 KCF - DR
 4 - 19 - 76

influence of the various bottom interactions increases as the receiver approaches either the bottom or the surface. Within region 2, the influence of the bottom is regular, i.e., independent of receiver depth.

3. Source Depth Dependence

Figures II-9 through II-12 present the average propagation losses computed by FACT for the mid-Pacific profile with a bottom depth of 3952 m. These figures plus Fig. II-6 present a series of curves for various source depths. For each source depth, propagation loss curves are presented for critical angles of 0° and 20° .

The propagation loss curves exhibit minima at the source depth and its conjugate depth. The maximum propagation loss between these two depths occurs at the channel axis (600 m). The differences between the curves for 0° and 20° critical angles have been computed and appear in Fig. II-13. The minimum difference increases as the source depth decreases. The amount of energy represented by the bottom refracting rays also decreases as the source depth decreases away from the axis. The significance of the bottom interacting energy will therefore increase as the source depth decreases. Figure II-14 presents these differences at a 600 m receiver depth along with the total amount of bottom reflecting energy. (This is represented as the total energy in decibels relative to the water refracted energy.) The bottom refracting energy is based on an omnidirectional source and is the ratio of the source angles for the first ray to intersect the bottom and the ray intersecting the bottom at 20° . The computed differences of the averages are within 2 dB of the calculated bottom refracting energy. The differences in the averages are calculated for the intensity and are expected to show only a reasonable agreement with the bottom refracting energy calculations.

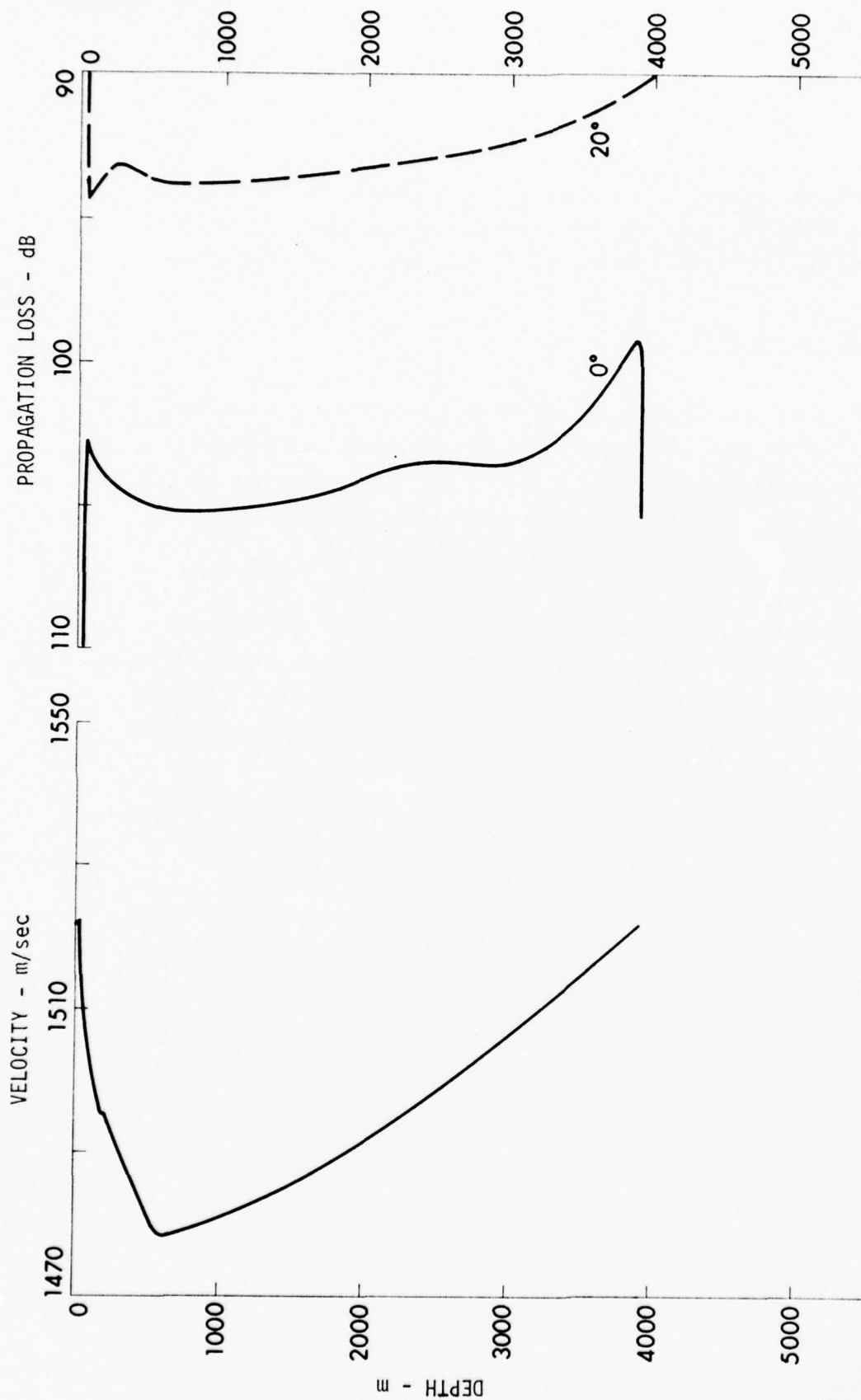


FIGURE II-9
 AVERAGE PROPAGATION LOSS
 Range Interval: 100-200 nm
 MID-PACIFIC PROFILE
 SOURCE DEPTH: 33.5 m, BOTTOM DEPTH: 3952 m, MODEL: FACT

ARL - UT
 AS-76-519
 KCF - DR
 4-19-76

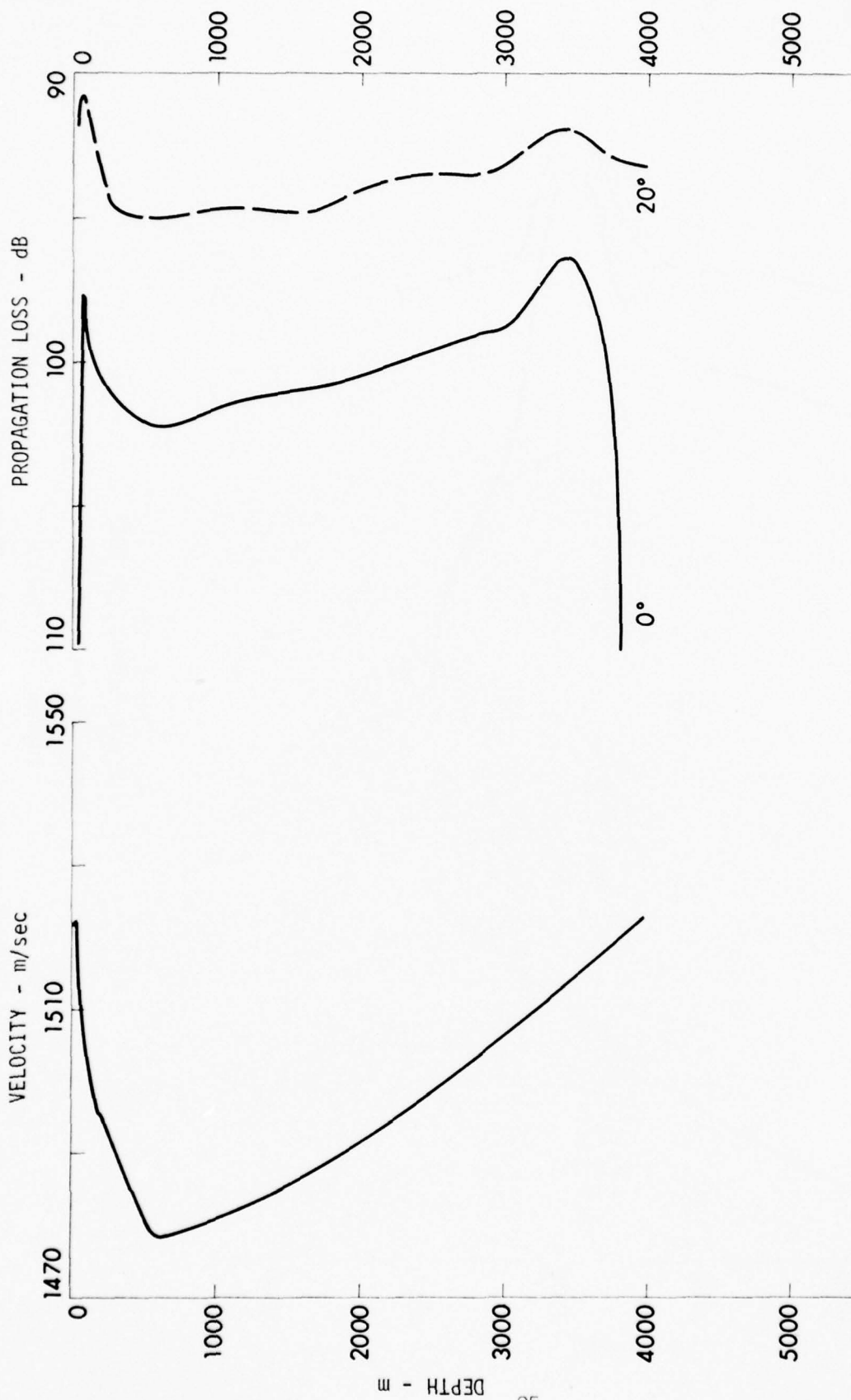


FIGURE II-10
AVERAGE PROPAGATION LOSS
Range Interval: 100-200 nm

MID-PACIFIC PROFILE

SOURCE DEPTH: 50m, BOTTOM DEPTH: 3952 m, MODEL: FACT

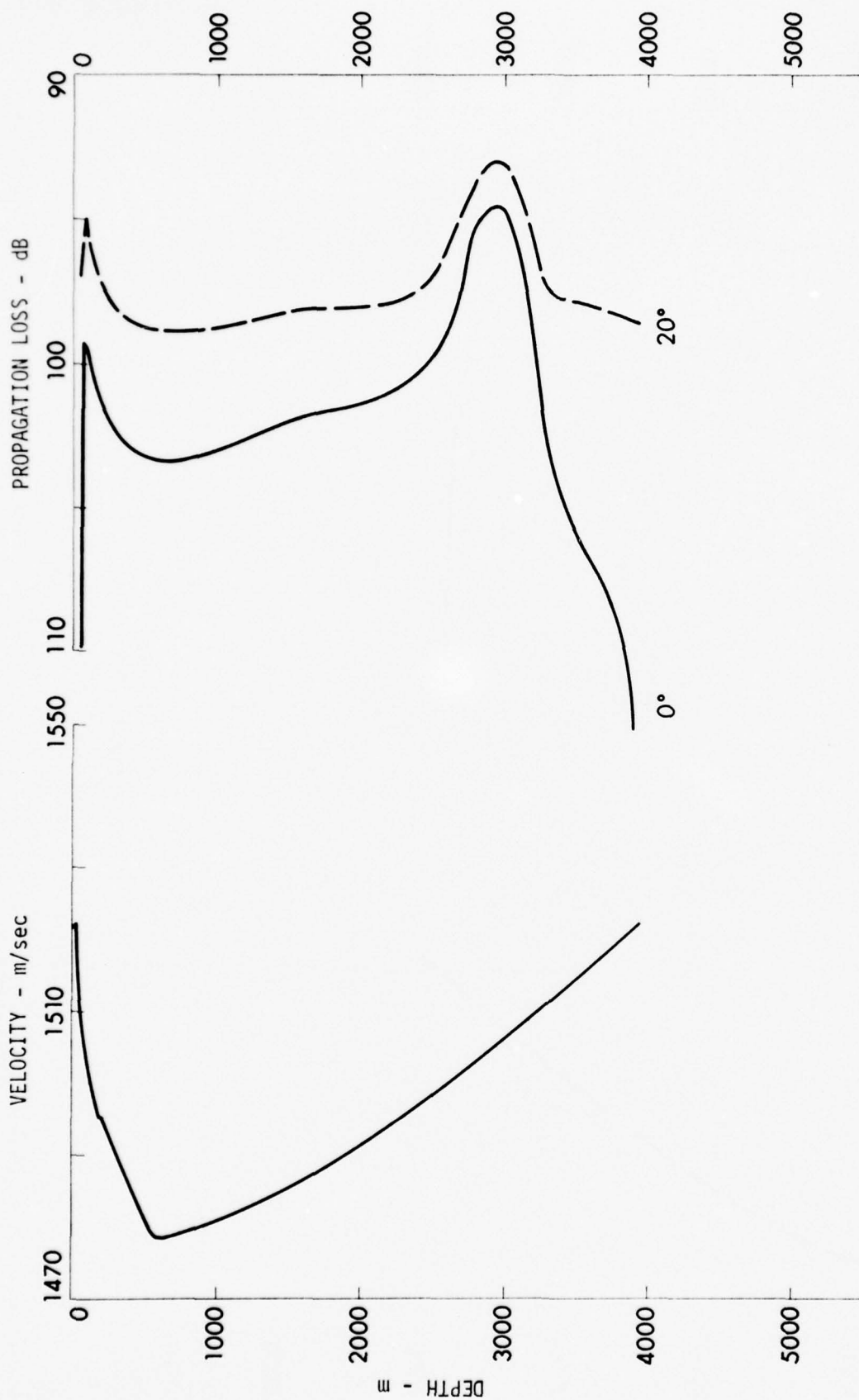


FIGURE II-11
AVERAGE PROPAGATION LOSS
Range Interval: 100-200 nm

MID-PACIFIC PROFILE

SOURCE DEPTH: 91 m, BOTTOM DEPTH: 3952 m, MODEL: FACT

ARL - UT
AS-76-521
KCF - DR
4-19-76

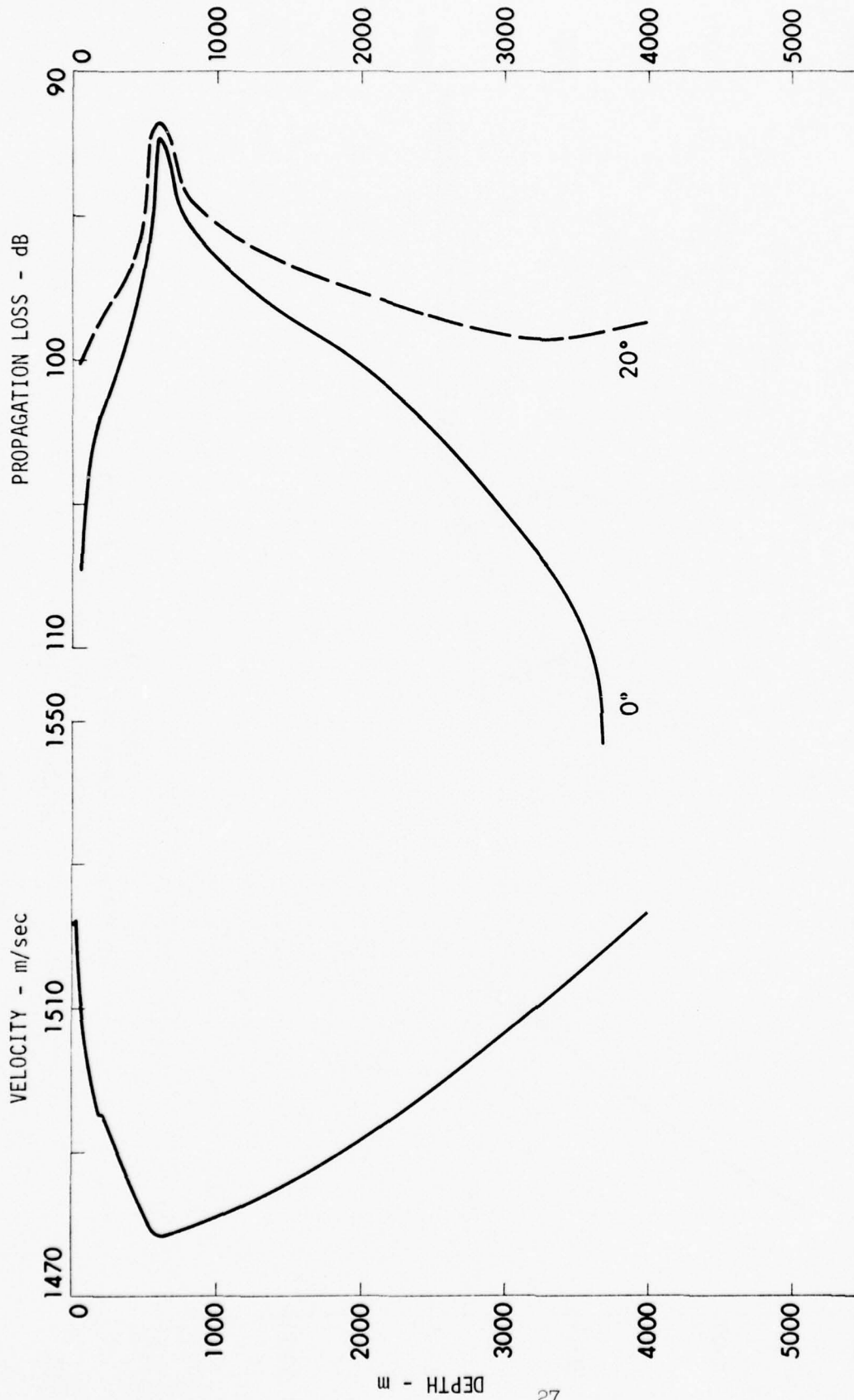


FIGURE II-12
 AVERAGE PROPAGATION LOSS
 Range Interval: 100-200 nm
 MID-PACIFIC PROFILE
 SOURCE DEPTH: 600 m, BOTTOM DEPTH: 3952 m, MODEL: FACT

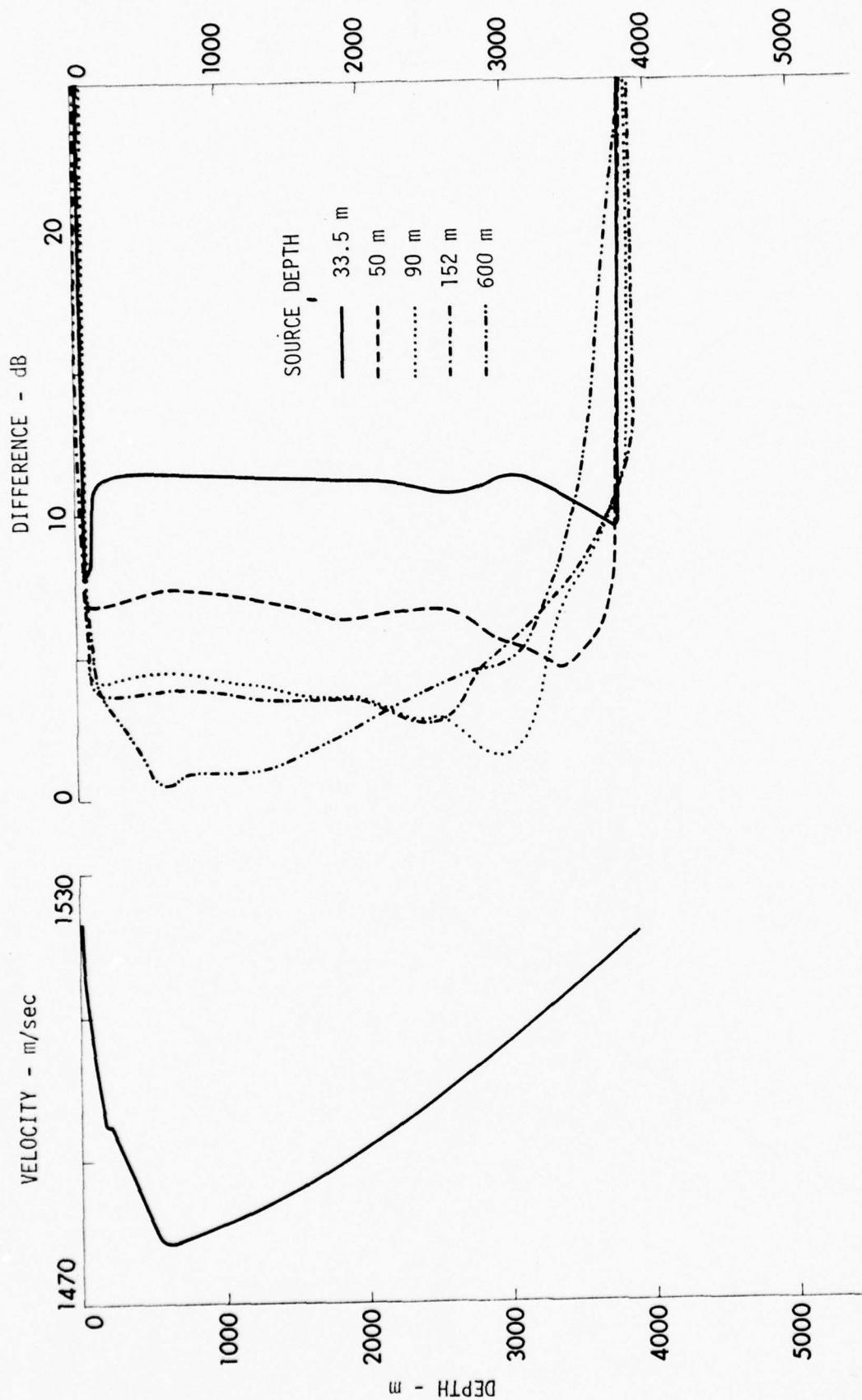


FIGURE II-13
DIFFERENCES BETWEEN THE 0° AND 20° BOTTOMS
FOR VARIOUS SOURCE DEPTHS

MID-PACIFIC PROFILE

BOTTOM DEPTH: 3952 m, MODEL: FACT

ARL - UT
AS-76-555
KCF - DR
4 - 19 - 76

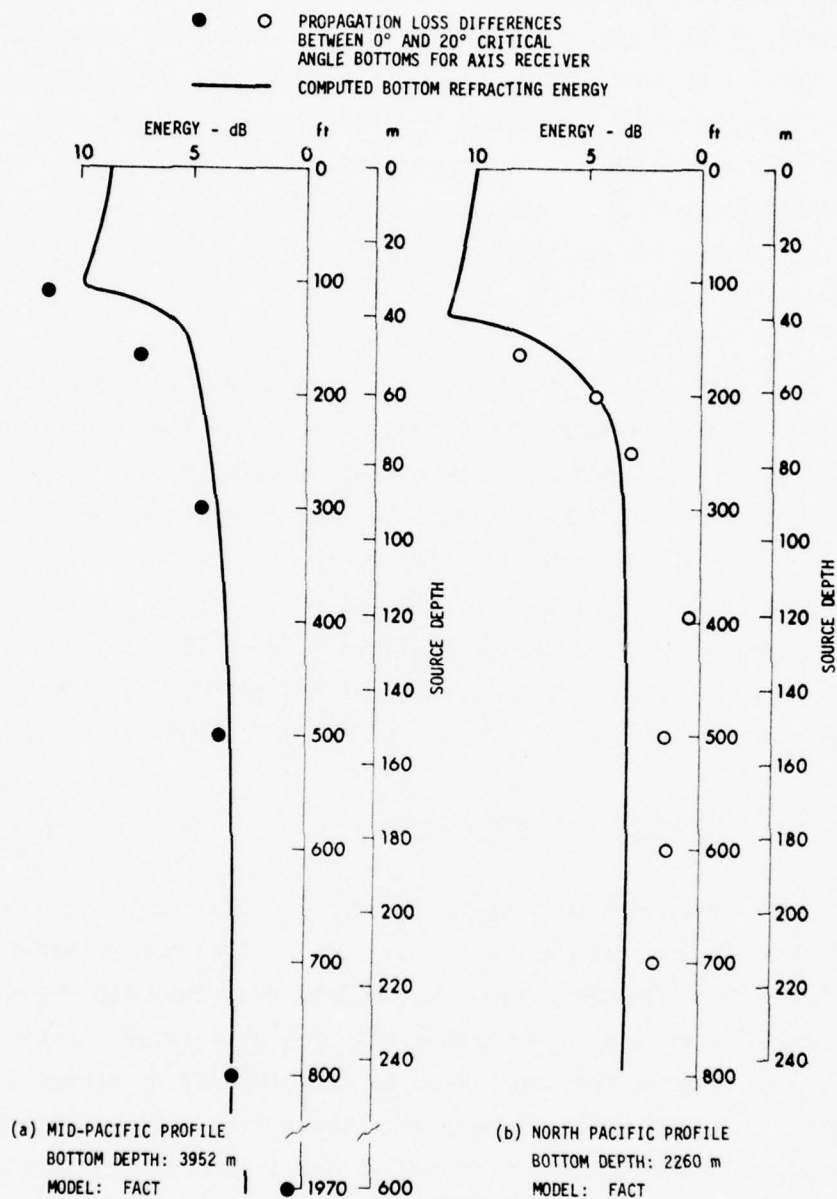


FIGURE II-14
 COMPARISON OF BOTTOM REFLECTED ENERGY AND AVERAGE
 INTENSITY OF THE BOTTOM REFRACTED PATHS

The propagation loss differences in Fig. II-13 display the regular bottom influences in the depth domain between the source and its conjugate depth. Ray theory predicts that all rays will pass through the depths between the source depth and its conjugate depth. Therefore, within this domain the energy contributions from the bottom interactions will be constant with receiver depth. Since bottom interactions do not lead to caustics, their contributions to the average intensities will result in the regular dependence seen in the model.

The one exception to this regular dependence was the 33.5 m source, where the near surface receivers below the source depth did not show this dependence. These model runs were made with surface image interference. When this interference was removed for the 33.5 m source, the differences went from 20 dB to 8 dB for the 33.5 m receiver and from 8.3 dB to 11.6 dB for the 50 m receiver. Within the rest of this domain, the differences remained 11 dB. The only other major effect of removing the interference was that the differences for the 18 m receiver decreased by 10 dB for all source depths.

4. Bottom Depth Dependence

Receivers between the source and its conjugate depth exhibit a regular dependence on the bottom loss. Using the parabolic equation (P.E.) model, average propagation losses were computed for the mid-Pacific profile with various bottom depths (Figs. II-15 through II-18) to examine the dependence of this regularity on the bottom depth. The propagation losses calculated with a 10° critical angle exhibit only a minimum dependence on the bottom depth to within 400 m of the bottom. As the bottom depth increases from 3647 m to 5543 m, the maximum decrease in propagation loss at any receiver depth is less than 1 dB for receivers more than 400 m off the bottom. Minimum losses occur at the source depth and its conjugate depth. Between these two depths, the maximum occurs at the axis. Outside this

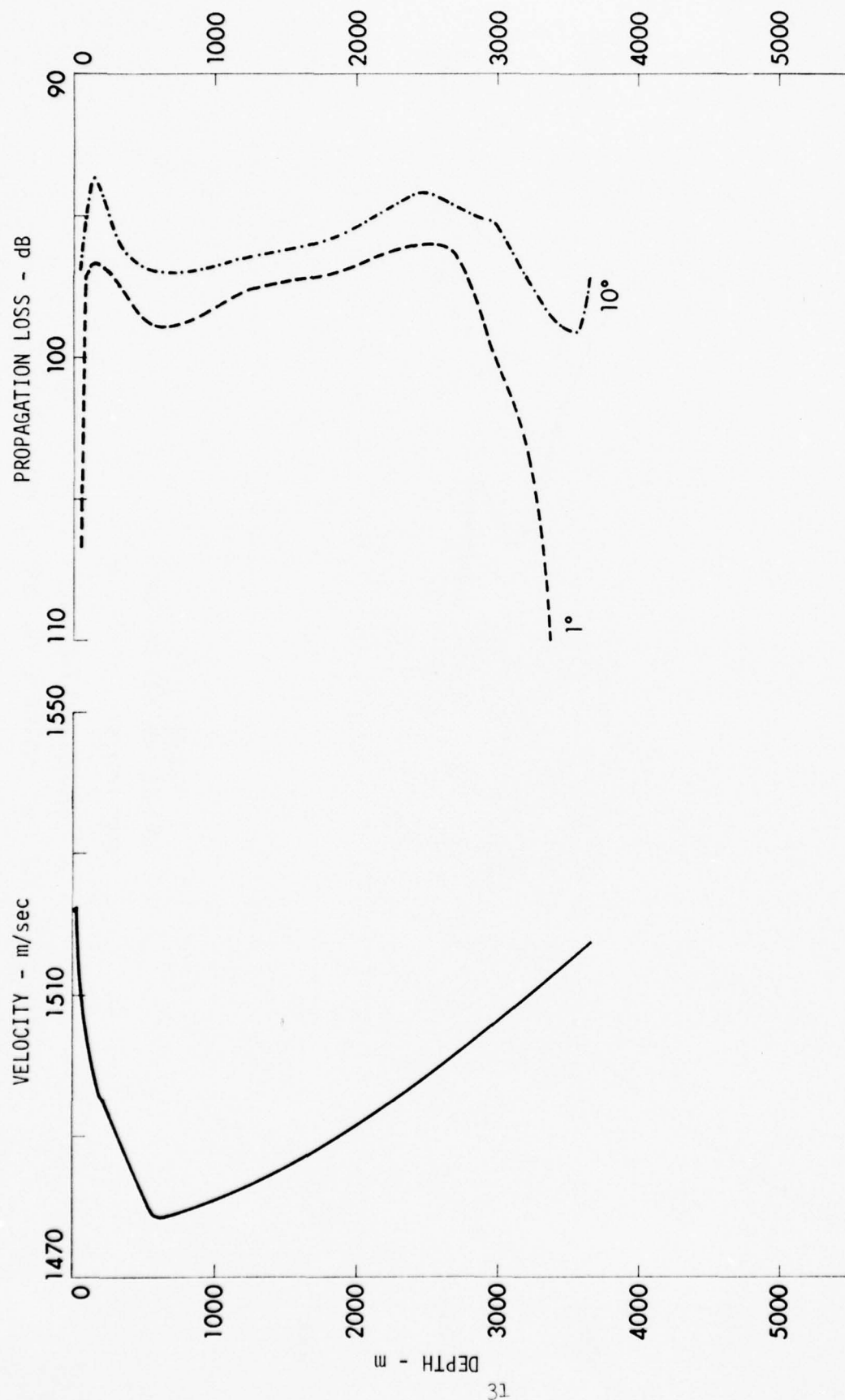


FIGURE II-15
 AVERAGE PROPAGATION LOSS
 Range Interval: 100-200 nm
 MID-PACIFIC PROFILE
 SOURCE DEPTH: 152 m, BOTTOM DEPTH: 3647 m, MODEL: P.E.

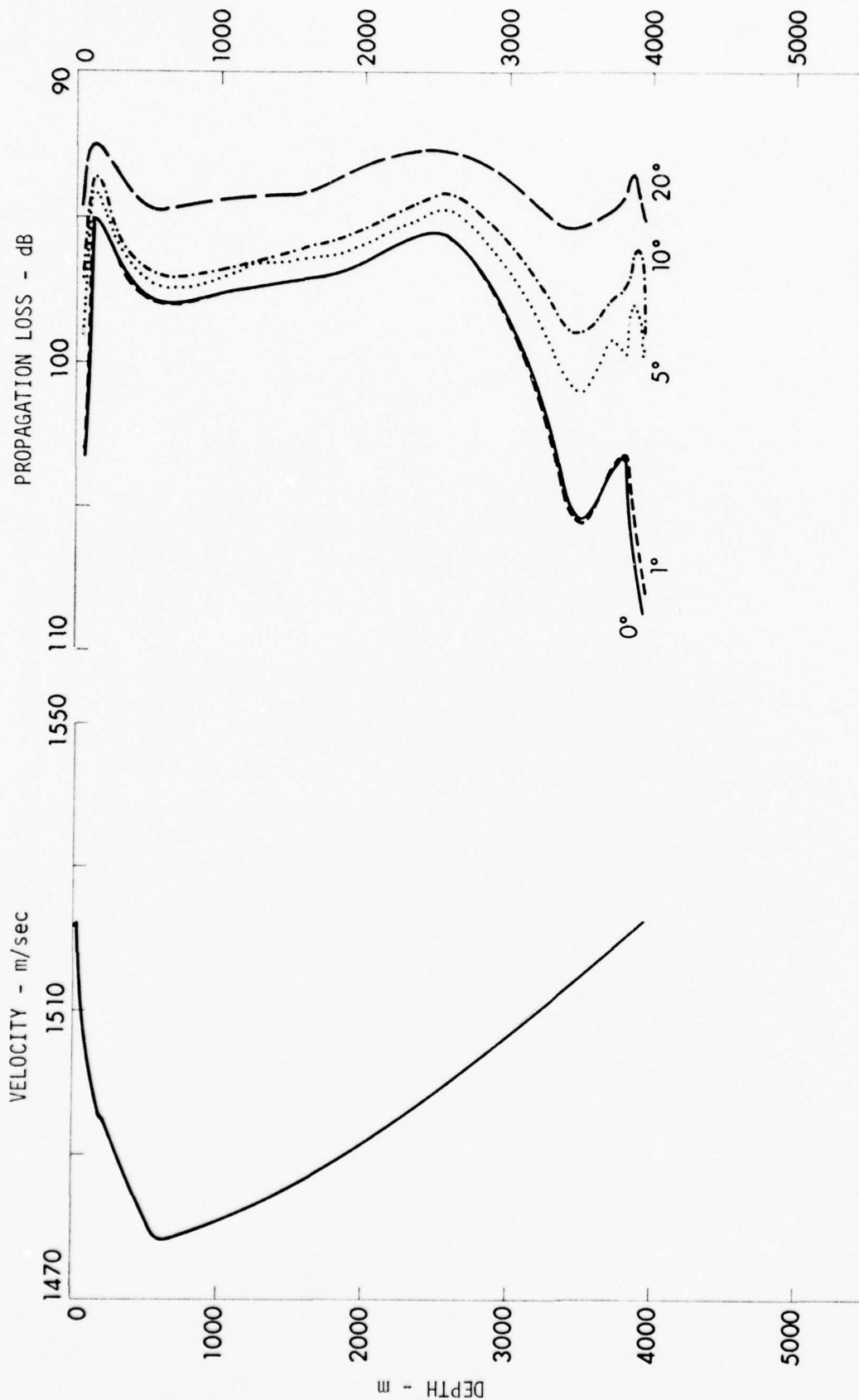


FIGURE II-16
AVERAGE PROPAGATION LOSS
Range Interval: 100-200 nm

MID-PACIFIC PROFILE
SOURCE DEPTH: 152.4 m, BOTTOM DEPTH: 3952 m, MODEL: P.E.



FIGURE II-17
AVERAGE PROPAGATION LOSS
Range Interval: 100-200 nm
MID-PACIFIC PROFILE

SOURCE DEPTH: 152 m, BOTTOM DEPTH: 4257 m, MODEL: P.E.

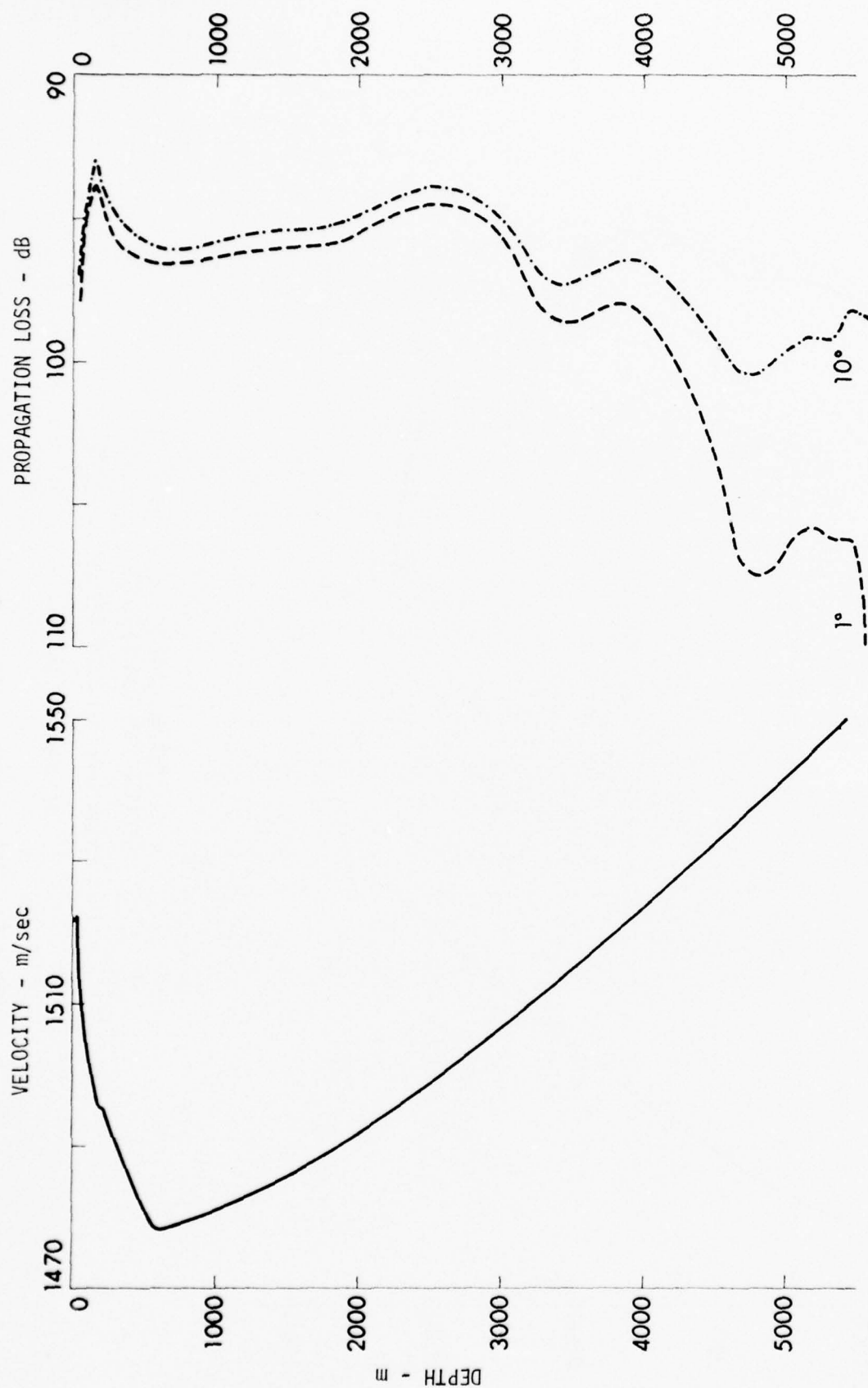


FIGURE II-18
AVERAGE PROPAGATION LOSS
Range Interval: 100-200 nm

MID-PACIFIC PROFILE

SOURCE DEPTH: 152 m, BOTTOM DEPTH: 5543 m, MODEL: P.E.

ARL - UT
AS-76-524
KCF - DR
4-19-76

domain the propagation loss has a generally increasing trend as the receiver approaches the bottom or surface.

Figure II-19 presents the differences between the averages computed with the 1° and 10° critical angles. The depths between the source depth and the source conjugate depth exhibit the regular bottom loss dependence for all bottom depths. With bottom depths 1000 m greater than the source conjugate depth, an increase of as much as 2000 m in the bottom depth leads to a change less than 1.5 dB in the differences between the source depth and its conjugate depth.

The receiver depths greater than the source conjugate depth show a decrease in the bottom loss dependence as the bottom depth increases. The bottom loss dependence increases as the receiver depth increases to within 700 m of the bottom. Within 400 m to 700 m, the bottom loss dependence as a function of depth varies with the bottom depth.

D. Considerations of Additional Profiles

A sound speed profile from the mid-Pacific has been used in the initial investigations of propagation sensitivity. The profile has a single sound channel with an axis depth of 600 m and represents the "classical" profile. Profiles from the North Pacific and from the Indian Ocean, both single channel profiles, are now used to extend the area of investigation. The North Pacific profile has a channel axis at 120 m and presents a "narrow" sound channel (critical depth 2260 m). The profile from the Indian Ocean has a channel axis of 1676 m and presents a "broad" sound channel (critical depth 4800 m). Again, these profiles are shown accompanying the respective propagation loss plots.

Average propagation losses computed by FACT and P.E. are shown in Figs. II-20 through II-27 for the North Pacific Profile. The average propagation losses for the Indian Ocean appear in Figs. II-28 through

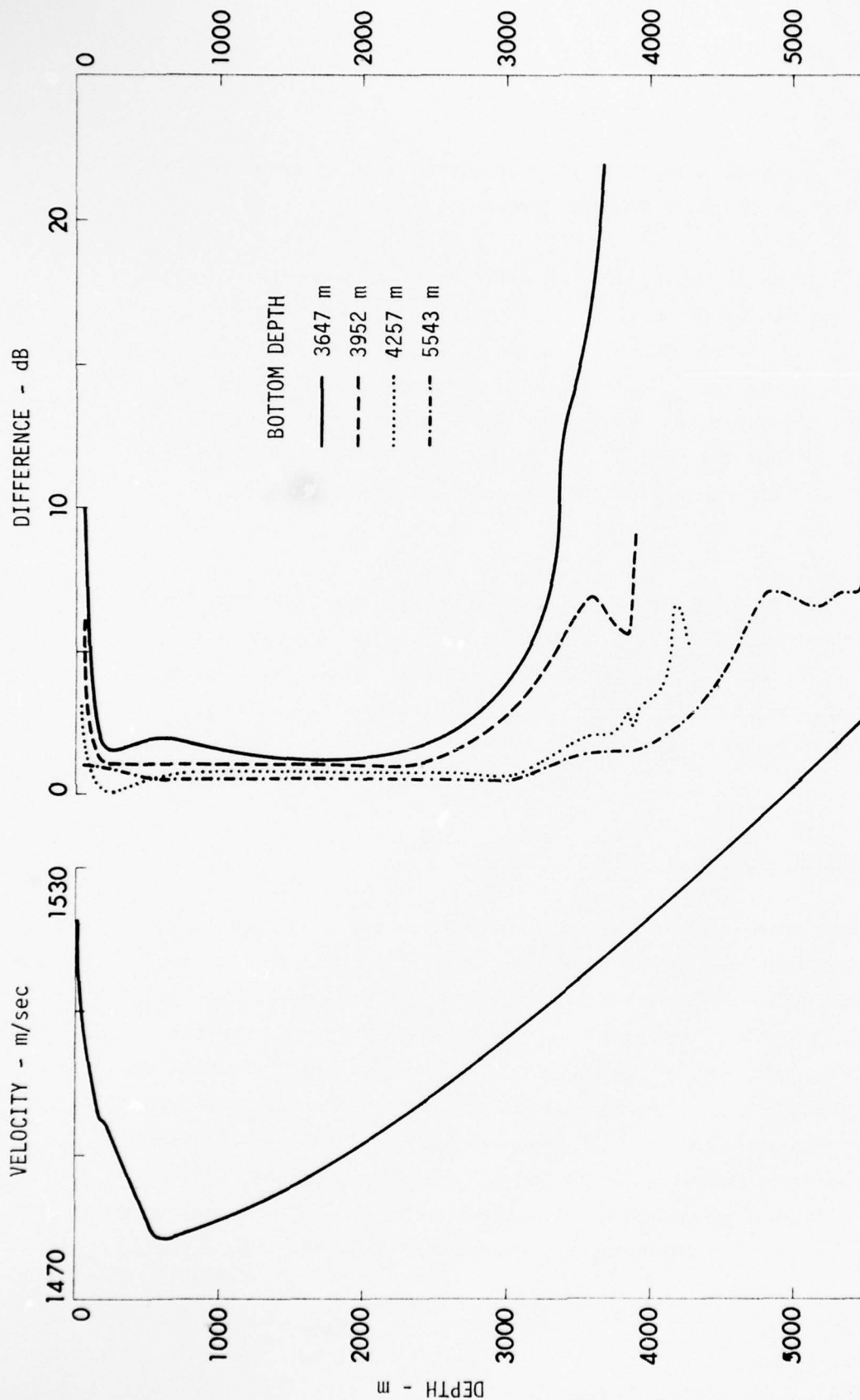


FIGURE II-19
 DIFFERENCES IN 1° AND 10° BOTTOMS FOR VARYING BOTTOM DEPTHS
 MID-PACIFIC PROFILE
 SOURCE DEPTH: 152 m, MODEL: P.E.

ARL - UT
 AS-76-554
 KCF - DR
 4-19-76

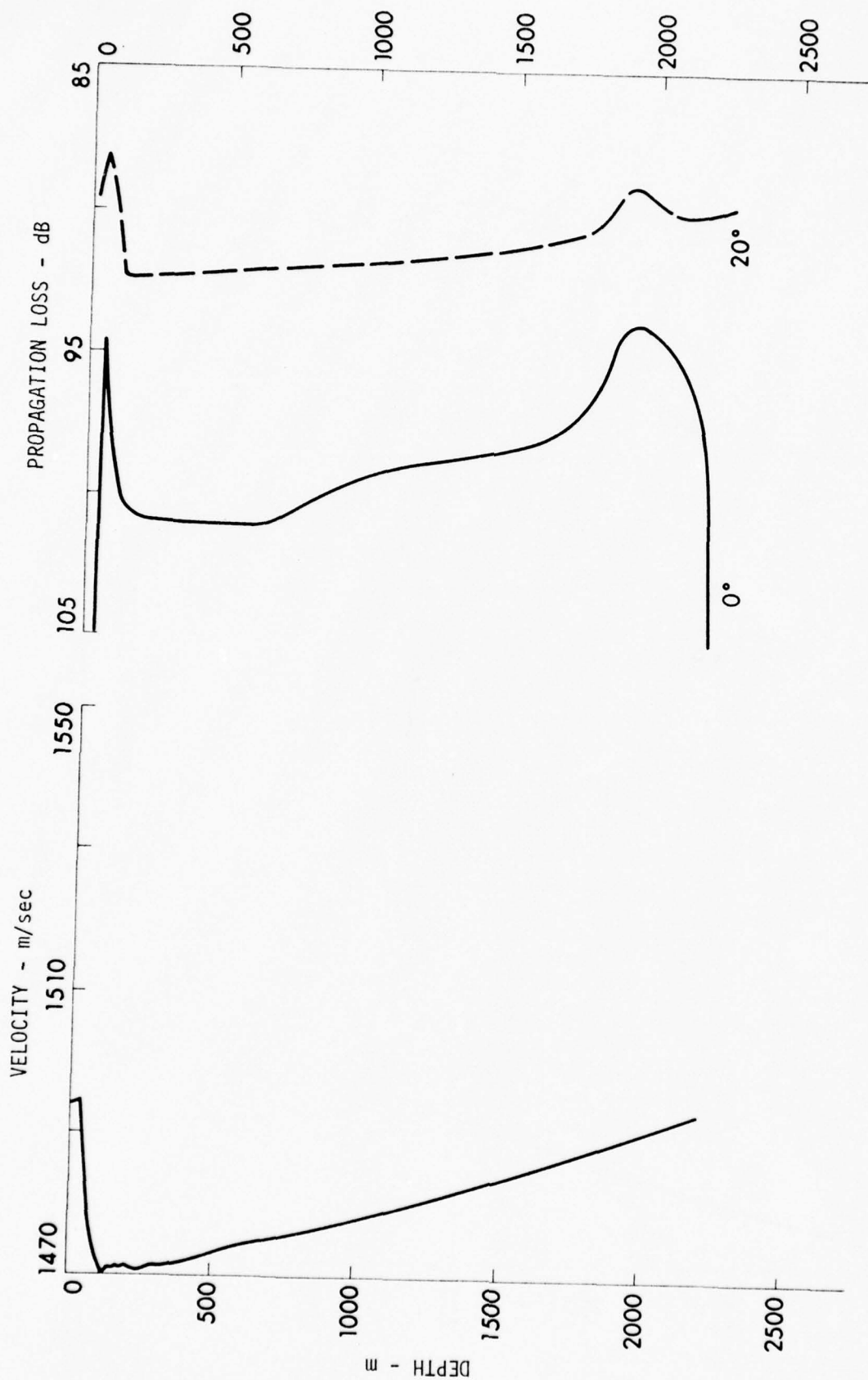


FIGURE II-20
AVERAGE PROPAGATION LOSS
Range Interval: 100-200 nm

NORTH PACIFIC PROFILE

SOURCE DEPTH: 50 m, BOTTOM DEPTH: 2260 m, MODEL: FACT

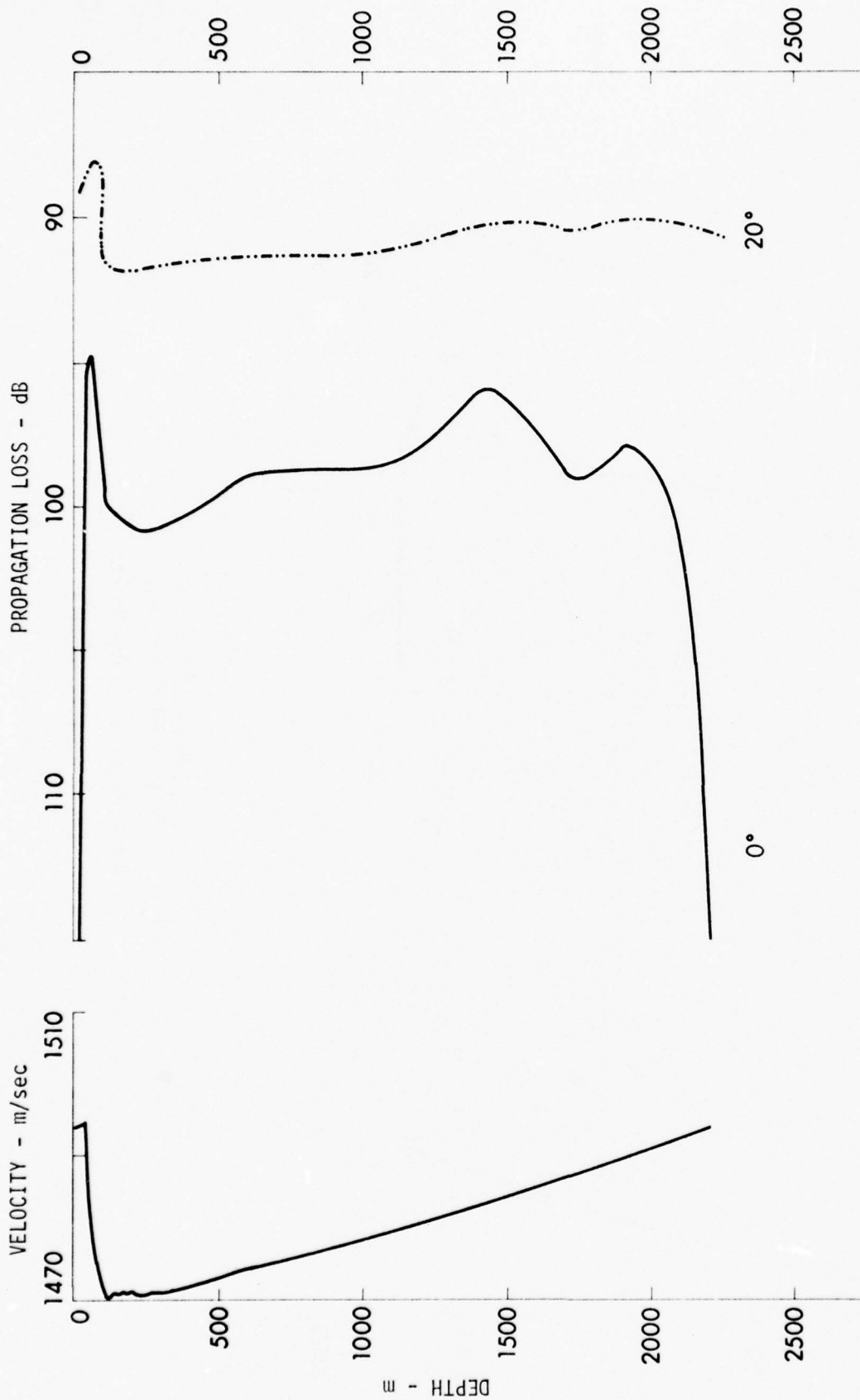


FIGURE II-21
 AVERAGE PROPAGATION LOSS
 NORTH PACIFIC PROFILE
 SOURCE DEPTH: 60 m, BOTTOM DEPTH: 2260 m, MODEL: FACT

ARL - UT
 AS-76-603
 KCF - DR
 5-12-76

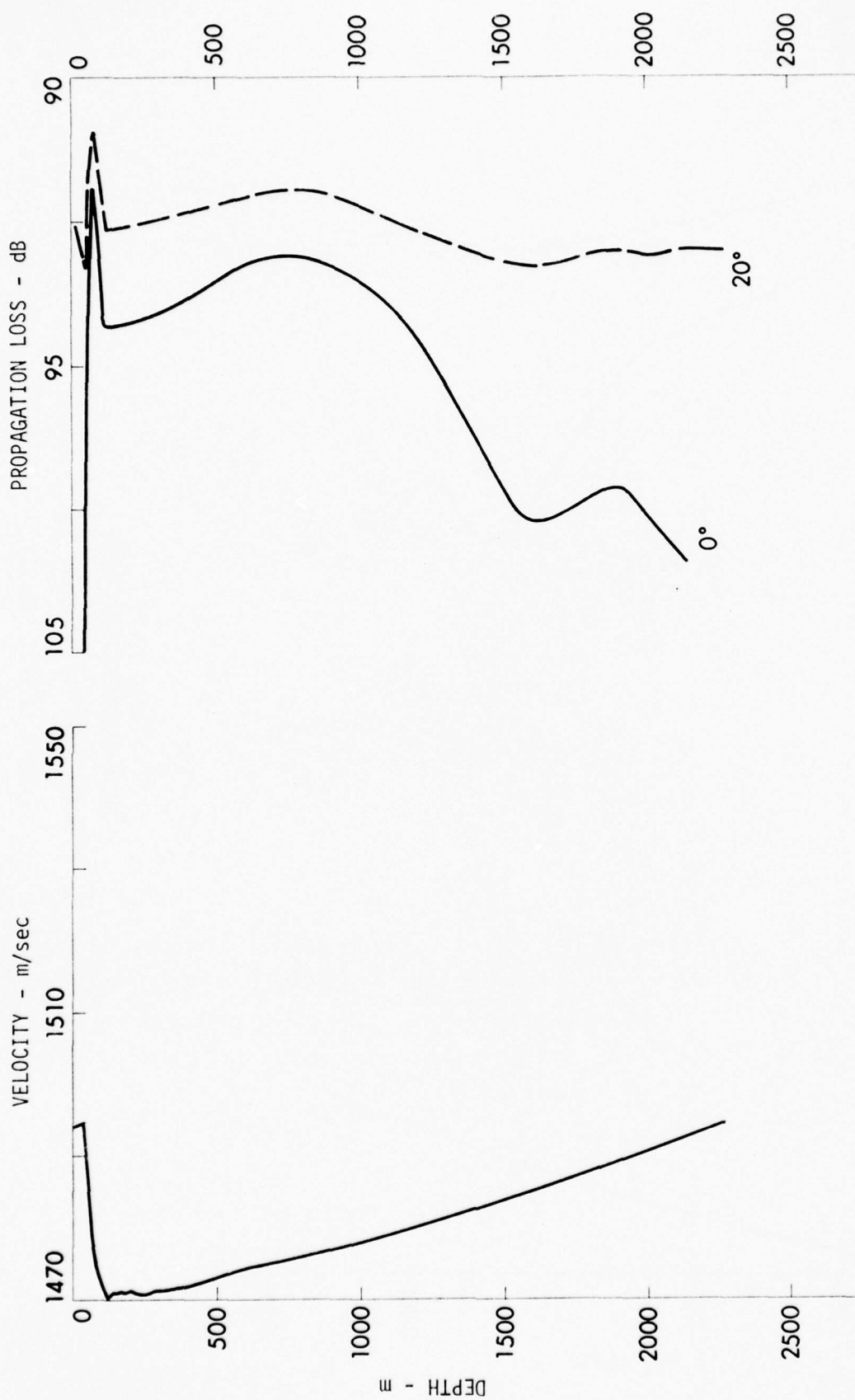


FIGURE II-22
AVERAGE PROPAGATION LOSS
Range Interval: 100-200 nm

NORTH PACIFIC PROFILE

SOURCE DEPTH: 76 m, BOTTOM DEPTH: 2260 m, MODEL: FACT

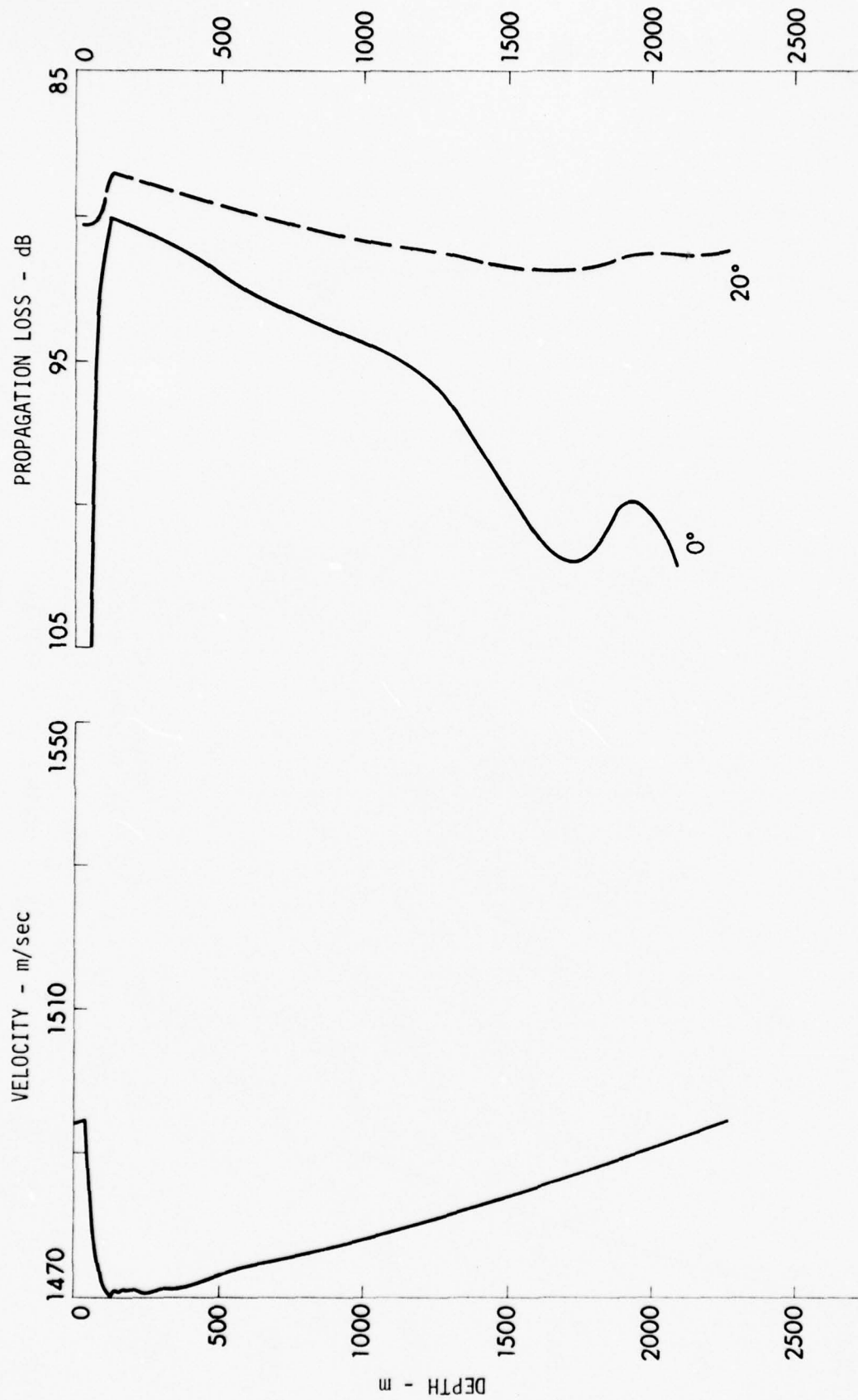


FIGURE II-23
AVERAGE PROPAGATION LOSS
Range Interval: 100-200 nm

NORTH PACIFIC PROFILE

SOURCE DEPTH: 152 m, BOTTOM DEPTH: 2260, MODEL: FACT

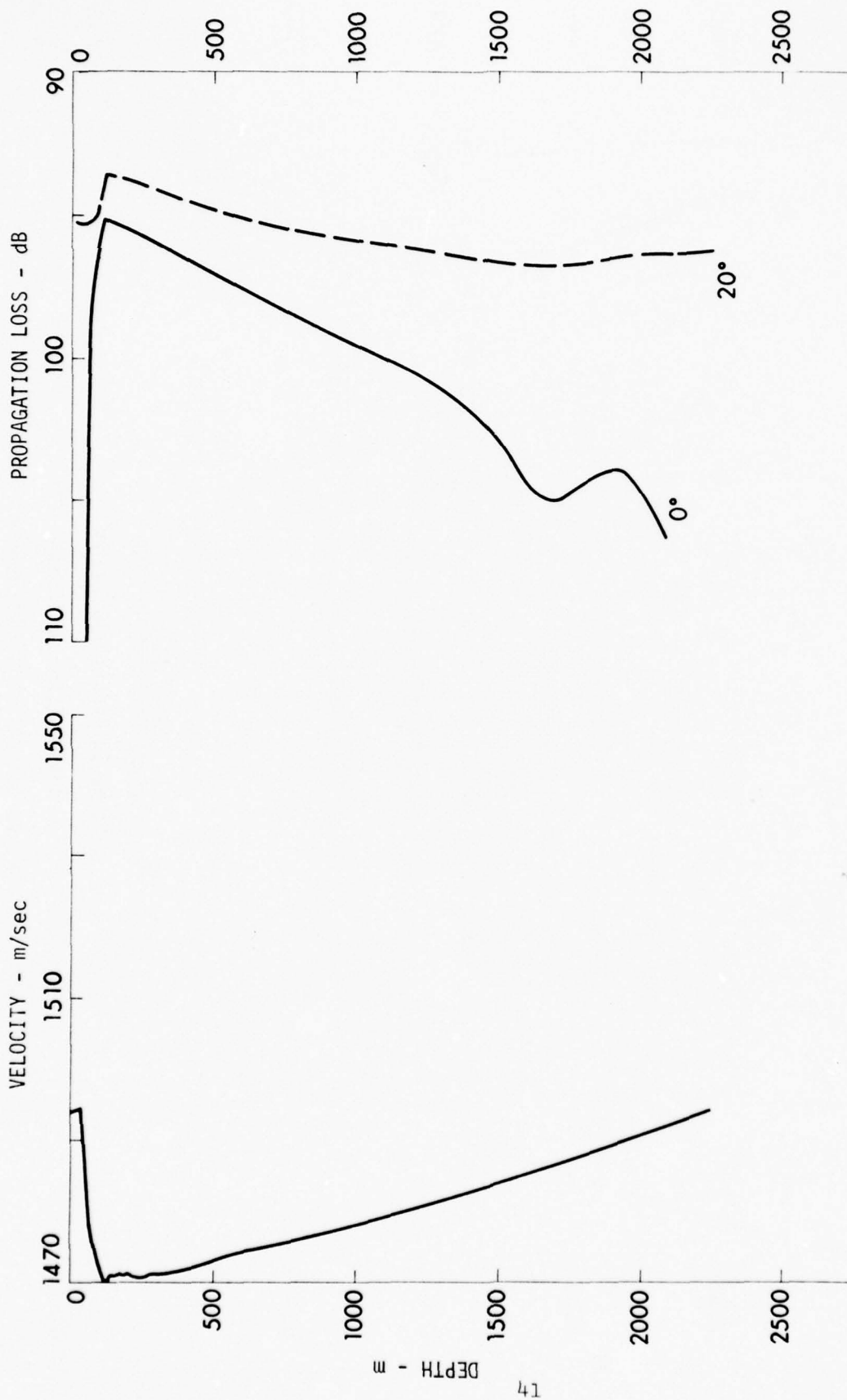


FIGURE II-24
AVERAGE PROPAGATION LOSS
Range Interval: 400-480 nm

NORTH PACIFIC PROFILE

SOURCE DEPTH: 152 m, BOTTOM DEPTH: 2260 m, MODEL: FACT

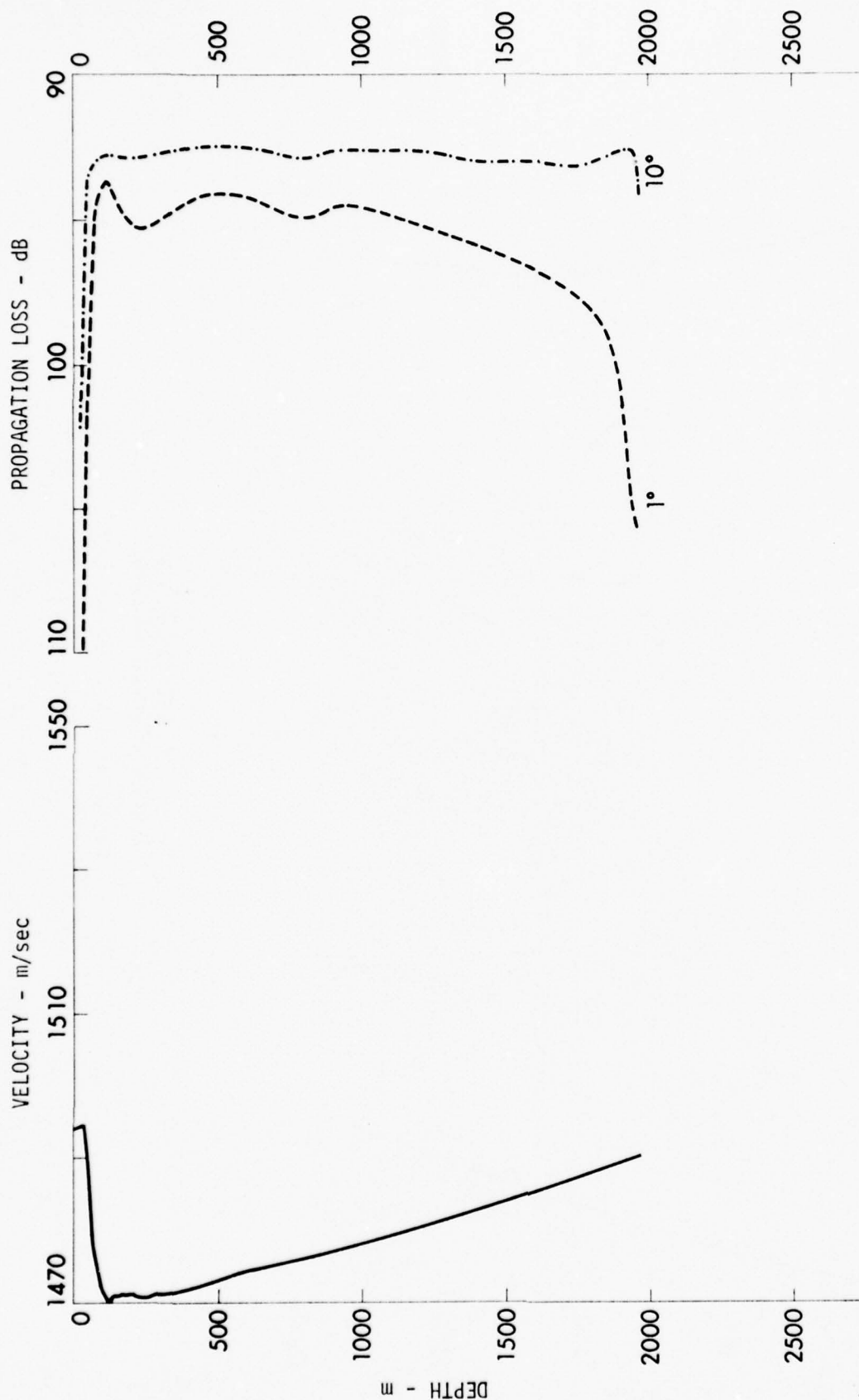


FIGURE II-25
AVERAGE PROPAGATION LOSS
Range Interval: 100-200 nm

NORTH PACIFIC PROFILE

SOURCE DEPTH: 76 m, BOTTOM DEPTH: 1955 m, MODEL: P.E.

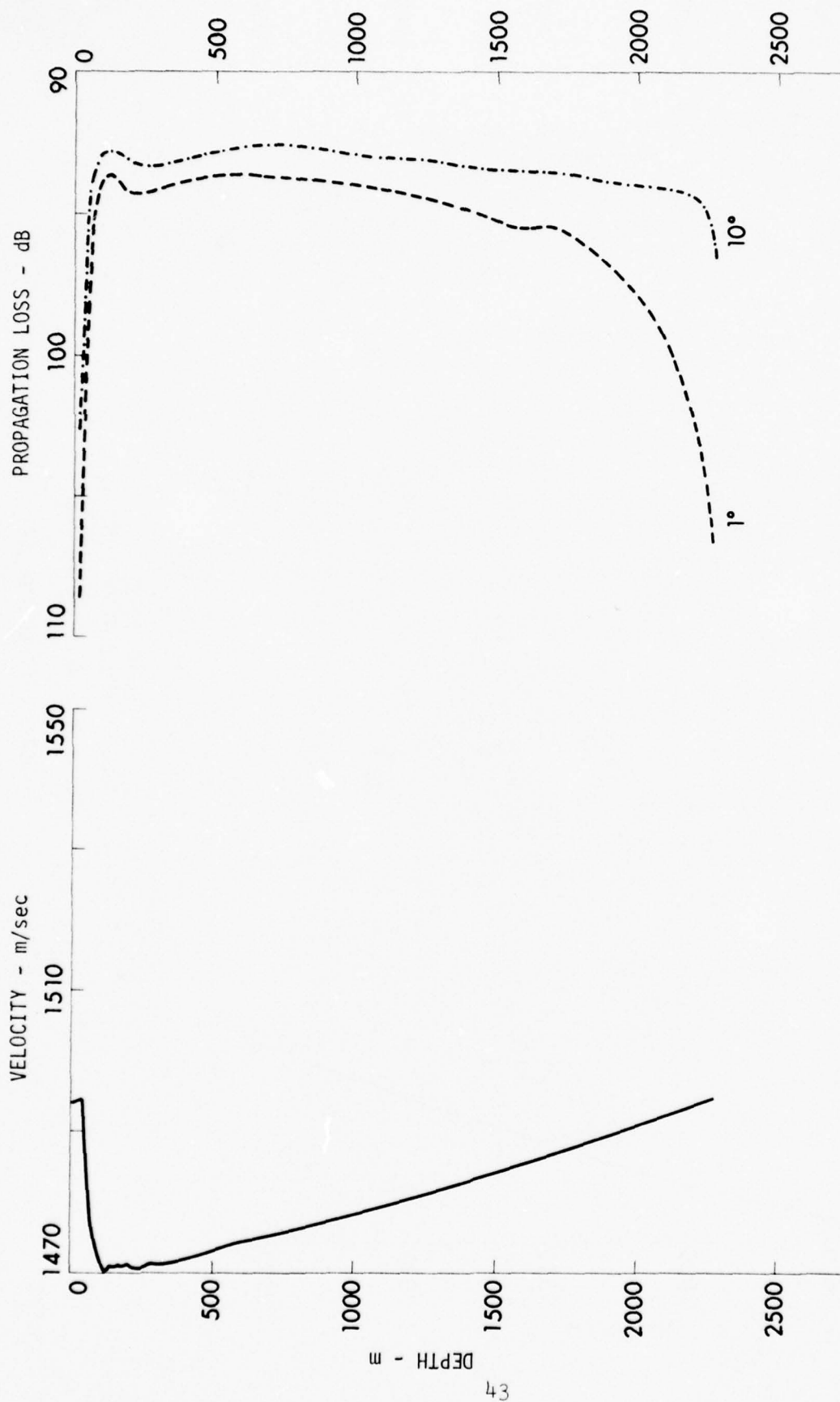


FIGURE II-26
AVERAGE PROPAGATION LOSS
Range Interval: 100-200 nm

NORTH PACIFIC PROFILE

SOURCE DEPTH: 76 m, BOTTOM DEPTH: 2260 m, MODEL: P.E.

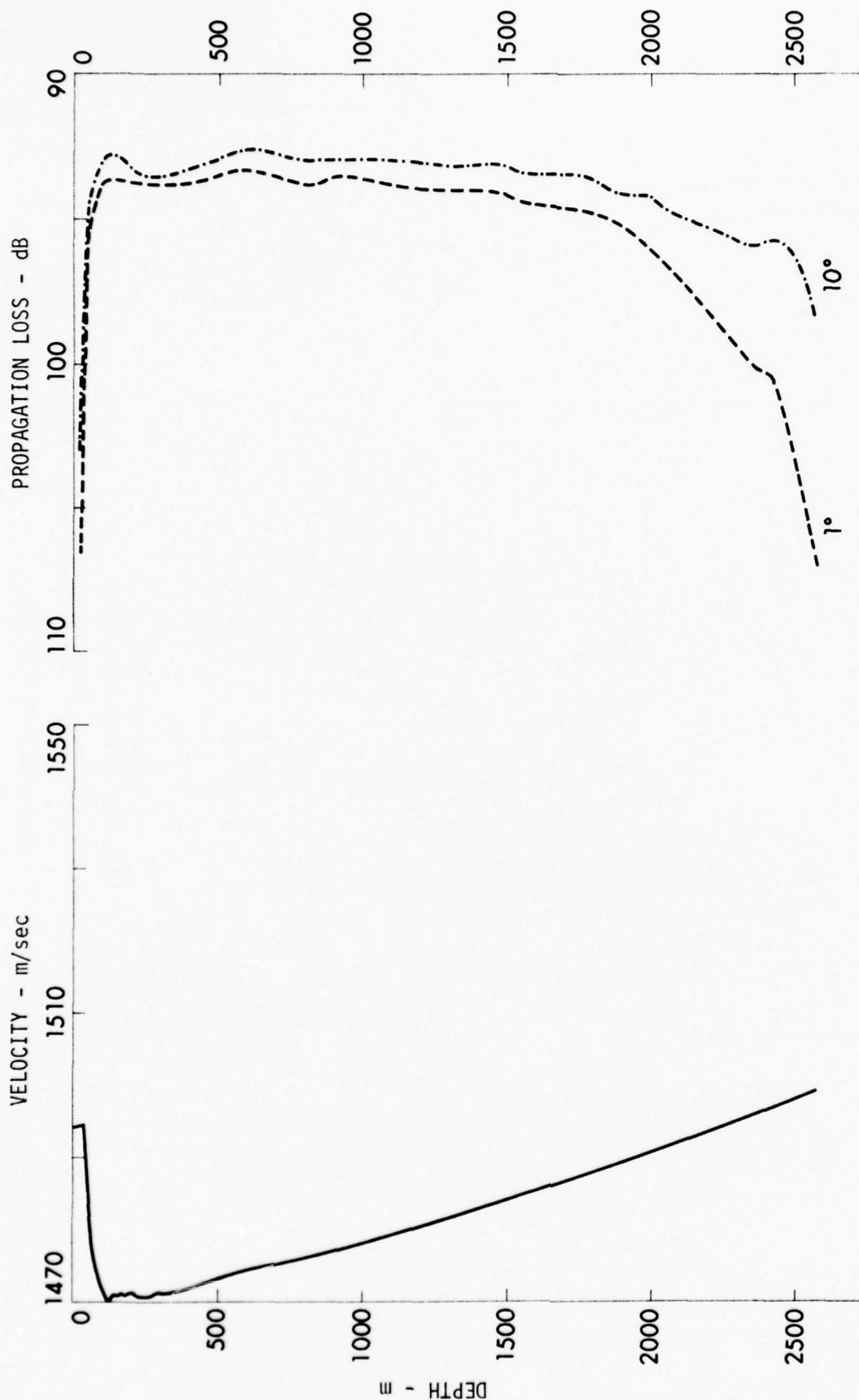


FIGURE 11-27
 AVERAGE PROPAGATION LOSS
 Range Interval: 100-200 nm

NORTH PACIFIC PROFILE

SOURCE DEPTH: 76 m, BOTTOM DEPTH: 2565 m, MODEL: P.E.

ARL - UT
 AS-76-531
 KCF - DR
 4 - 19 - 76

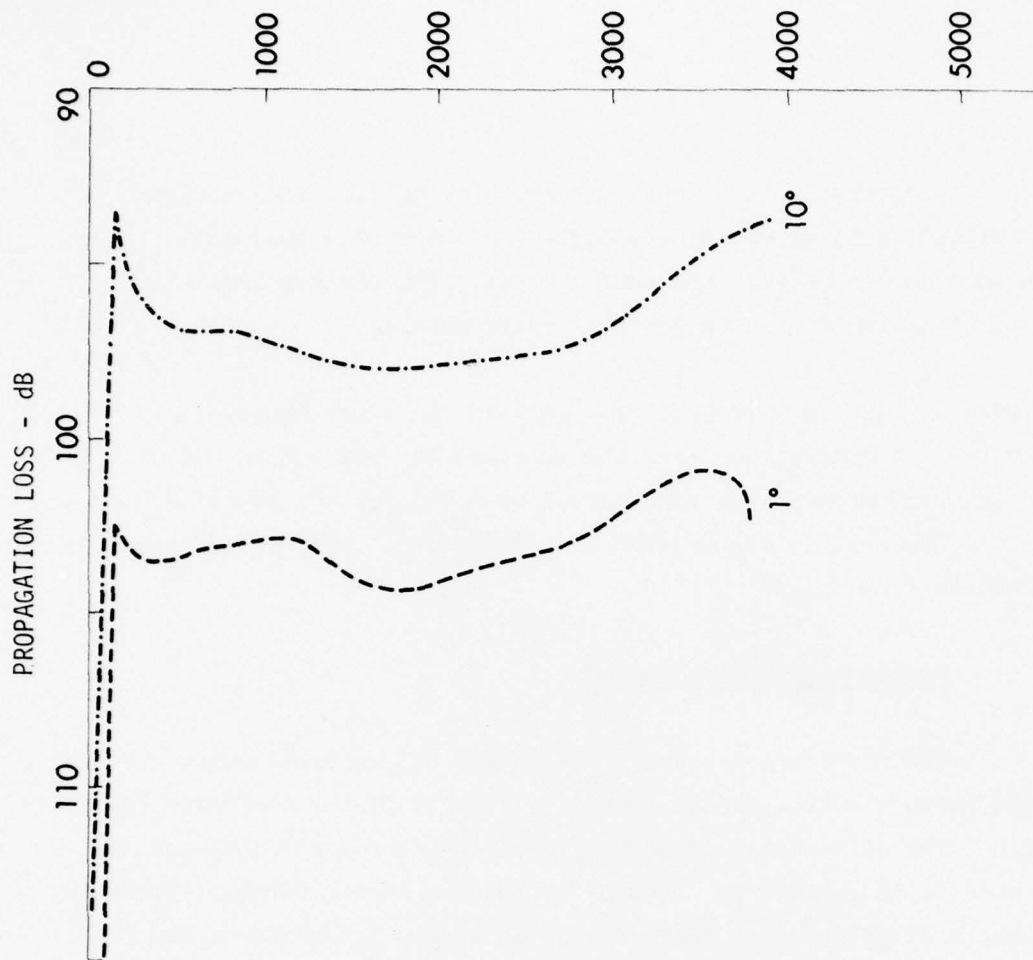
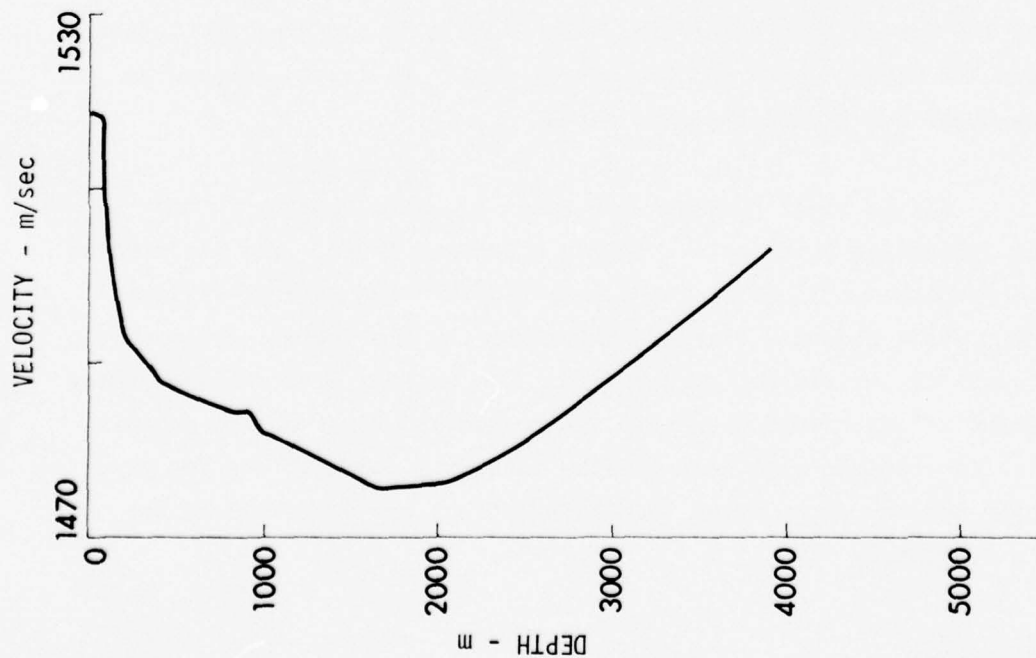


FIGURE II-28
AVERAGE PROPAGATION LOSS
Range Interval: 100-200 nm

INDIAN OCEAN PROFILE

SOURCE DEPTH: 152 m, BOTTOM DEPTH: 3880 m, MODEL: P.E.

II-34. These curves, like those for the mid-Pacific, show minimum propagation losses at the source depth and the source conjugate depth for sources outside the surface duct. The maximum loss between these two depths in general occurs on axis.

Figures II-23 and II-24 differ only in the range interval. Except for a 5 dB displacement, the averages for the 400 to 480 nm range interval present the same curves as those for the 100 to 200 nm interval. The 100 to 200 nm averages, therefore, represent the general propagation losses.

1. Source Depth Dependence

The differences between the 0° and 20° critical angle curves for the various source depths appear in Fig. II-35 for the North Pacific profile. The differences for depths between the source depth and its conjugate depth exhibit the regular dependence on the bottom. There is, however, a slight general decrease in the bottom influence as the receiver approaches the source conjugate depth. For receivers outside this domain, the differences increase as the receiver depths approach either the bottom or the surface. The minimum differences for depths between the source depth and the source conjugate depth decrease as the source depth approaches the axis depth.

Figure II-14 presents the total amount of energy in the bottom reflecting paths as a function of source depth. The differences in the propagation losses for the axis receiver are generally within 1.5 dB of this computed energy, exhibiting the same relationship as that seen for the mid-Pacific profile. The maximum error between these two calculations occurs when both the source and receiver are on axis. Caustic corrections will dominate the intensity calculations for this geometry and the propagation loss computations are dominated by the bottom refracting rays.

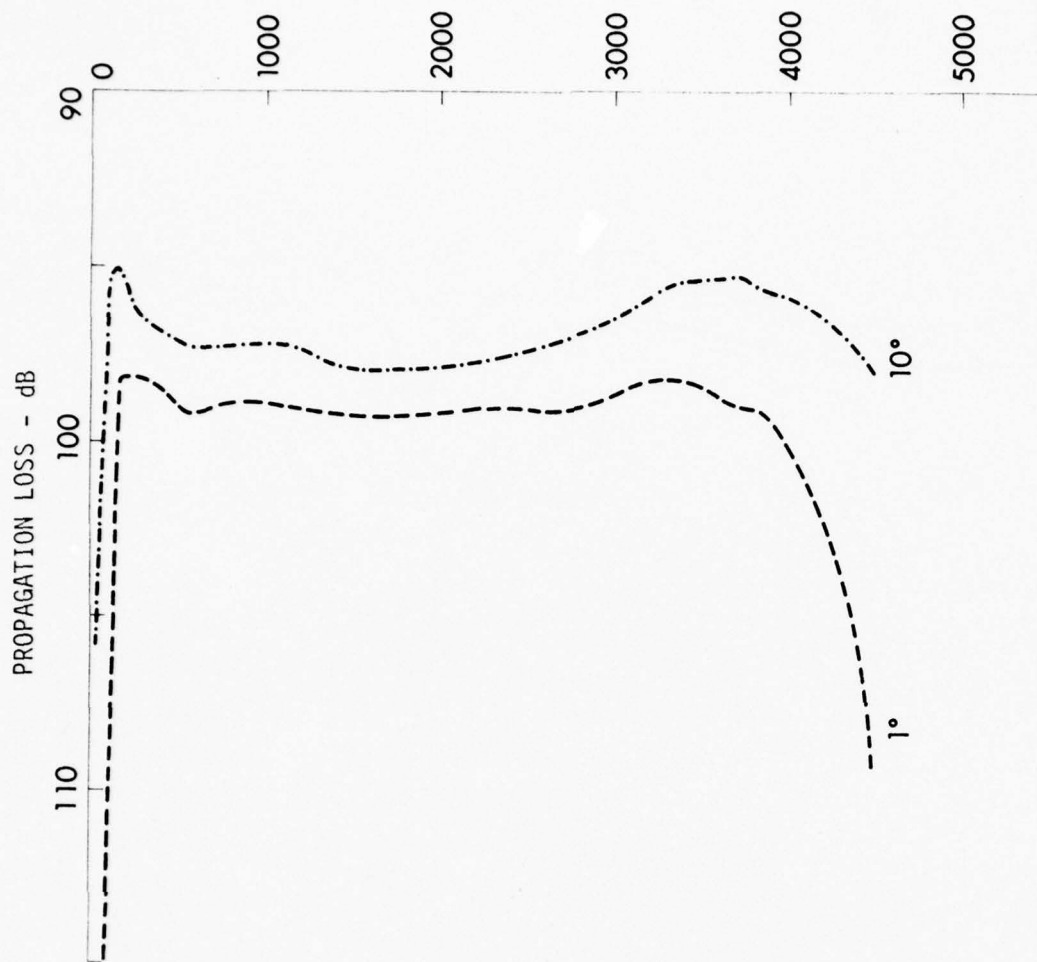
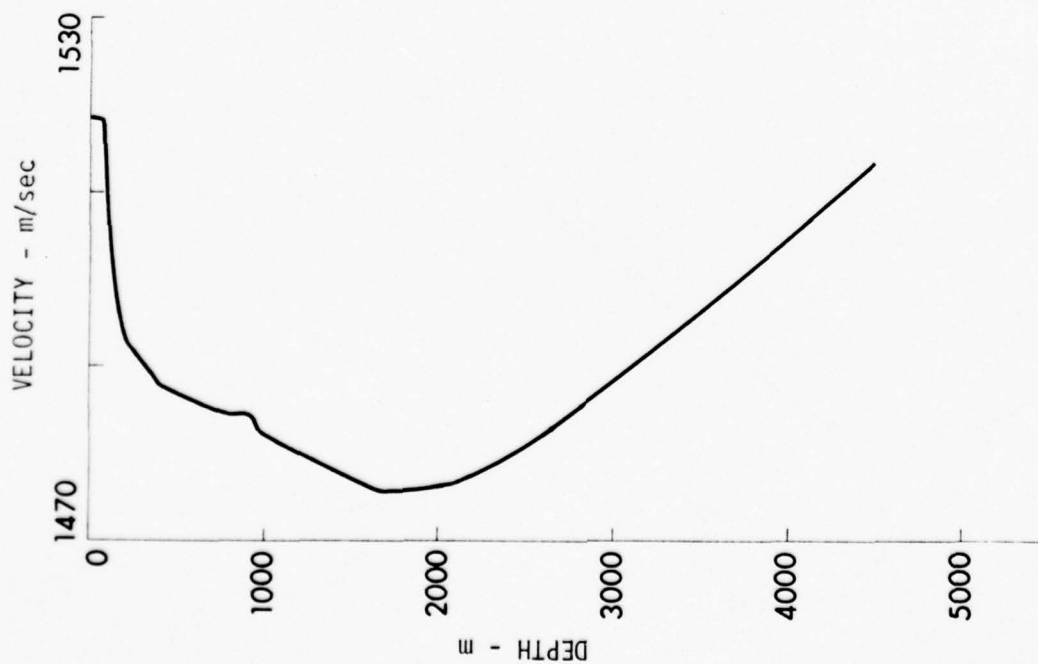


FIGURE II-29
AVERAGE PROPAGATION LOSS
Range Interval: 100-200 nm

INDIAN OCEAN PROFILE

SOURCE DEPTH: 152 m, BOTTOM DEPTH: 4490 m, MODEL: P.E.

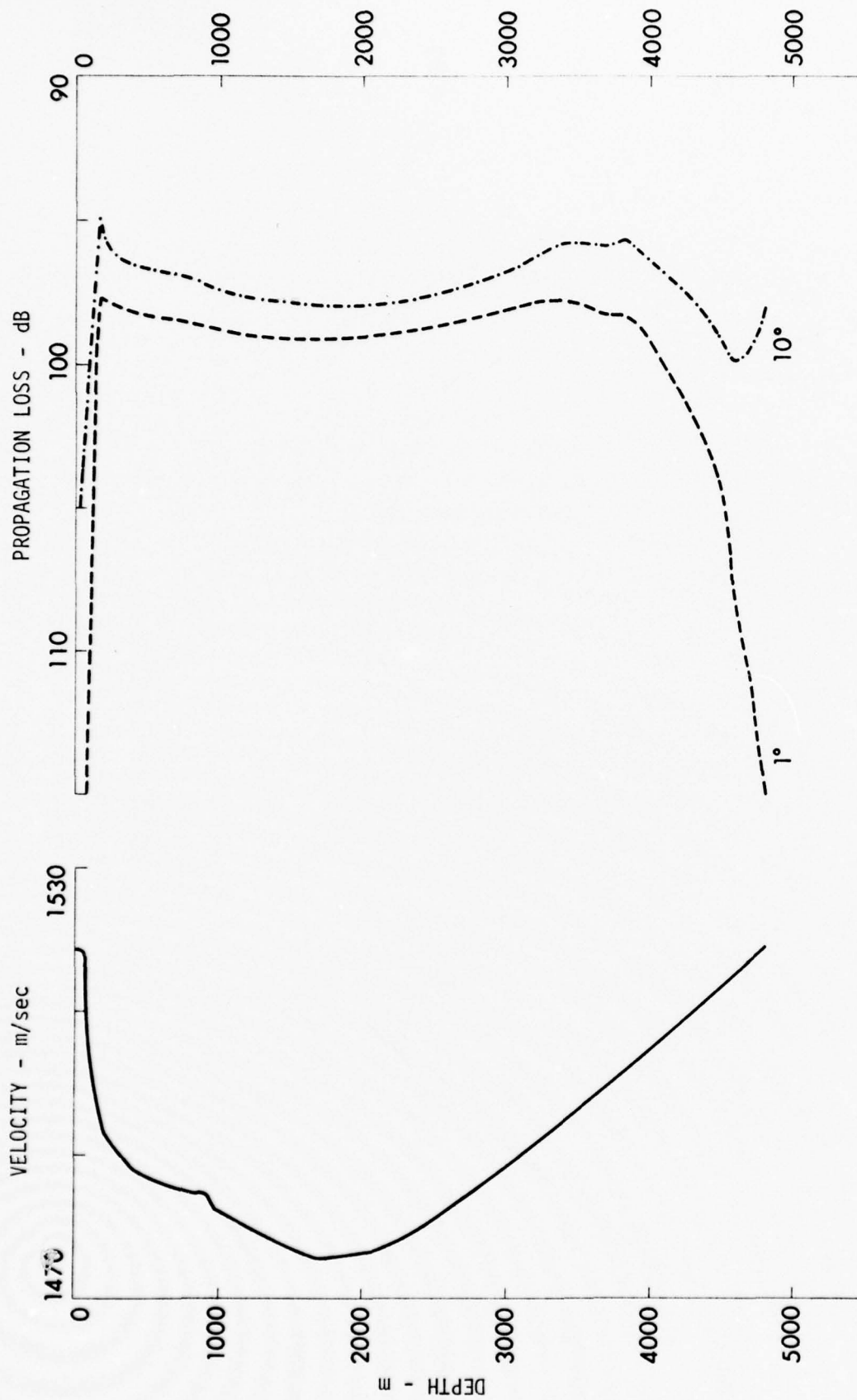


FIGURE II-30
AVERAGE PROPAGATION LOSS
Range Interval: 100-200 nm

INDIAN OCEAN PROFILE

SOURCE DEPTH: 152 m, BOTTOM DEPTH: 4795 m, MODEL: P.E.

ARL - UT
AS-76-539
KCF - DR
4-19-76

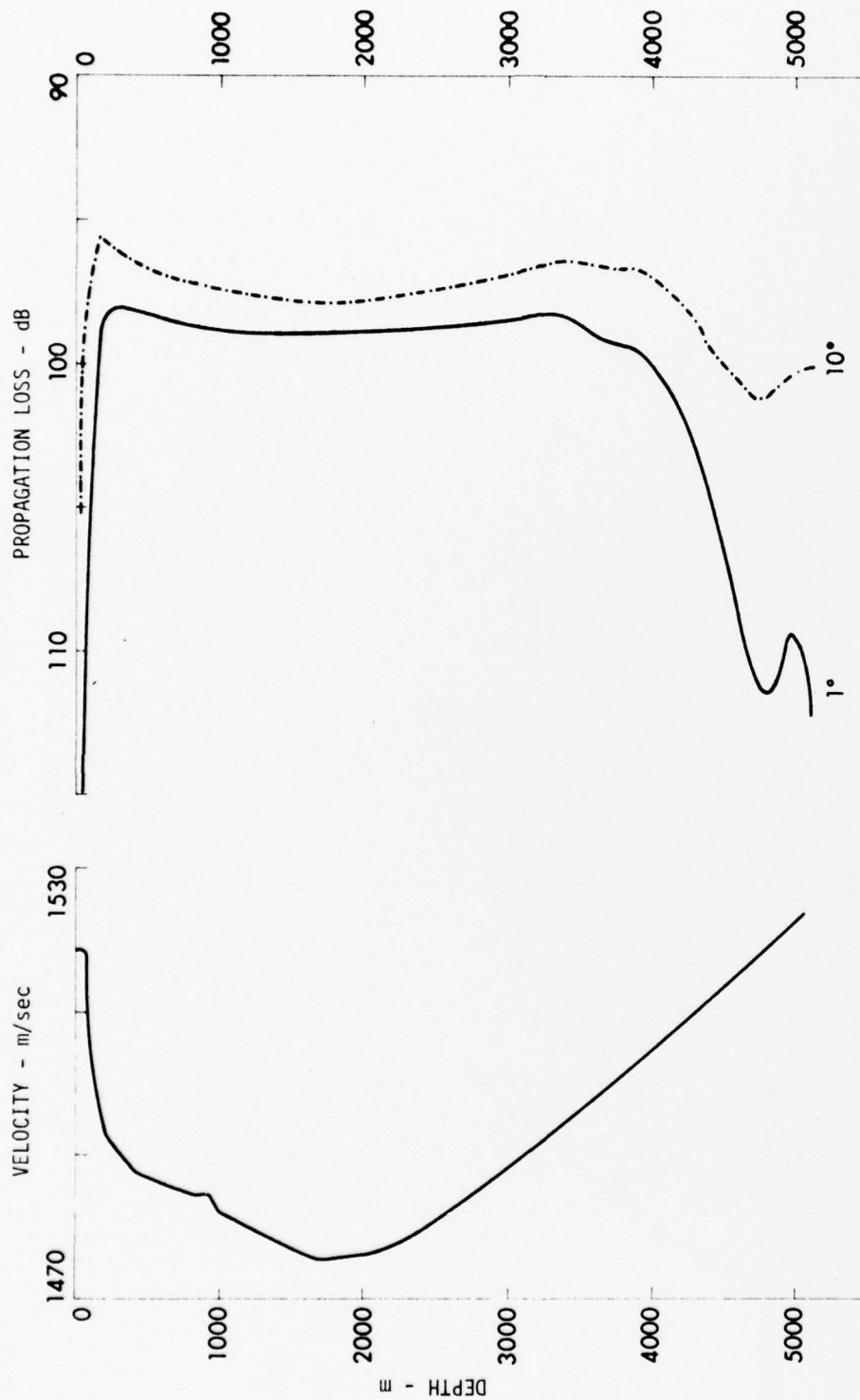


FIGURE II-31
AVERAGE PROPAGATION LOSS
Range Interval: 100-200 nm

INDIAN OCEAN PROFILE
SOURCE DEPTH: 152 m, BOTTOM DEPTH: 5100 m, MODEL: P.E.

ARL - UT
AS-76-538
KCF - DR
4 - 19 - 76

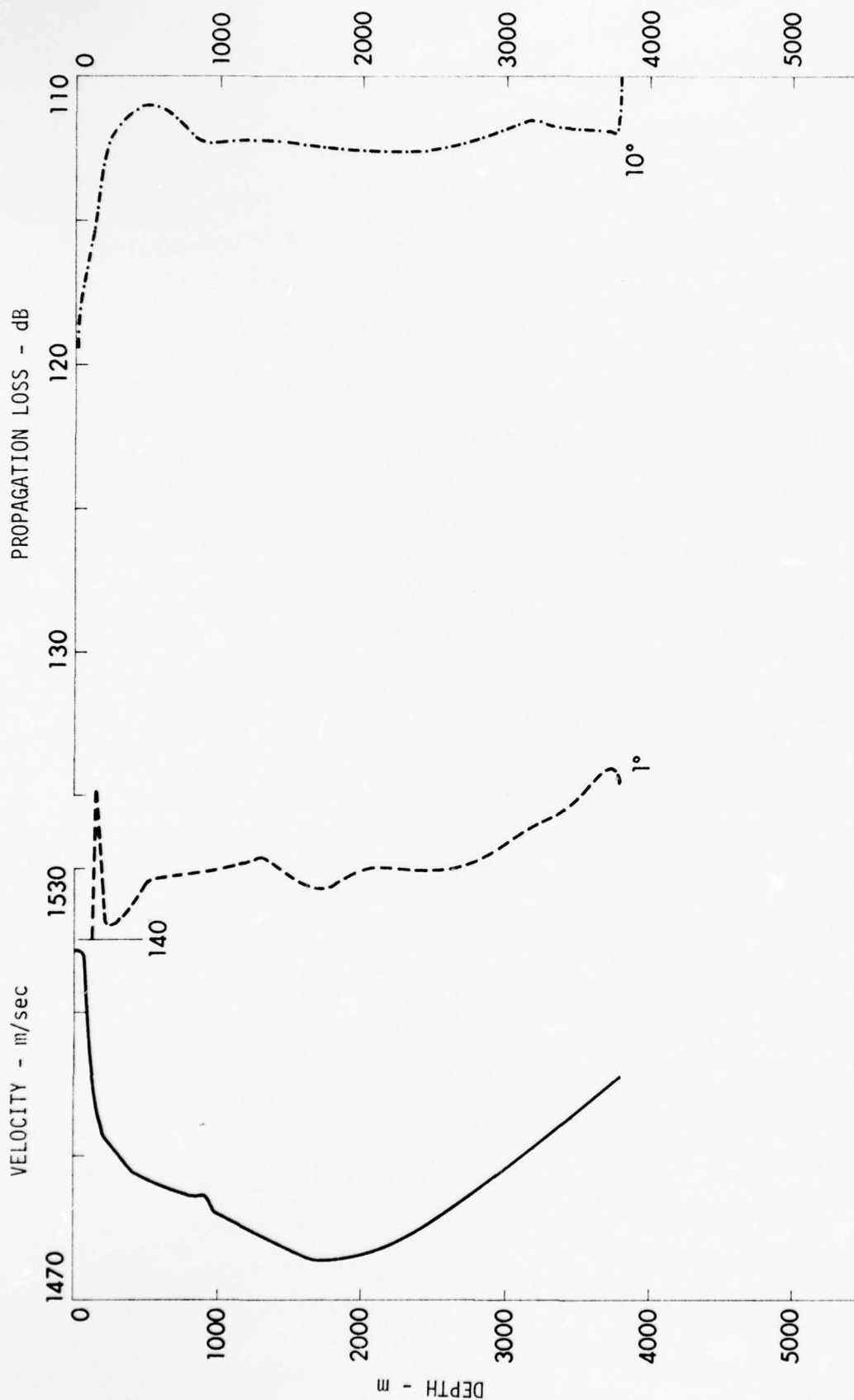


FIGURE II-32
 AVERAGE PROPAGATION LOSS
 Range Interval: 100-200 nm
 INDIAN OCEAN PROFILE
 SOURCE DEPTH: 18 m, BOTTOM DEPTH: 3880 m, MODEL: P.E.

ARL - UT
 AS-76-544
 KCF - DR
 4-19-76

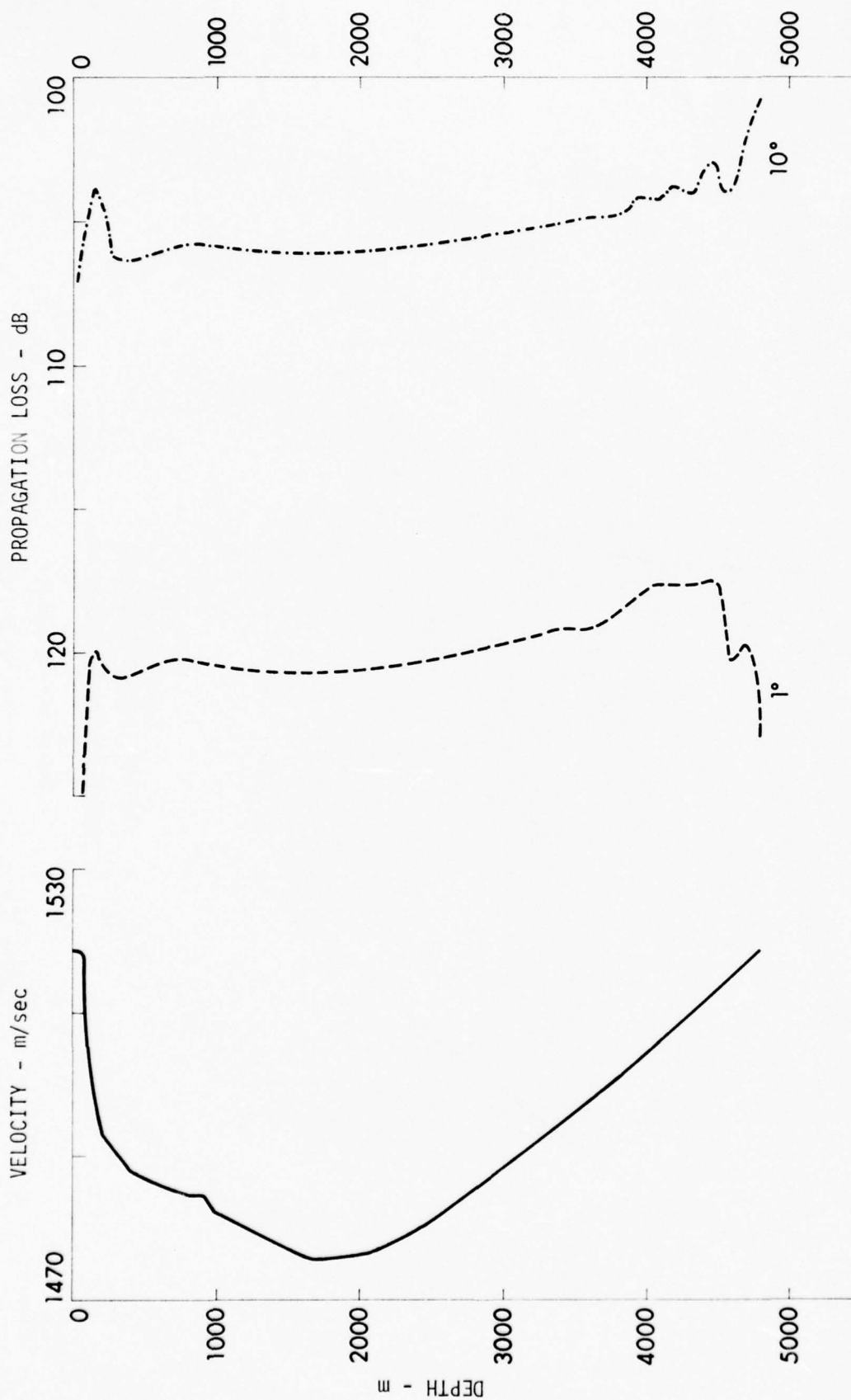


FIGURE II-33
AVERAGE PROPAGATION LOSS
Range Interval: 100-200 nm

INDIAN OCEAN PROFILE

SOURCE DEPTH: 18 m, BOTTOM DEPTH: 4795 m, MODEL: P.E.

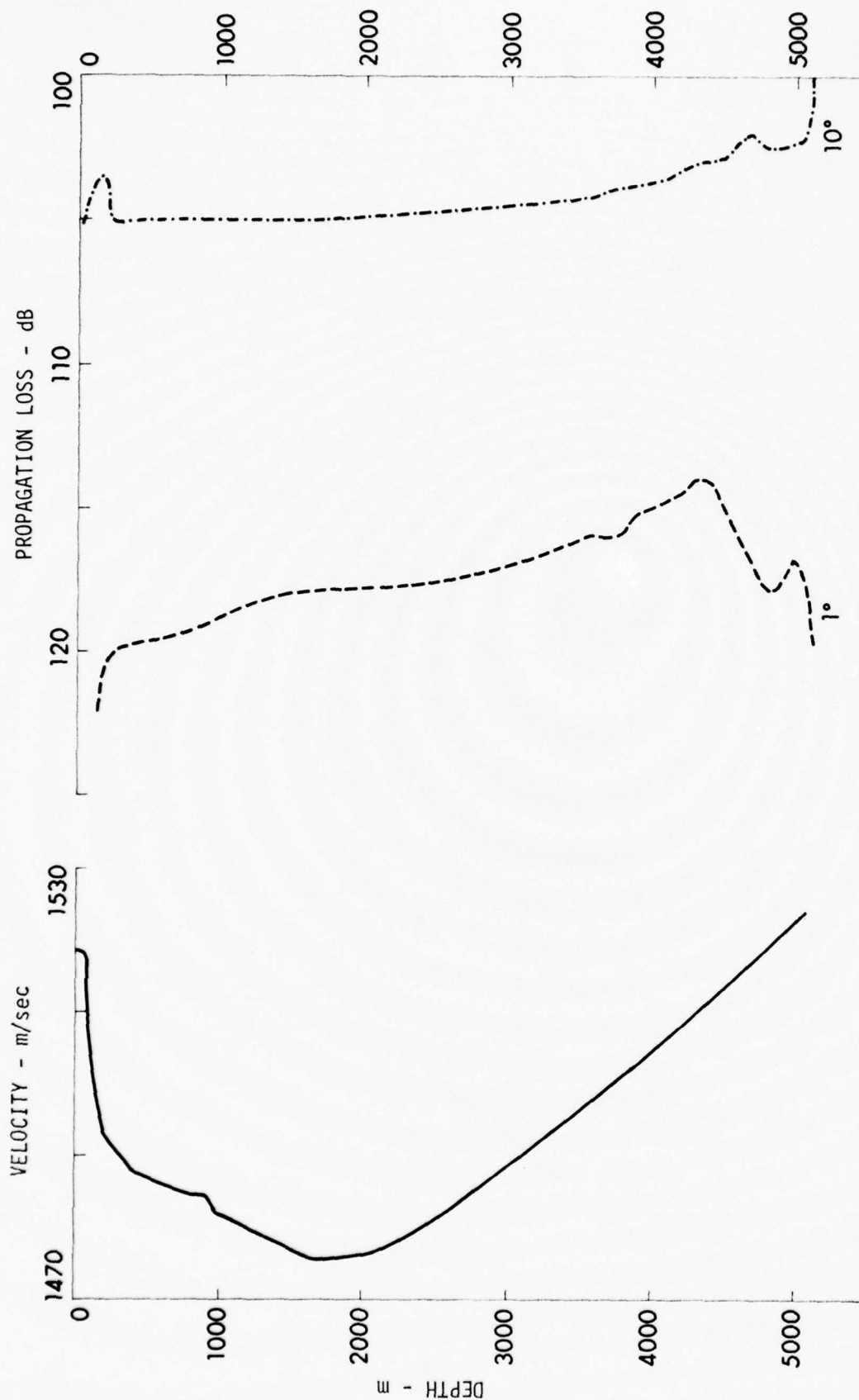


FIGURE II-34
 AVERAGE PROPAGATION LOSS
 Range Interval: 100-200 nm
 INDIAN OCEAN PROFILE
 SOURCE DEPTH: 18 m, BOTTOM DEPTH: 5100 m, MODEL: P.E.

ARL - UT
 AS-76-537
 KCF - DR
 4-19-76

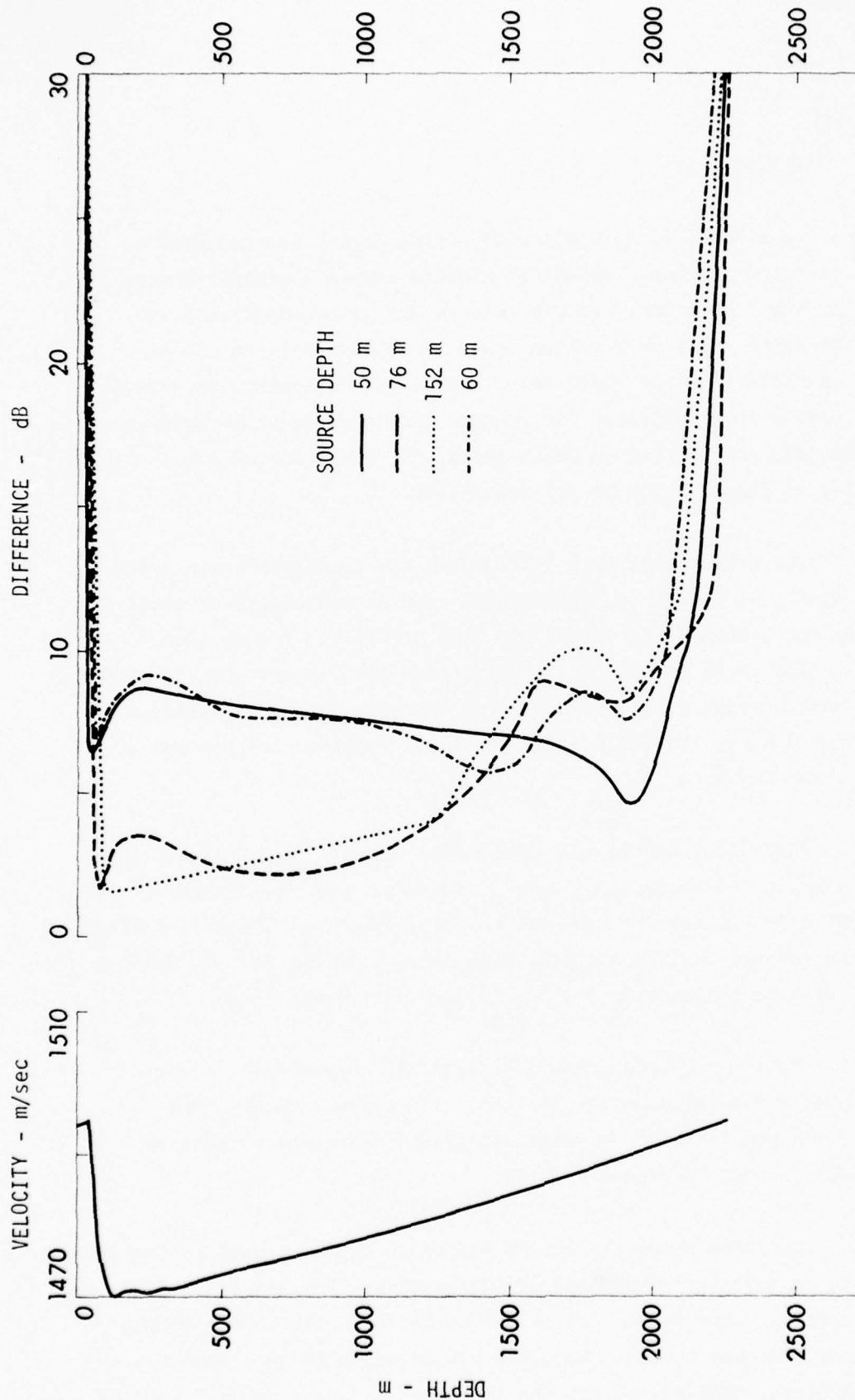


FIGURE II-35
 PROPAGATION LOSS DIFFERENCES BETWEEN 0° AND 20°
 BOTTOM CASES WITH VARYING SOURCE DEPTHS

NORTH PACIFIC PROFILE
 BOTTOM DEPTH: 2260 m, MODEL: FACT

ARL - UT
 AS-76-567
 KCF - DR
 4-27-76

2. Bottom Depth Dependence

Considered as a function of bottom depth, the propagation losses computed for the mid-Pacific profile showed a minimal change (1 dB) in the bottom loss effects between the source depth and its conjugate depth. The propagation loss differences between 10° and 1° bottom critical angles have been computed to determine the changes in the bottom loss influence for changes in bottom depth in both the North Pacific and the Indian Ocean profiles. These curves are presented in Figs. II-36, II-37, and II-38.

The propagation loss differences for receivers between the source depth and source conjugate depth remain independent of receiver depth as the bottom depth varies for both profiles. For an 18 m source, which is in the Indian Ocean surface duct, a decrease of 1200 m in the bottom depth resulted in a 11 dB increase in the differences. Even in this case, the differences generally remained independent of the receiver depth.

Variations of 300 m in the bottom depth result in less than 1 dB change in the propagation loss differences when the source conjugate depth is greater than 700 m off the bottom. These variations, including the mid-Pacific profile, were larger (± 1 dB) for the North Pacific profile and smaller for the Indian Ocean (± 0.2 dB).

The 152 m source conjugate depth was only 200 m above the bottom when a realistic bottom depth of 3880 m was used with the Indian Ocean profile. The propagation loss differences between the 1° and 10° bottoms increased by 5 dB.

Receivers below the source conjugate depth present bottom loss dependencies which are functions of the profile. For all three profiles, a small region close to the bottom can be defined which shows strong influences from the bottom. When the bottom depth is less than the critical depth, this region appears to extend up about 400 m. For

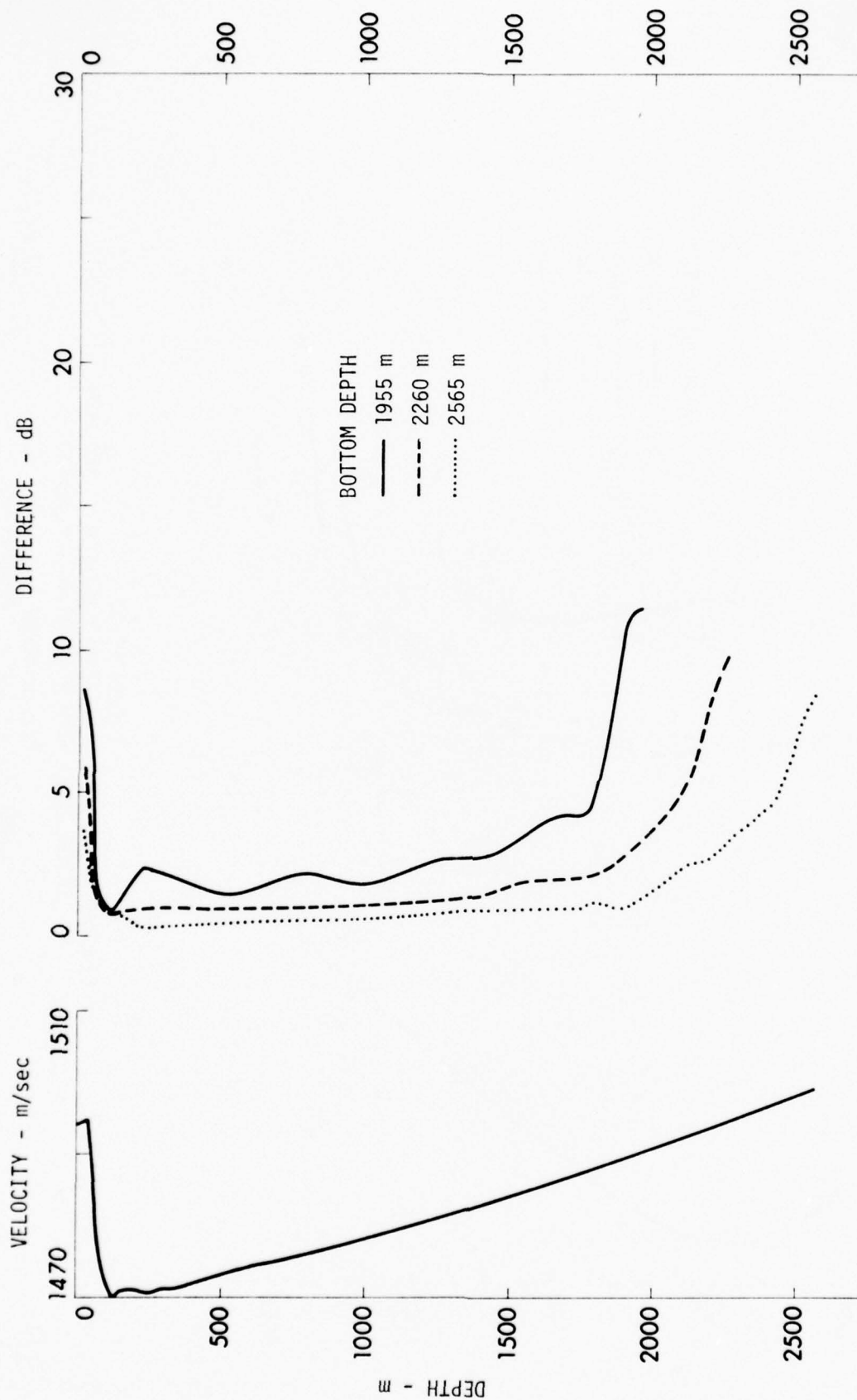


FIGURE II-36
 PROPAGATION LOSS DIFFERENCES BETWEEN 1° AND 10°
 BOTTOM CASES WITH VARYING BOTTOM DEPTHS
 NORTH PACIFIC PROFILE
 SOURCE DEPTH: 76 m, MODEL: P.E.

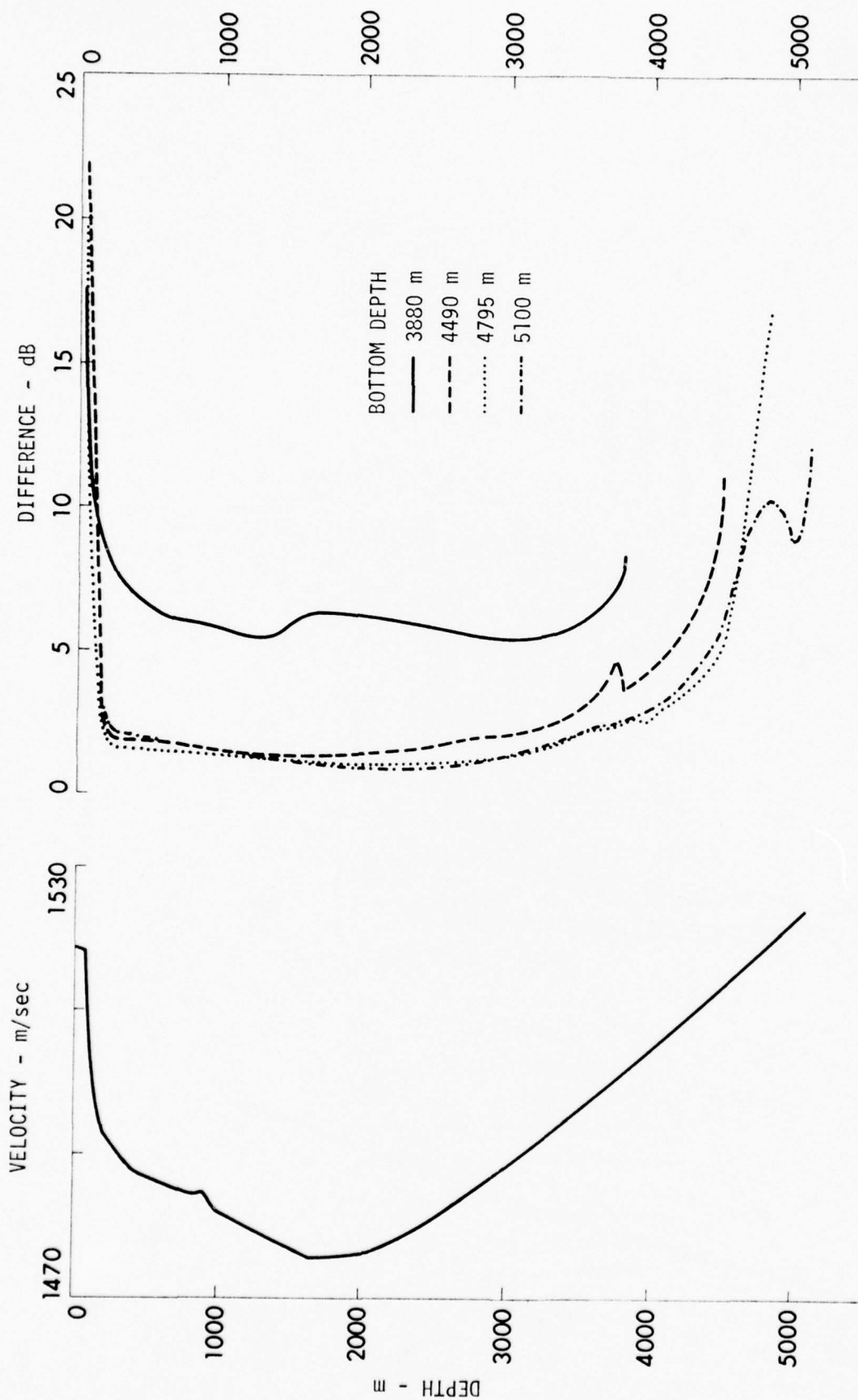


FIGURE II-37
 PROPAGATION LOSS DIFFERENCES BETWEEN 1° AND 10°
 BOTTOM CASES WITH VARYING BOTTOM DEPTHS
 INDIAN OCEAN
 SOURCE DEPTH: 152 m, MODEL: P.E.

ARL - UT
 AS-76-565
 KCF - DR
 4-27-76

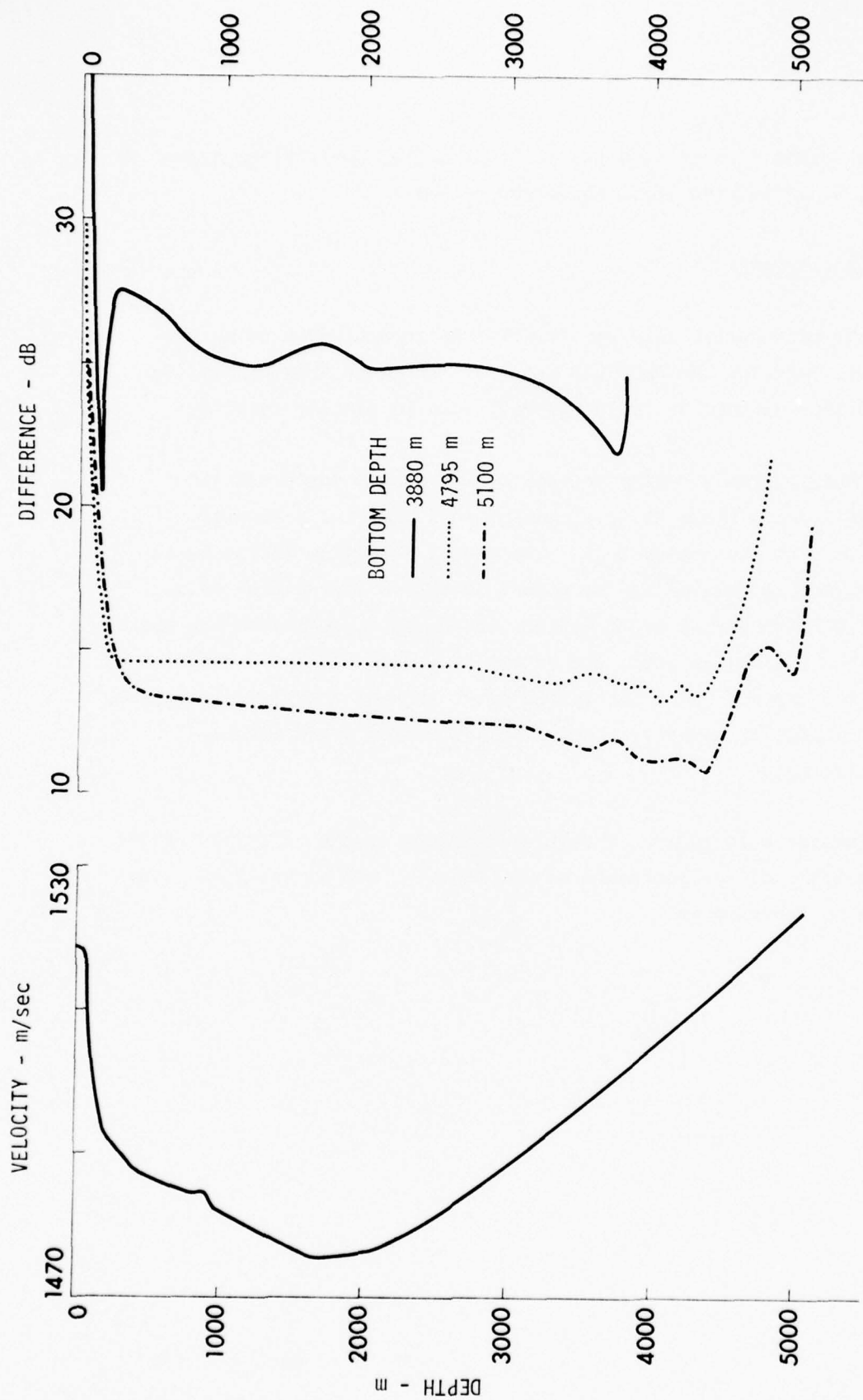


FIGURE II-38
 PROPAGATION LOSS DIFFERENCES BETWEEN 1° AND 10°
 BOTTOM CASES WITH VARYING BOTTOM DEPTHS
 INDIAN OCEAN
 SOURCE DEPTH: 18 m, MODEL: P.E.

bottom depths greater than the critical depth, the regions appear to extend to as much as 700 m above the bottom.

E. Conclusions

The propagation loss sensitivity was investigated using two different models, the FACT and the P.E. Although they handle the bottom interactions differently, both lead to similar results.

There exists a region defined by the source depth and its conjugate depth where the propagation loss exhibits a regular dependence on the bottom loss. The amount of bottom influence in this region is related to the amount of bottom refracting rays. Since both the source depth and the bottom depth determine the amount of bottom refracting rays, the bottom influence becomes a function of these two depths. Once the bottom depth exceeds the source conjugate depth by 1000 m, however, changes in the bottom depth become insignificant.

Outside this region of regular dependence, the influence of the bottom interactions increases as the receiver approaches either the bottom or the surface.

CHAPTER III

BOTTOM LOSS SENSITIVITY

A. Introduction

The previous chapter has dealt extensively with the problem of the sensitivity of propagation loss to variations in bottom loss. The present chapter deals with the other side of this problem, namely, the factors which might be the cause of particular changes in bottom loss. More specifically, the general problem is one of determining the changes in bottom loss arising from variations in the geoacoustic description of the bottom.

This problem contains many factors, the most important of which are the following:

- (1) sediment layering configuration,
- (2) sediment type within each layer,
- (3) specification of sediment attenuation and its frequency dependence,
- (4) sediment sound speed and density profiles,
- (5) nature and importance of the rock basement,
- (6) shear wave effects within sediment layers and at interfaces,
and
- (7) bulk and rough surface scattering.

The bottom loss model, BOTLOSS, developed to investigate the bottom loss sensitivity problem (see Hawker and Foreman⁸) is capable of treating all of these factors except the last two. The effects of bulk scattering within the subbottom will not be considered in this report. Rough surface effects are to be considered in a later report issued under

this contract. In the interest of simplicity, the effects of sediment shear waves are ignored, although they could be incorporated in the bottom loss model if desired.

The remaining five problem areas still constitute a large number of degrees of freedom. Consequently, the straightforward encyclopedia approach of direct parameter variation is far too cumbersome and the problem must be subdivided.

One obvious restriction is to impose a limitation on the range of grazing angles to be considered. If there is any bottom loss whatsoever, rays encountering the bottom at high angles will soon suffer prohibitively large losses because of their large number of bottom bounces. This effect is illustrated in Fig. III-1, which shows the results of five FACT runs using the mid-Pacific profile and geometry of Fig. II-3. Figure III-1 shows propagation loss versus range for critical angles of 0° , 5° , 10° , 15° , and 20° . However, unlike Fig. II-3, the present case employs a bottom loss which is always 0 at 0° , rises to 0.5 dB at the critical angle, and then jumps to 50 dB above the critical angle, where it remains constant. The zero degree critical angle case is therefore identical with the corresponding curve of Fig. II.3. It can be observed that the bottom interacting energy which fills in the shadow zones not only diminishes with range but does so more rapidly for the energy returned from the bottom at high angles.

On the basis of such considerations, it was decided that the bulk of the bottom loss sensitivity study would be carried out over the grazing angle range $0 \leq \theta \leq 25^\circ$. Although higher angles can be important for certain geometries, this angular range is sufficiently broad to include all effects important in long range propagation.

A second and equally important restriction on the general problem is a depth limitation. It is reasonable to suppose that there is a

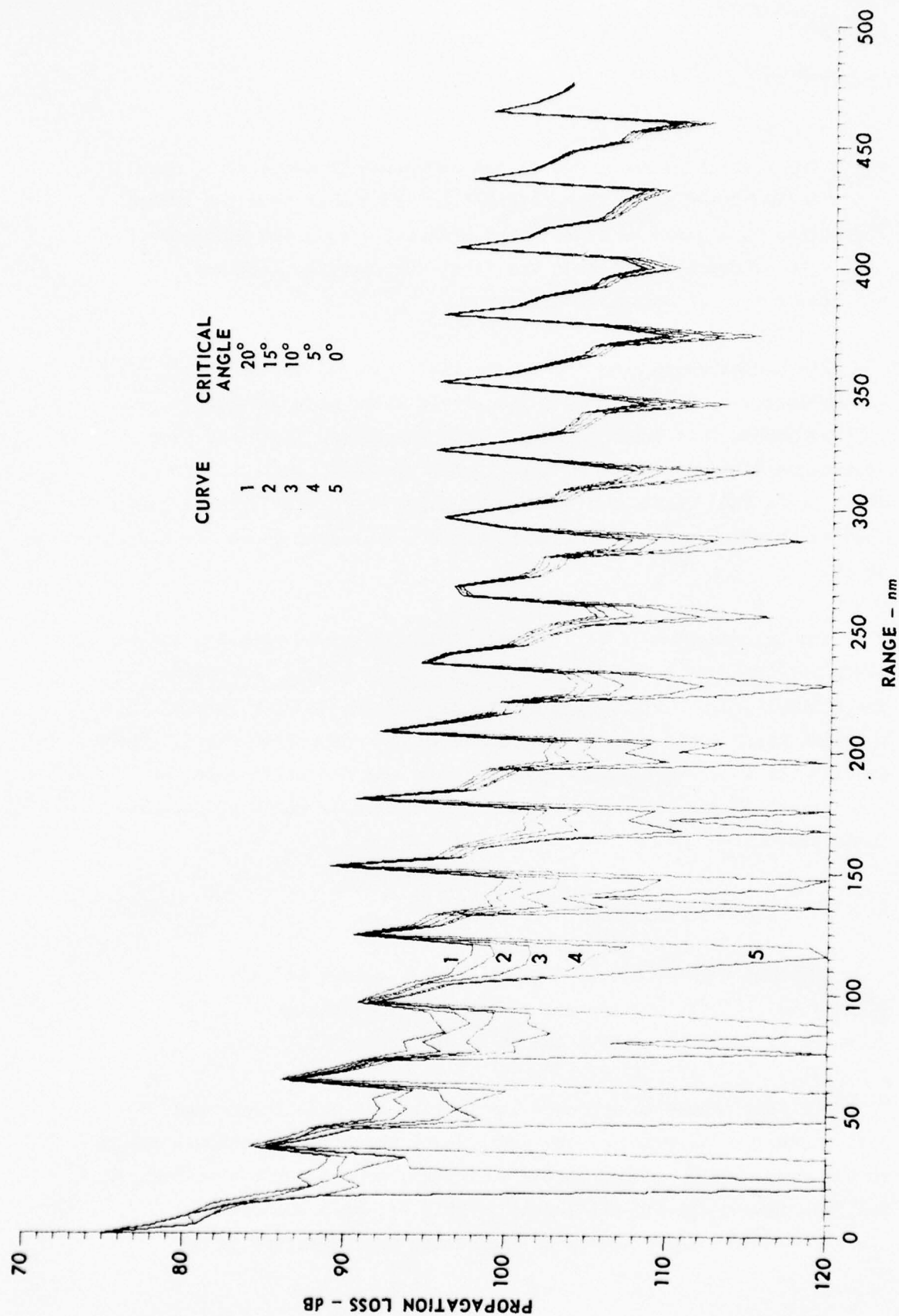


FIGURE III - 1
PROPAGATION LOSS versus RANGE FOR VARIOUS CRITICAL ANGLES
WITH A MID-PACIFIC TYPE SOUND SPEED PROFILE

ARL - UT
AS-76-743
KEH - DR
7-5-76

depth below which no knowledge of the subbottom is necessary. Such a limitation could arise from attenuation effects or from the upward refraction of a positive sound speed gradient within the sediments. This type of depth restriction was first discussed by Williams,⁹ who referred to it as the hidden depth.

The hidden depth question is, in fact, central to the entire bottom loss sensitivity problem and provides the most important restriction on this broad problem. Once the hidden depth has been determined for a given set of sound speed profiles, sediment types, etc., it is then meaningful to inquire about the sensitivity of bottom loss to changes in these various parameters occurring above the hidden depth.

The next section of this chapter deals in detail with the hidden depth problem and its dependence on sound speed profile, frequency, and sediment type. The following section then deals with some of the problems which occur once the hidden depth has been established. These include the importance of the rock basement and its solid aspects (shear wave supporting material) and the problem of sediment parameter variations.

B. The Hidden Depth Problem

Although the concept of a hidden depth appears to be clear intuitively, a more precise and quantitative definition will be required if specific results are to be obtained.

Williams⁹ chose to approach the problem via mode theory and defined the hidden depth as the depth below which the fractional change in the eigenvalues, caused by the introduction of a perfect reflector, was less than a specified tolerance. This approach necessitates specifying which modes are to be considered and therefore is not

independent of the propagation geometry. Williams obviated a particular choice of modes by averaging over a chosen set of modes.

An alternative approach, and the one adopted in this report, is to define the hidden depth in terms of the fractional change in the bottom loss caused by the introduction of a perfect reflector at some depth. When this change is less than a certain tolerance, the hidden depth has been reached. Here, again, some elements of the propagation geometry are hidden since the grazing angle, or angular interval, must be specified.

Also, in addition to choosing the tolerance, there is the possibility of modifying the definition to examine the difference between a normal sediment column and one with an absorber underneath, or perhaps the difference between the reflector and absorber cases. The most extreme contrast is obtained by comparing situations in which a column of sediment alternately overlies a perfect reflector and a perfect absorber. This definition will be adopted in this report. That is, the hidden depth, Z_H , is defined as the depth at which a reflector and then an absorber can be inserted in the sediment such that $\Delta(Z_H) = |20 \log (|R|_{\text{Reflection}}/|R|_{\text{Absorber}})| \leq \epsilon$, where $|R|$ is the modulus of the plane wave reflection coefficient and ϵ is the tolerance. Investigation has shown that the precise nature of the comparison cases is not of great importance and the results would be little changed if the definition were somewhat altered.

In the remainder of this section we shall examine the hidden depth problem for two sediment types, a fine clay and a coarse silt. The clay sediment has a density ratio (relative to seawater) of 1.206, a sound speed ratio of 0.991, and a porosity of 87%. The silt sediment has a density ratio of 1.595, a sound speed ratio of 0.986, and a porosity of 63%. The frequency was chosen to be 50 Hz and, at this frequency, the attenuations were 0.00285 dB/m for clay and 0.012 dB/m

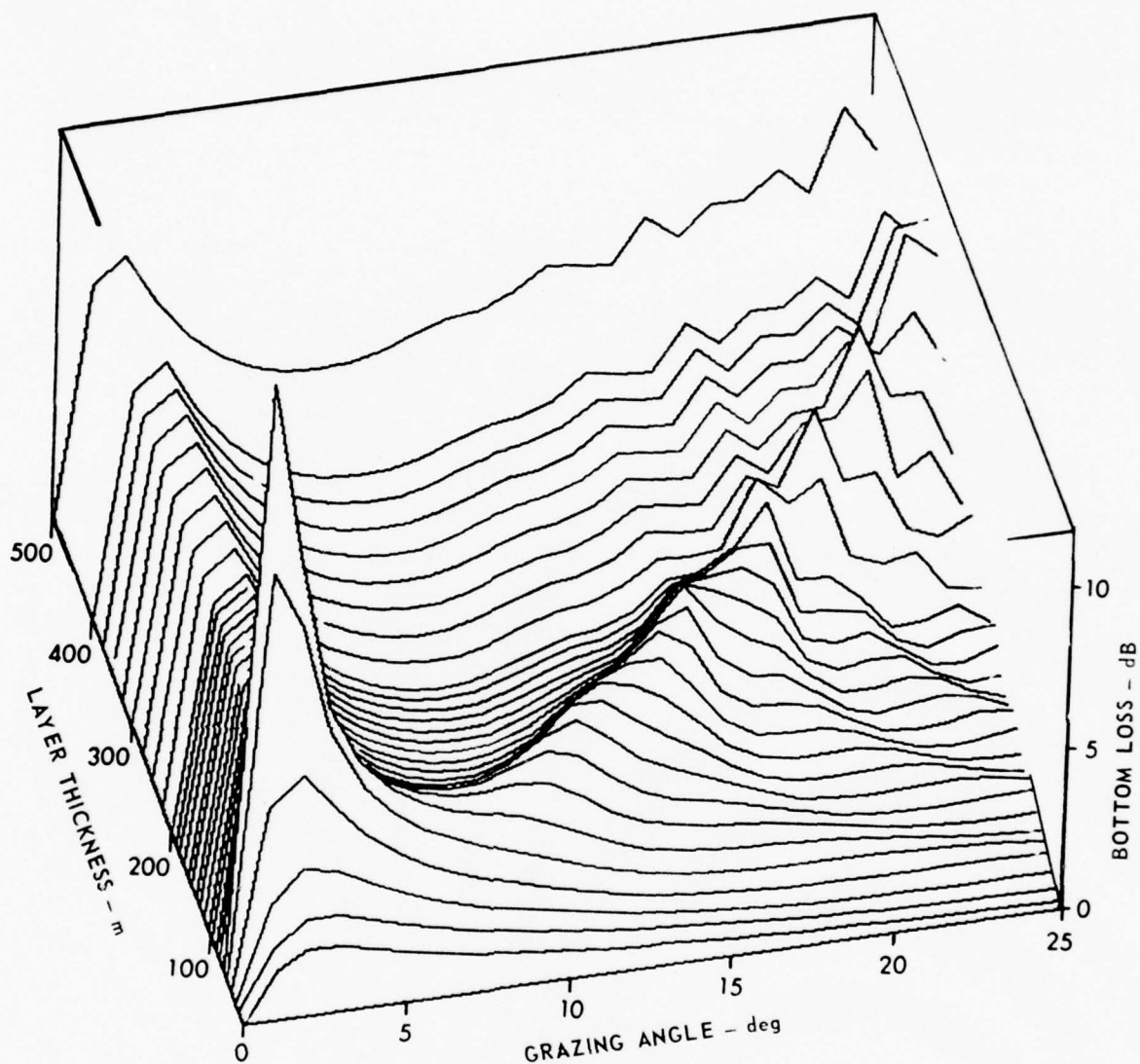
for silt. The sediment properties and their relationship to porosity follows the work of Hamilton,¹⁰ Akal,¹¹ and Hamilton.¹²

Figures III-2 through III-4 show the bottom loss versus grazing angle versus layer thickness for a clay layer overlying a perfectly reflecting surface. These bottom loss curves, as well as all others appearing in this report, were computed using the BOTLOSS model. The sound speed profile was assumed to be linear $C(z)=C(0)+gz$, and the gradients g are 0.5 sec^{-1} , 1.0 sec^{-1} , and 1.5 sec^{-1} in the three drawings. This range of sound speed gradients includes those most commonly found in deep ocean sediments.

All three figures display a prominent diagonal ridge where orientation with respect to the grazing angle axis decreases with increasing gradient. For any given angle, at depths beyond this ridge, the bottom loss is seen to be independent of any further increase in layer thickness. This independence of layer thickness is an indication that, at this angle, the hidden depth has been reached. Moreover, the decreasing inclination of the ridge shows that, at a fixed angle, the hidden depth is reached more quickly for greater sound speed gradients. This effect is caused by the increased upward refraction of the sound speed profile for larger gradients.

Figures III-5 through III-7 show the quantity $\Delta(\theta, z)$ plotted versus grazing angle θ and layer thickness z for this same clay layer, with the same three sound speed gradients as in Figs. III-2 through III-4. The quantity $\Delta(\theta, z)$ is defined as the absolute value of the difference between the bottom losses in the case of a perfectly reflecting plane and a perfect absorber inserted at a depth z . This difference can be seen to be

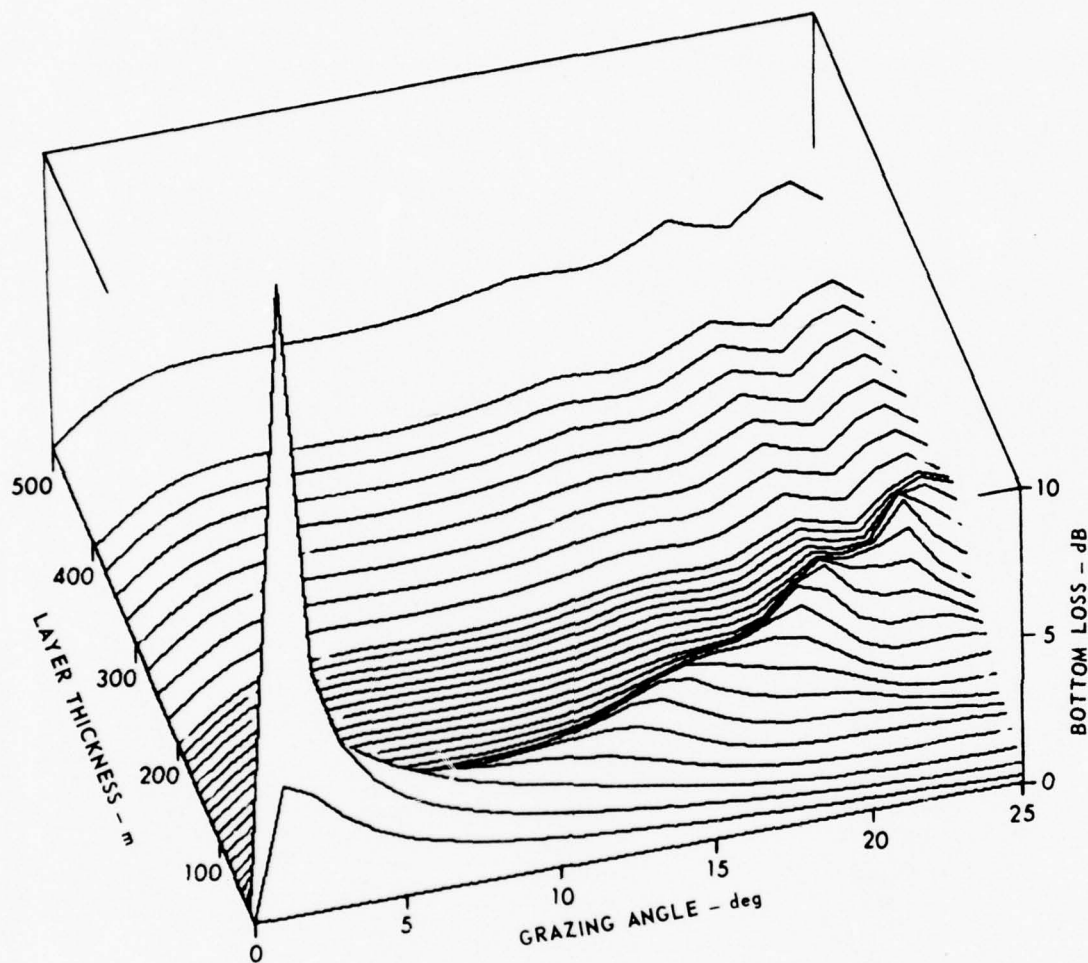
$$\begin{aligned}\Delta(\theta, z) &= |-20 \log(|R|_{\text{Reflector}}) + 20 \log(|R|_{\text{Absorber}})| \\ &= 20 |\log(|R|_{\text{Reflector}}/|R|_{\text{Absorber}})| \quad ,\end{aligned}$$



FREQUENCY: 50 Hz
 MATERIAL: CLAY
 GRADIENT: 0.5 sec⁻¹

FIGURE III - 2
 BOTTOM LOSS versus GRAZING ANGLE versus LAYER THICKNESS
 WITH A SOUND SPEED GRADIENT OF 0.5 sec⁻¹

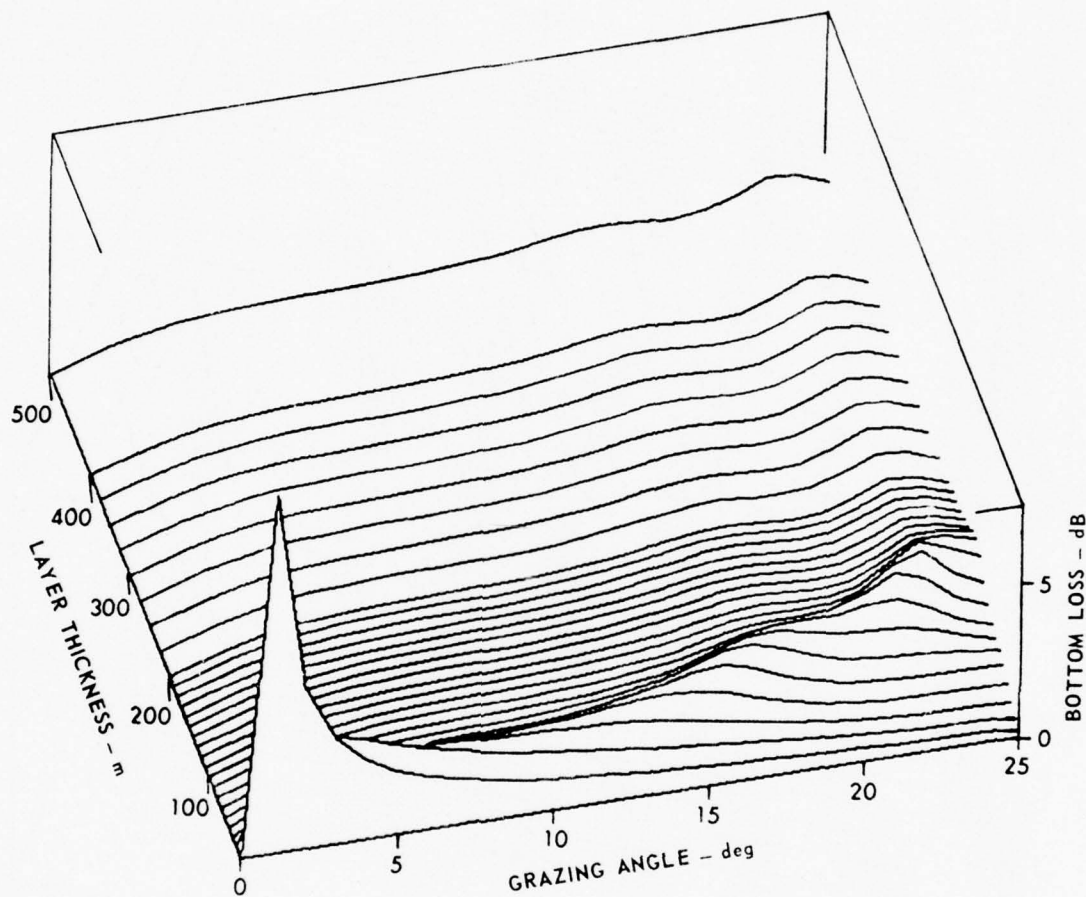
ARL - UT
 AS-76-623
 KEH - DR
 6 - 7 - 76



FREQUENCY: 50 Hz
 MATERIAL: CLAY
 GRADIENT: 1.0 sec^{-1}

FIGURE III - 3
 BOTTOM LOSS versus GRAZING ANGLE versus LAYER THICKNESS
 WITH A SOUND SPEED GRADIENT OF 1.0 sec^{-1}

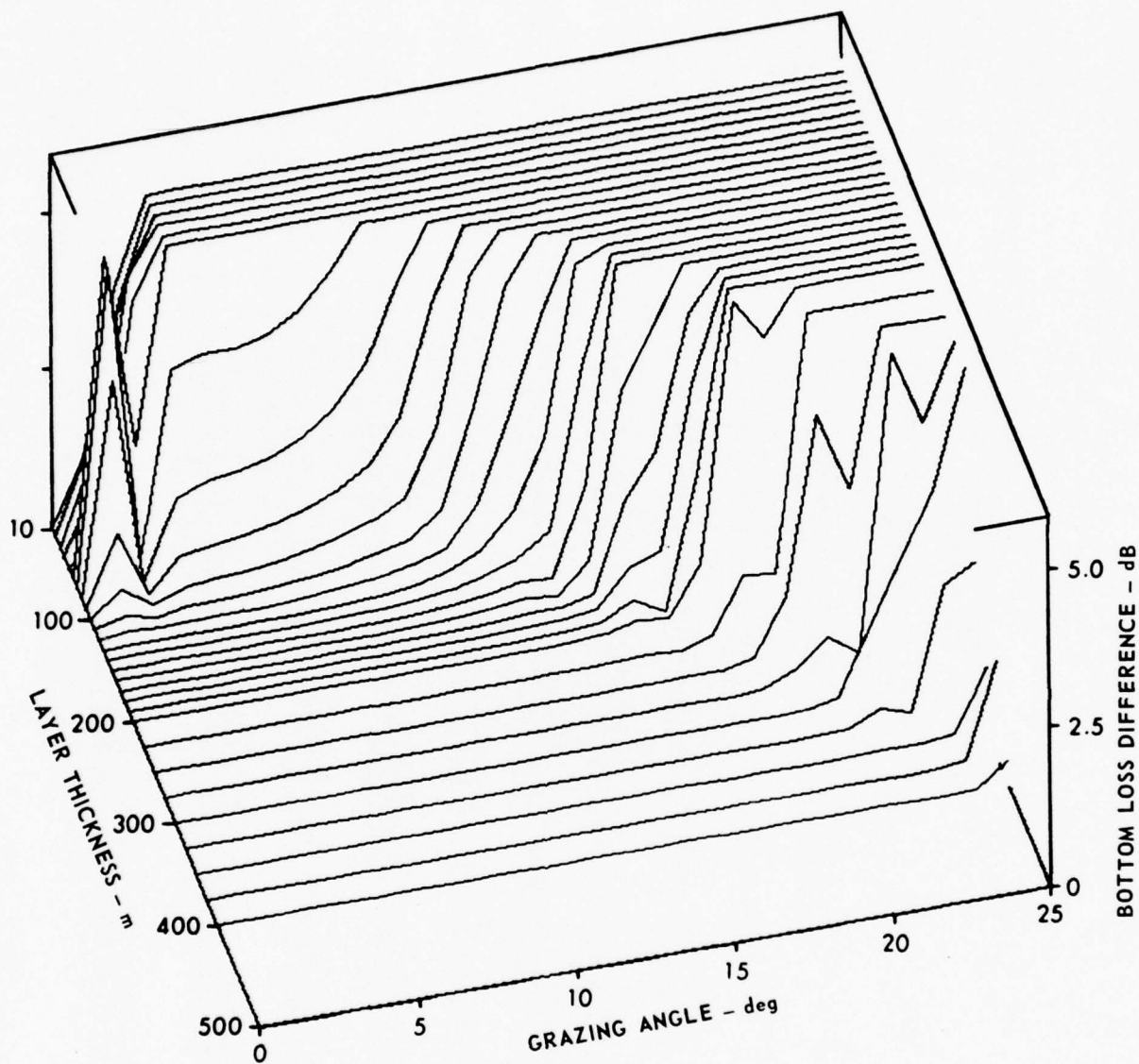
ARL - UT
 AS-76-624
 KEH - DR
 6 - 7 - 76



FREQUENCY: 50 Hz
 MATERIAL: CLAY
 GRADIENT: 1.5 sec^{-1}

FIGURE III - 4
 BOTTOM LOSS versus GRAZING ANGLE versus LAYER THICKNESS
 WITH A SOUND SPEED GRADIENT OF 1.5 sec^{-1}

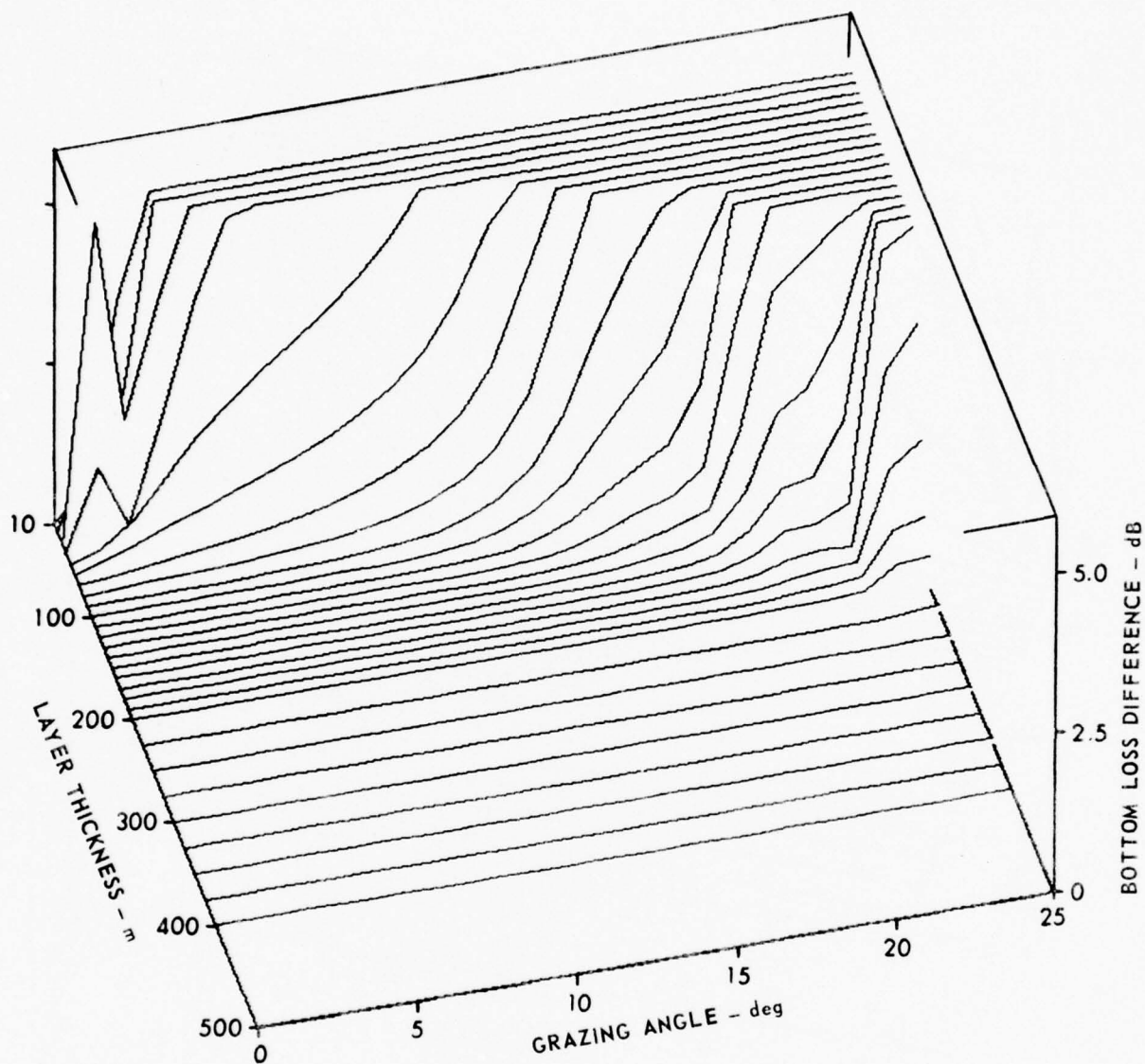
ARL - UT
 AS-76-625
 KEH - DR
 6 - 7 - 76



FREQUENCY: 50 Hz
 MATERIAL: CLAY
 GRADIENT: 0.5 sec^{-1}

FIGURE III - 5
 INTENSITY RATIO FOR REFLECTOR-ABSORBER SUBSTRATES
 WITH A SOUND SPEED GRADIENT OF 0.5 sec^{-1}

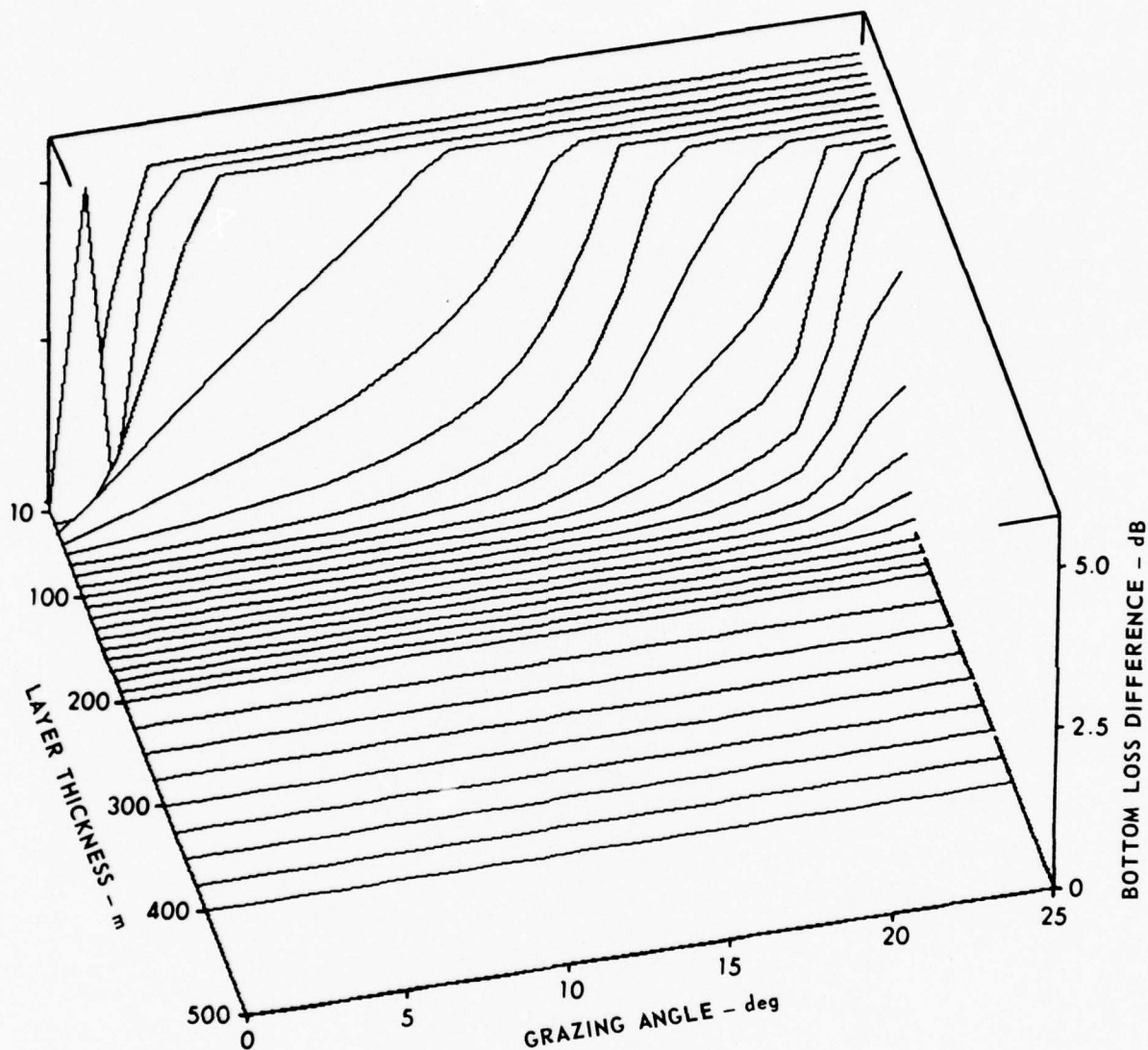
ARL - UT
 AS-76-629
 KEH - DR
 6 - 7 - 76



FREQUENCY: 50 Hz
 MATERIAL: CLAY
 GRADIENT: 1.0 sec^{-1}

FIGURE III - 6
 INTENSITY RATIO FOR REFLECTOR-ABSORBER SUBSTRATES
 WITH A SOUND SPEED GRADIENT OF 1.0 sec^{-1}

ARL - UT
 AS-76-630
 KEH - DR
 6 - 7 - 76



FREQUENCY: 50 Hz
 MATERIAL: CLAY
 GRADIENT: 1.5 sec^{-1}

FIGURE III - 7
 INTENSITY RATIO FOR REFLECTOR-ABSORBER SUBSTRATES
 WITH A SOUND SPEED GRADIENT OF 1.5 sec^{-1}

ARL - UT
 AS-76-631
 KEH - DR
 6 - 7 - 76

which is simply the intensity ratio in the two cases expressed in decibels. The fact that these curves have been clipped at 5.0 dB accounts for the flat portion of the surface above the prominent "cliff."

There are several important points to be noted concerning Figs. III-5 through III-7. The most obvious feature is, of course, the very steep "cliff" below which $\Delta(\theta, z)$ rapidly approaches 0. Moreover, if the curve defining the bottom of the cliff were drawn on the figures, it would change its inclination with respect to the angle axis in a fashion analogous to the ridge in the preceding three figures. That is, the larger the gradient, the more rapidly a given small value of $\Delta(\theta, z)$ is achieved.

The hidden depth, defined by $\Delta(\theta, z) \leq \epsilon$, is directly obtainable from these figures once the tolerance ϵ is chosen. Since there is no particular reason to choose any particular value for ϵ (in a specific problem ϵ might be fixed), it might seem at first that a considerable element of arbitrariness remains in the problem. It is just at this stage, however, that the steepness of the surface in the vicinity of the cliff plays a role. By inspection it is clear that a change of ϵ from, say, 0.1 dB to 0.01 dB, will cause very little change in the derived value of the hidden depth. In other words, the concept of a hidden depth will be a useful one and the tolerance ϵ need not be specified very precisely.

Figure III-8 shows the hidden depth, defined with $\epsilon = 0.1$ dB, plotted versus grazing angle for the three sound speed gradients shown in the preceding groups of figures. For comparison purposes, Fig. III-9 shows the ray turning depth versus grazing angle for these same gradients. It will be observed that the hidden depth always lies several wavelengths below the turning depth. This close association of hidden depth and turning depth is not surprising since it is at the turning depth that the pressure field changes from oscillatory

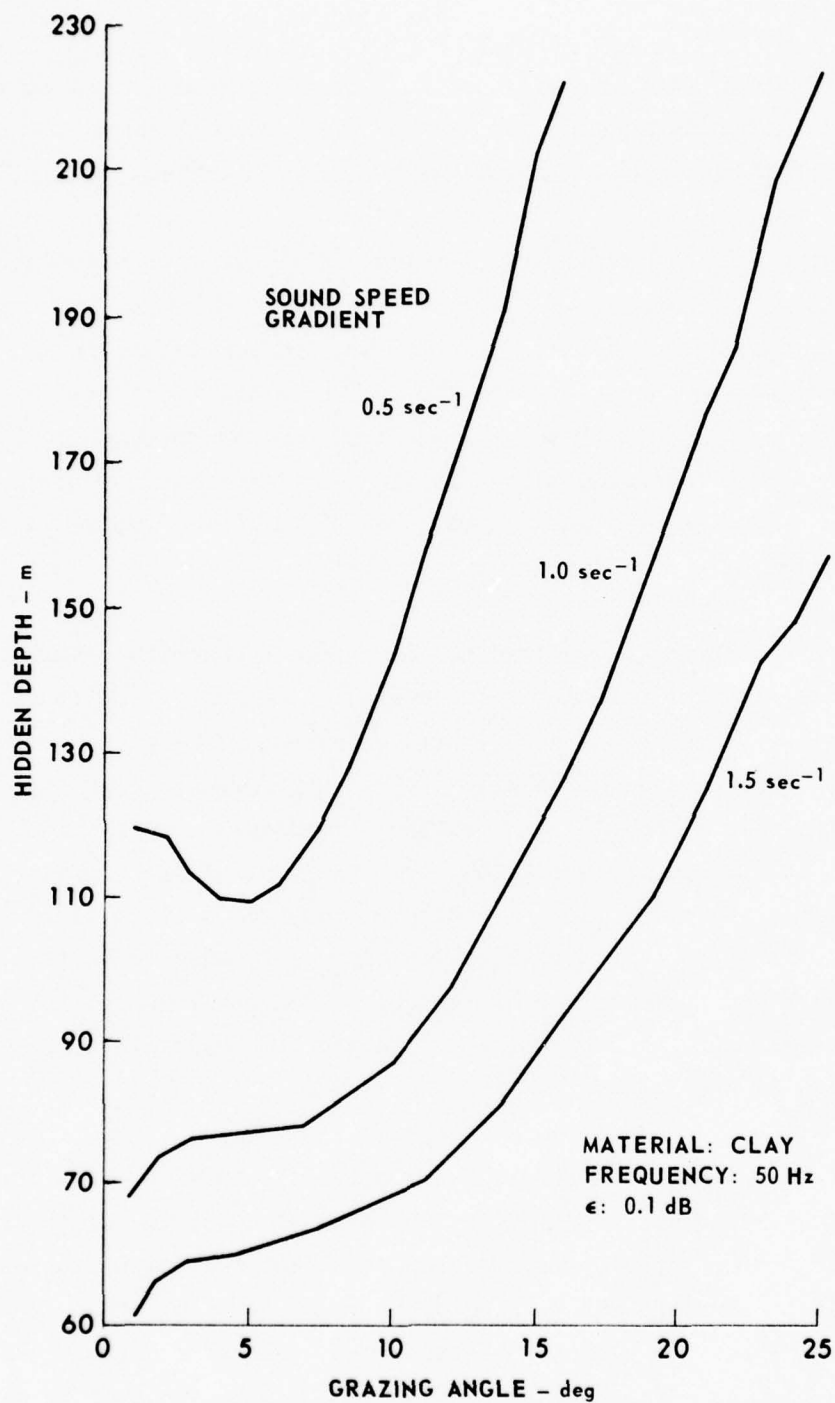


FIGURE III - 8
HIDDEN DEPTH versus GRAZING ANGLE FOR A CLAY
LAYER WITH VARIOUS SOUND SPEED GRADIENTS

ARL - UT
AS-76-740
KEH - DR
7 - 5 - 76

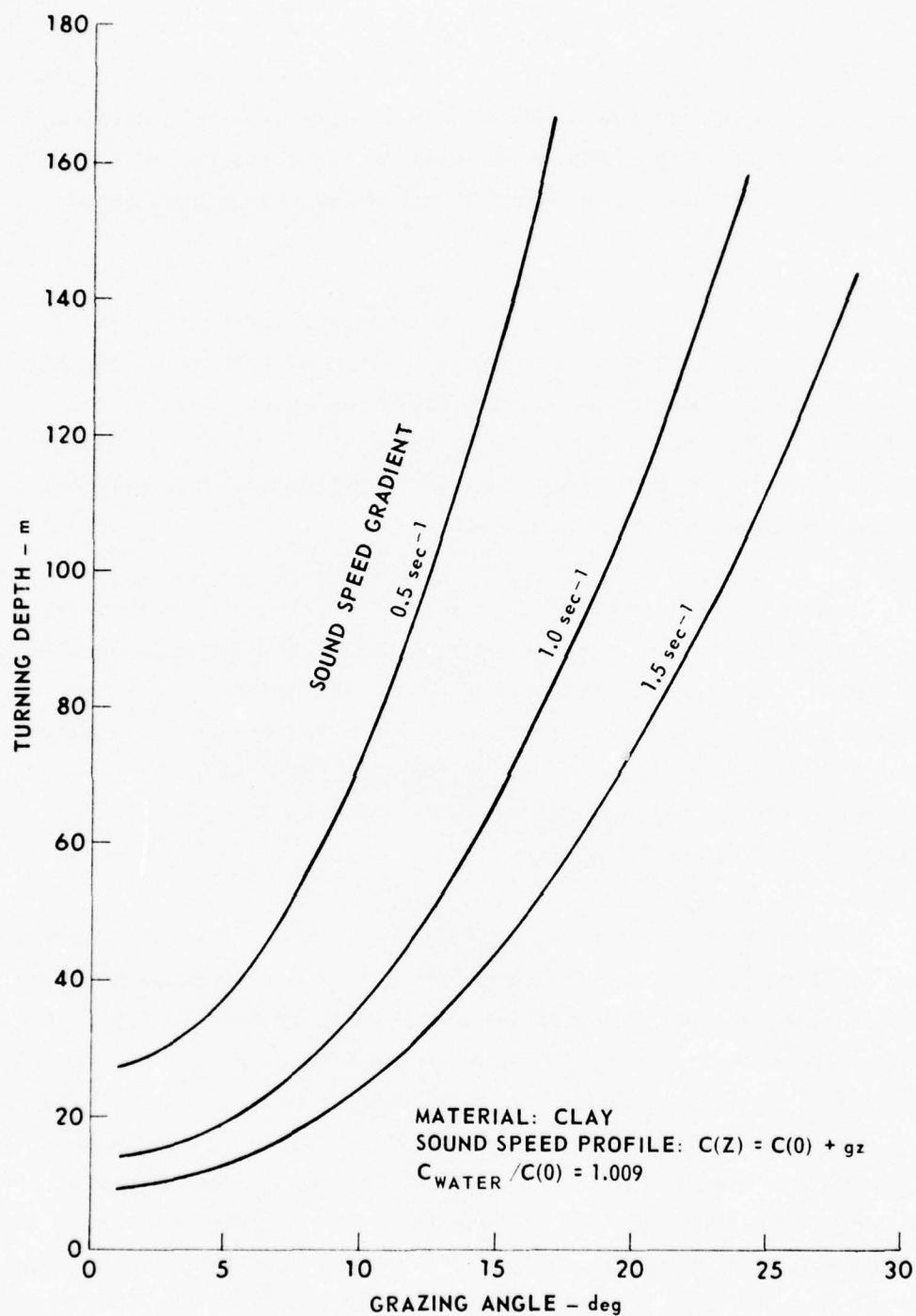


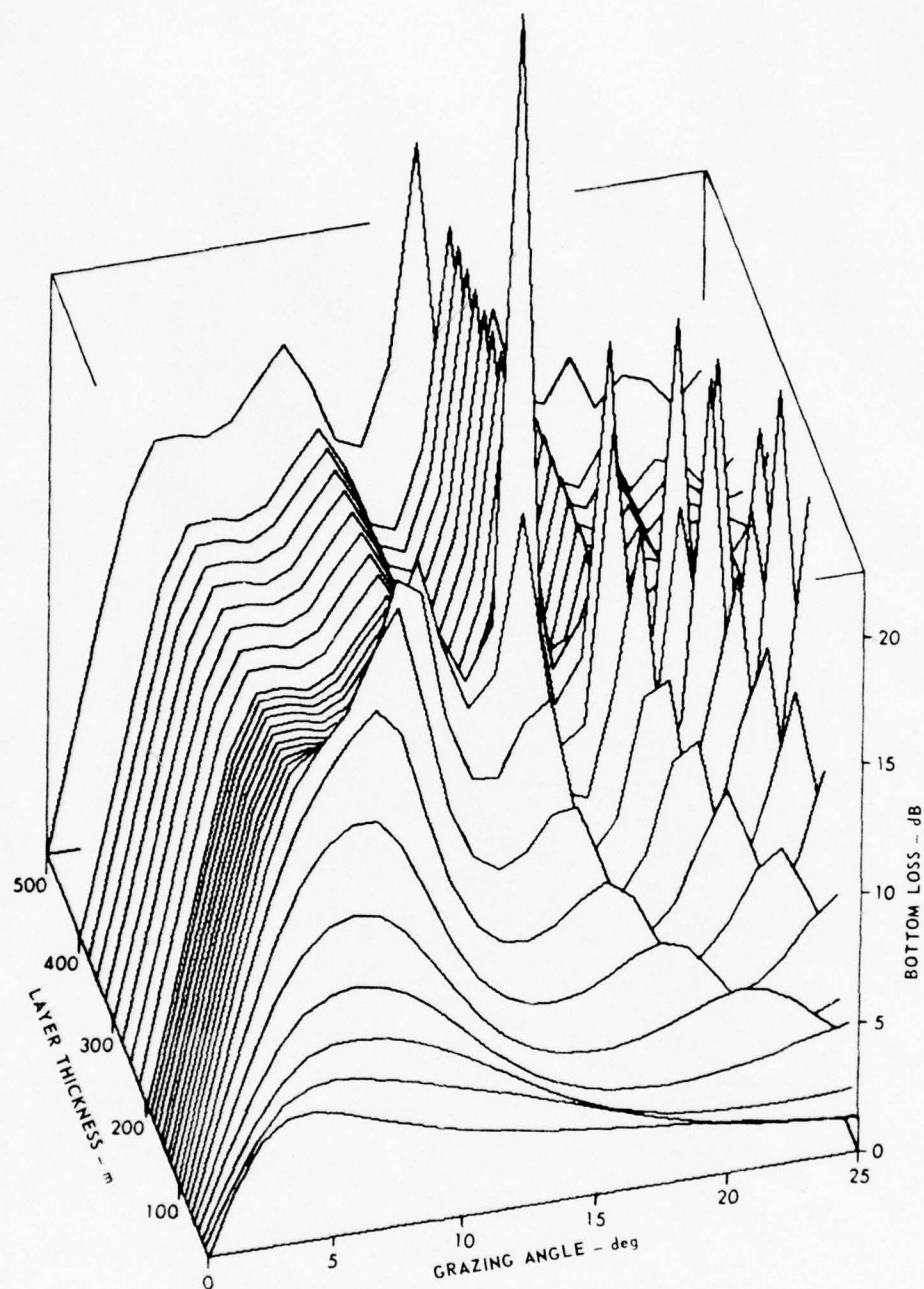
FIGURE III - 9
 TURNING DEPTH versus GRAZING ANGLE FOR A CLAY
 LAYER HAVING VARIOUS SOUND SPEED GRADIENTS

to exponentially decaying behavior. In the investigation carried out by Williams,⁹ the hidden depth was, in fact, referenced to the turning depth and was again found to lie a few wavelengths below it.

Having established the hidden depth in one particular case, we come to the general question of the variation of the hidden depth with changes in sediment type, with different sound speed profiles, with frequency, etc. Although these questions have not yet been completely resolved and these lines of investigation are still being pursued, some results have been obtained.

Figures III-10 through III-12 show the bottom loss versus grazing angle versus layer thickness for a coarse silt layer overlying a perfect reflector. These curves together with the corresponding ones for the perfect absorber are combined to produce the difference plots shown in Figs. III-13 through III-15. As in the clay layer case, these two groups of figures are based on a linear sound speed model with gradients of 0.5 sec^{-1} , 1.0 sec^{-1} , and 1.5 sec^{-1} .

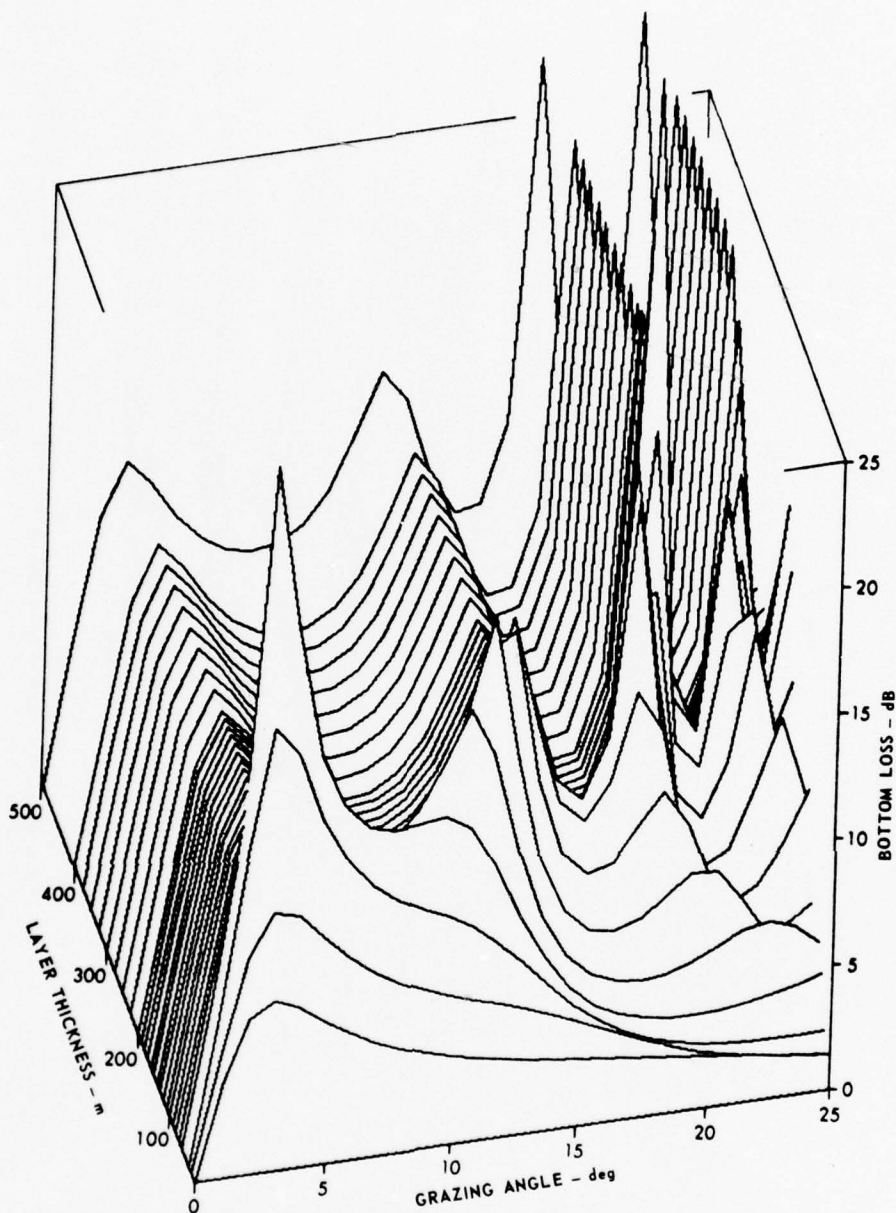
The same general features are present in these curves as in the clay layer case, although the increased amount of structure tends to obscure some trends. The most important point to note is that, once again, the concept of a hidden depth is seen to be a well-defined one. The very abrupt flattening of the Δ surface below the "cliff" will lead to a very narrow range of hidden depth values for a broad range of values of ϵ . Figure III-16 shows the hidden depth, for this silt layer, plotted versus grazing angle for the three sound speed gradients. Once again the hidden depth lies within several wavelengths of the tuning depth (which is computed according to $Z_T = g^{-1} [c_w / \cos \theta - c_s(0)]$ where c_w is the water sound speed and $c_s(0)$ is the sediment sound speed at the top of the layer).



FREQUENCY: 50 Hz
 MATERIAL: SILT
 GRADIENT: 0.5 sec^{-1}

ARL - UT
 AS-76-724
 KEH - DR
 6 - 7 - 76

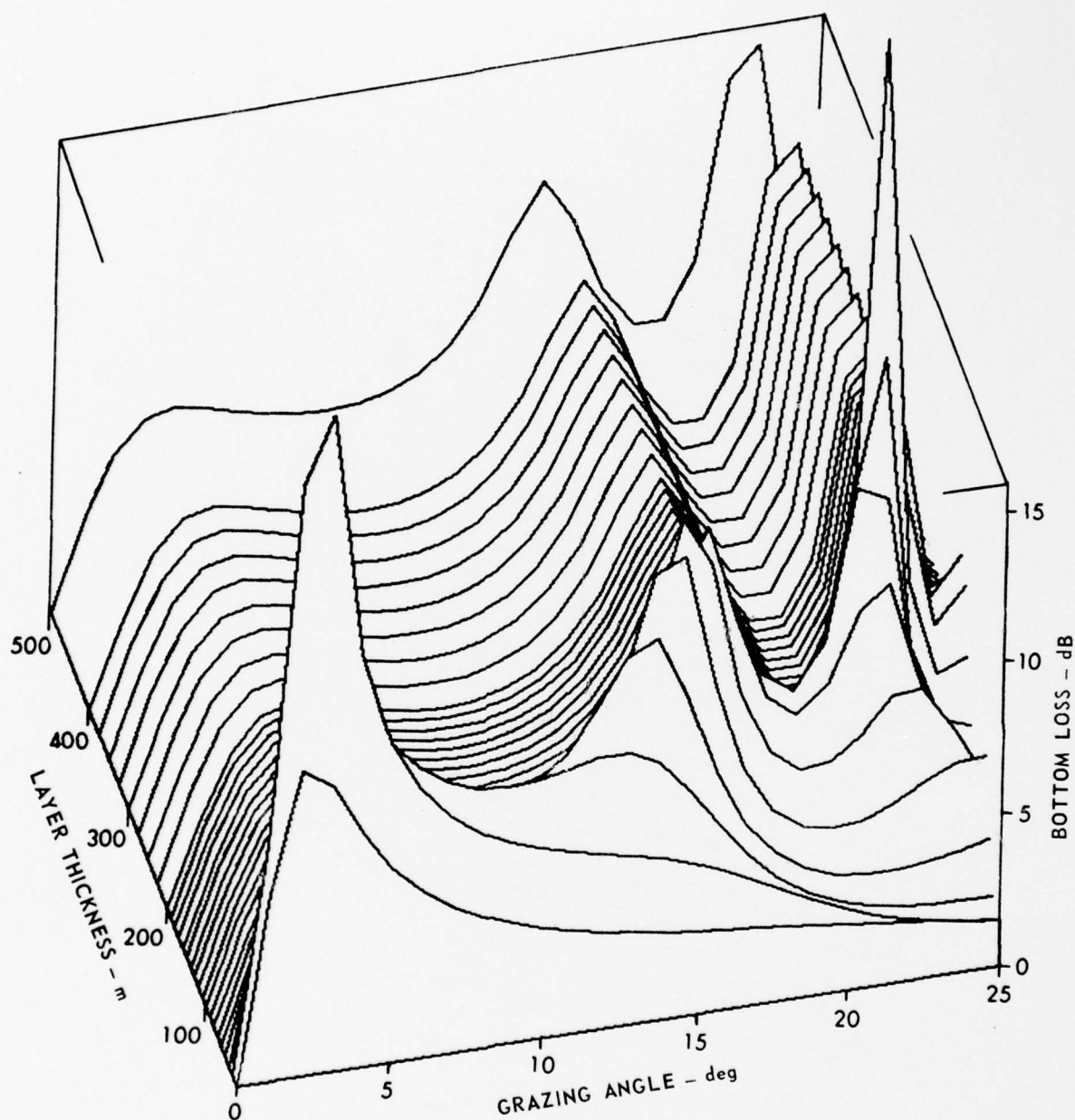
FIGURE III.10
 BOTTOM LOSS versus GRAZING ANGLE versus LAYER THICKNESS
 WITH A SOUND SPEED GRADIENT OF 0.5 sec^{-1}



FREQUENCY: 50 Hz
 MATERIAL: SILT
 GRADIENT: 1.0 sec⁻¹

FIGURE III - 11
 BOTTOM LOSS versus GRAZING ANGLE versus LAYER THICKNESS
 WITH A SOUND SPEED GRADIENT OF 1.0 sec⁻¹

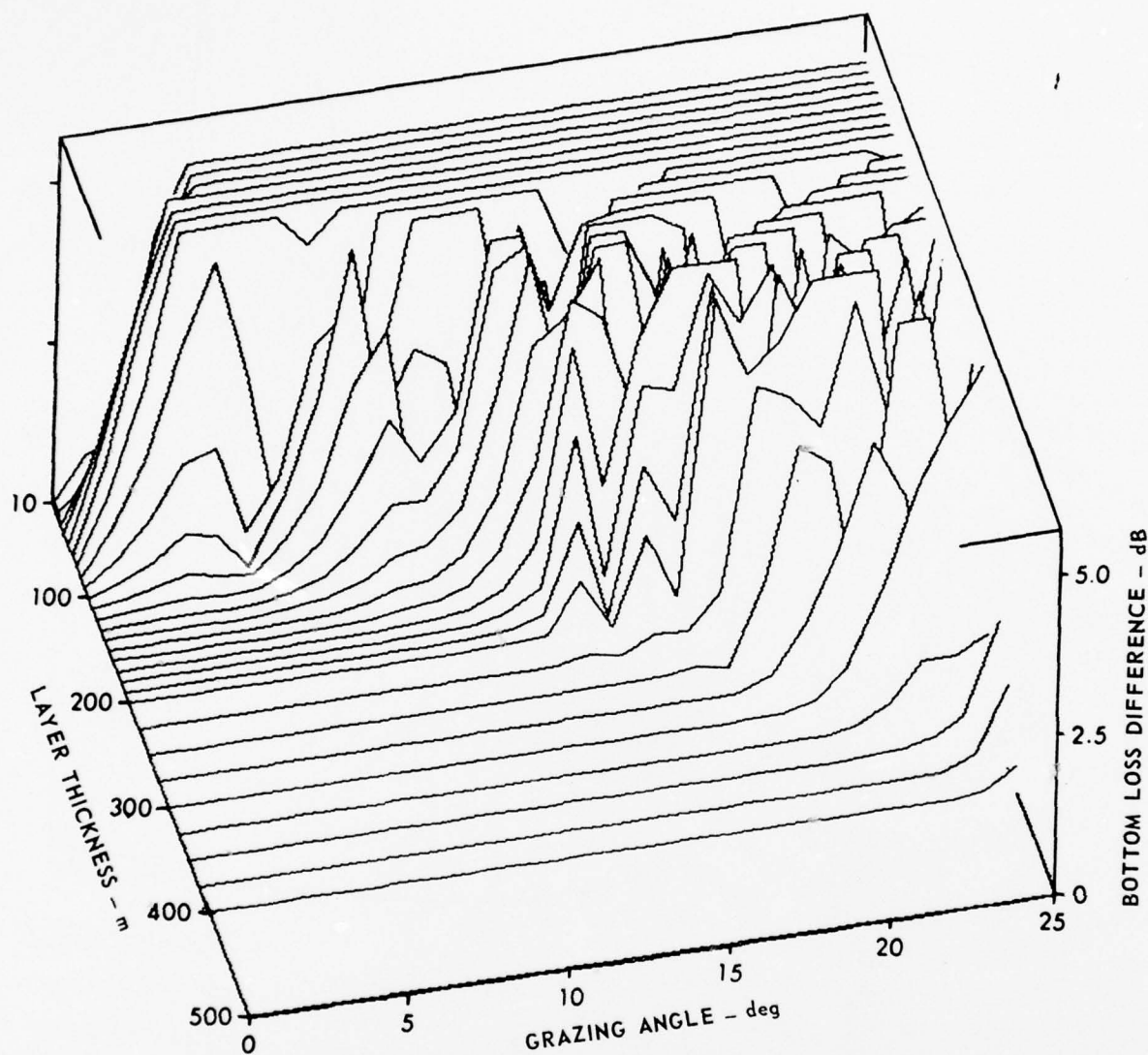
ARL - UT
 AS-76-627
 KEH - DR
 6 - 7 - 76



FREQUENCY: 50 Hz
 MATERIAL: SILT
 GRADIENT: 1.5 sec^{-1}

FIGURE III - 12
 BOTTOM LOSS versus GRAZING ANGLE versus LAYER THICKNESS
 WITH A SOUND SPEED GRADIENT OF 1.5 sec^{-1}

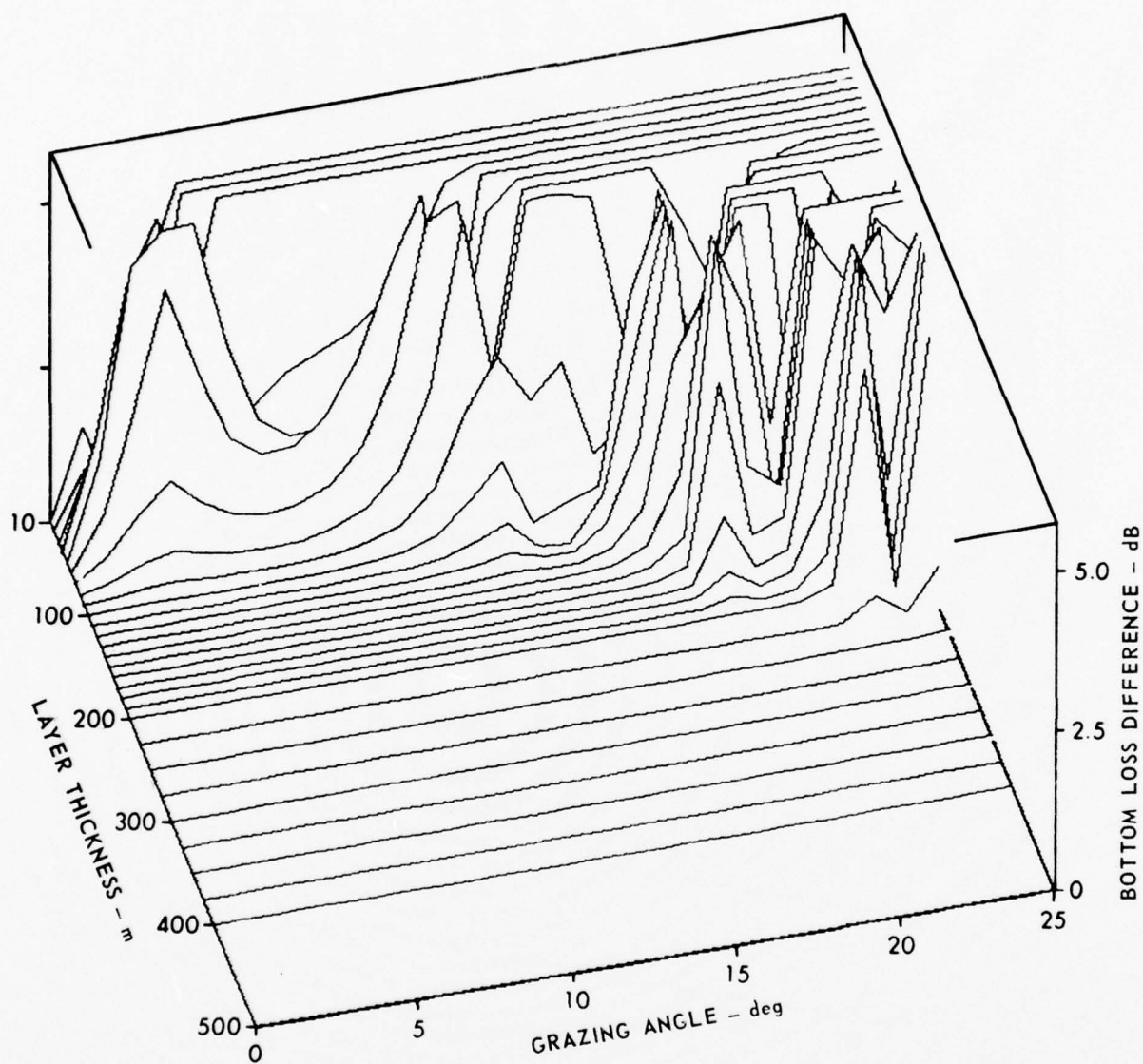
ARL - UT
 AS-76-628
 KEH - DR
 6 - 7 - 76



FREQUENCY: 50 Hz
 MATERIAL: SILT
 GRADIENT: 0.5 sec^{-1}

FIGURE III - 13
 INTENSITY RATIO FOR REFLECTOR-ABSORBER SUBSTRATES
 WITH A SOUND SPEED GRADIENT OF 0.5 sec^{-1}

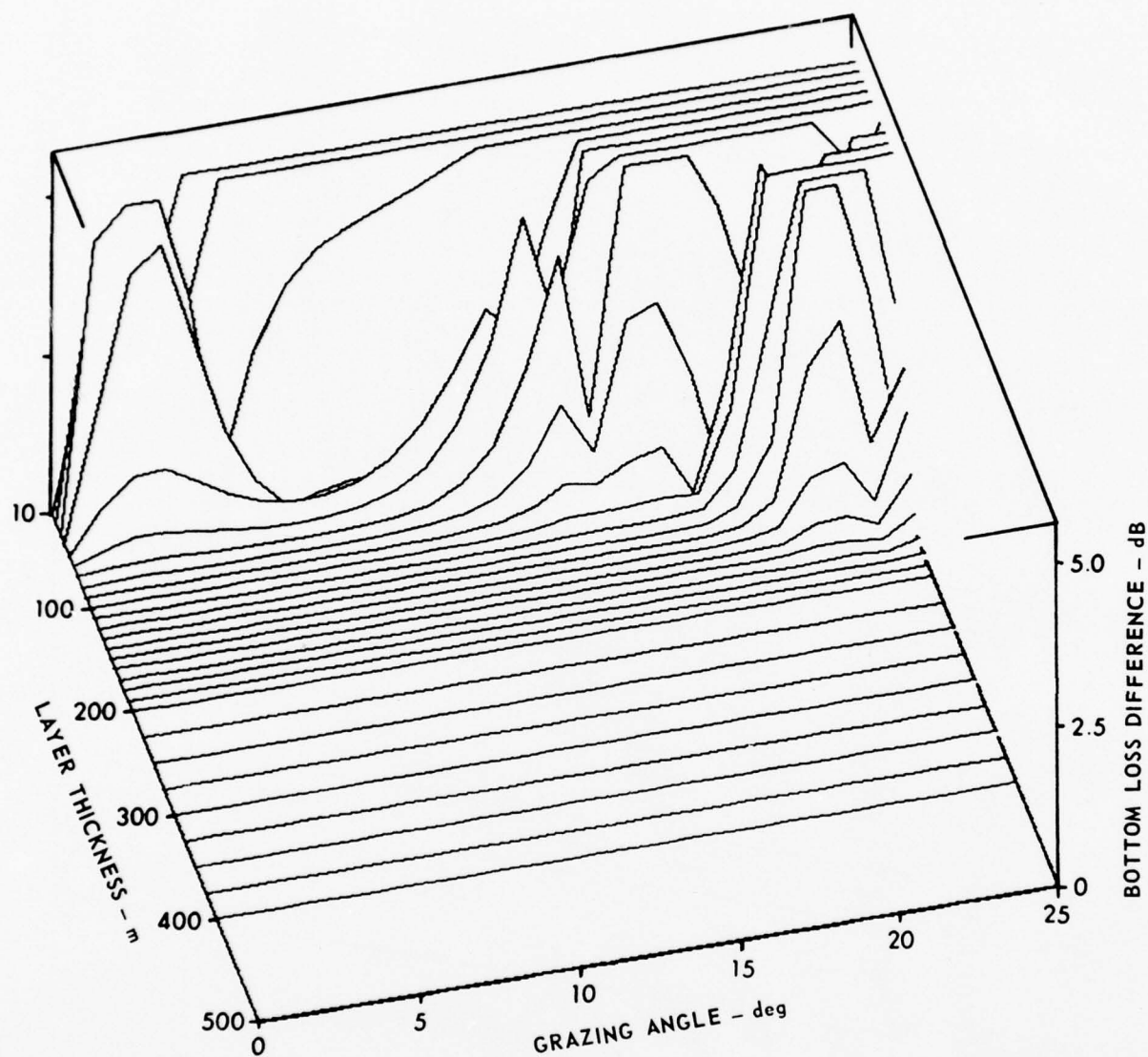
ARL - UT
 AS-76-632
 KEH - DR
 6 - 7 - 76



FREQUENCY: 50 Hz
 MATERIAL: SILT
 GRADIENT: 1.0 sec^{-1}

FIGURE III - 14
 INTENSITY RATIO FOR REFLECTOR-ABSORBER SUBSTRATES
 WITH A SOUND SPEED GRADIENT OF 1.0 sec^{-1}

ARL - UT
 AS-76-633
 KEH - DR
 6 - 7 - 76



FREQUENCY: 50 Hz
 MATERIAL: SILT
 GRADIENT: 1.5 sec^{-1}

FIGURE III-15
 INTENSITY RATIO FOR REFLECTOR-ABSORBER SUBSTRATES
 WITH A SOUND SPEED GRADIENT OF 1.5 sec^{-1}

ARL - UT
 AS-76-634
 KEH - DR
 6-7-76

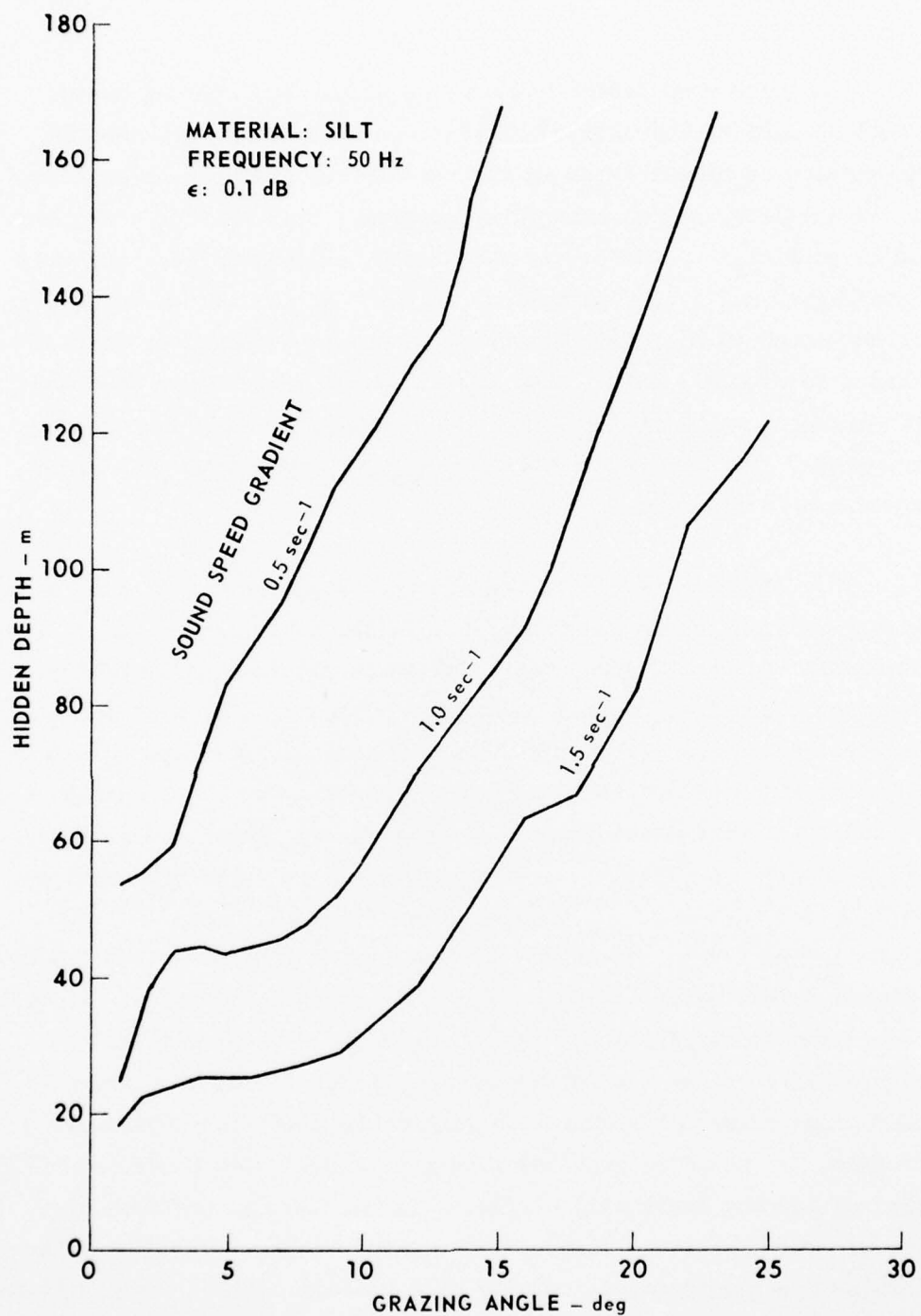


FIGURE III - 16
HIDDEN DEPTH versus GRAZING ANGLE FOR A SILT
LAYER WITH VARIOUS SOUND SPEED GRADIENTS

The close association between the hidden and turning depths leads at once to the conclusion that the apparently very complex dependence of hidden depth on all the various sediment parameters is in actuality not an overriding problem. Upon writing the hidden depth as $Z_H = Z_T + \delta\lambda$, where λ is some sound wavelength (say, the water wavelength) and δ is a parameter, we see that all of the complexity is contained in δ alone. Moreover, we now have reason to believe that δ is of order unity, that is, it is not much larger than one. In general, δ will depend on all the sediment parameters as well as on frequency. The dominant sound speed profile dependence should be contained in the term Z_T .

Thus far we have restricted our investigation to the case of a linear sediment sound speed profile. Although it is true that, in the uppermost sediment layers, the sound speed gradient is generally constant, seismic profiling measurements clearly show that the gradient decreases with depth. To gain some insight into how such behavior might affect the hidden depth picture, we shall examine the exponential sound speed profile proposed by Williams³ and given by $C(Z) = C(0)[1 + A^2(e^{-\beta Z} - 1)]^{-1/2}$. This profile is a three-parameter one with $C(\infty) = C(0)[1 - A^2]^{-1/2}$, $C'(Z) = C'(0)e^{-\beta Z}[1 + A^2(e^{-\beta Z} - 1)]^{-1/2}$, and $C'(0) = 1/2 \beta A^2 C(0)$. Figure III-17 shows $C'(Z)$ plotted versus depth for various values of $C(0)/C(\infty)$, with $C'(0)$ chosen to be unity. It will be observed that, for $C(0)/C(\infty) < 2/3$, $C'(Z) < 1$ for all depths. Figure III-18 shows the ray turning depth for the case of water overlying sediment that contains such an exponential sound speed profile. As would be expected from Fig. III-17, for $C(0)/C(\infty) > 2/3$, the ray turning depth will always be larger than in the case of a linear profile (dotted line). For a given value of $C(0)/C(\infty)$, the turning depth approaches infinity at a certain angle. These critical angles are denoted by the asymptotes.

The most important result contained in these figures concerns the deviation of Z_T from linear behavior at low angles. It will be noted

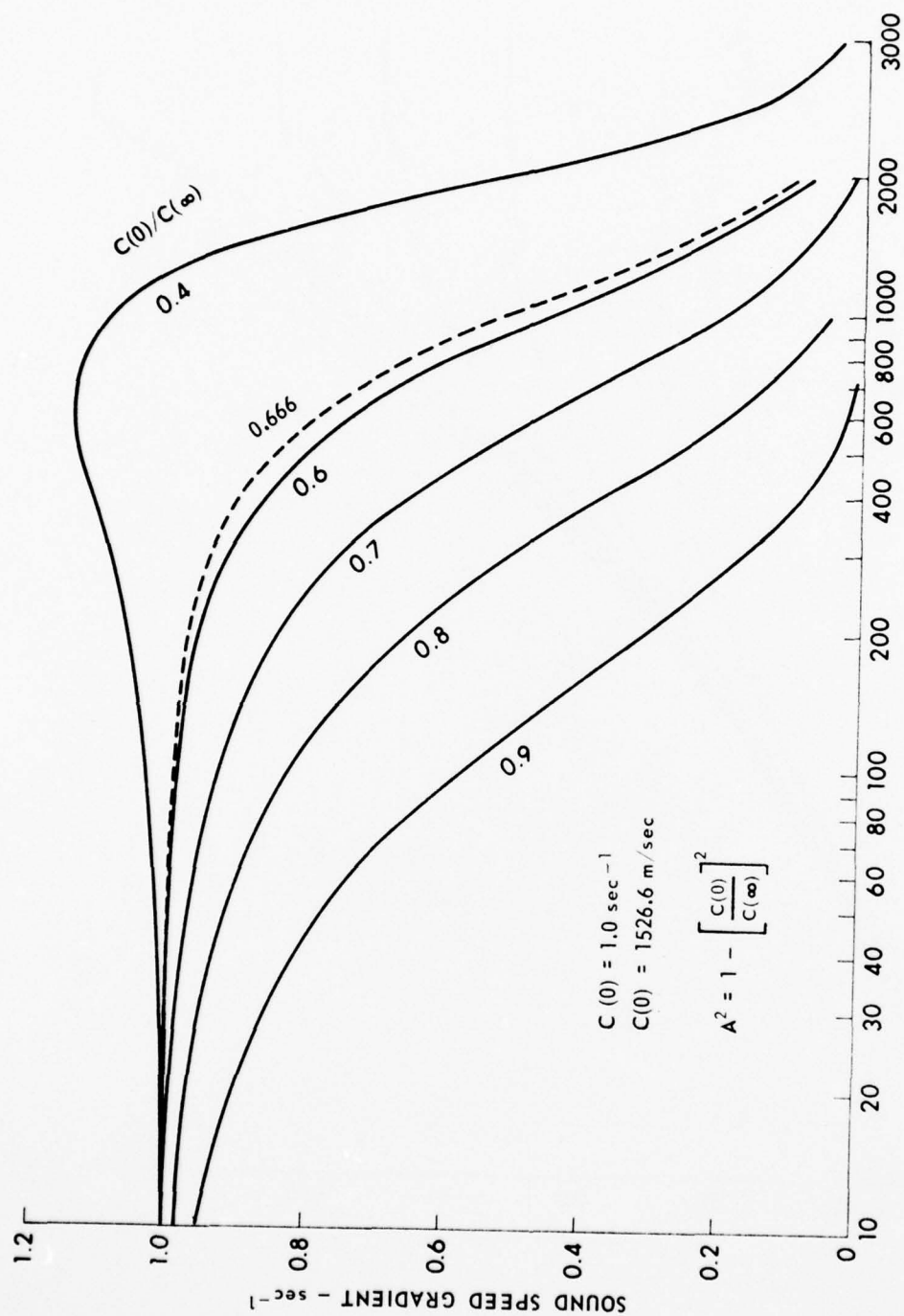


FIGURE III - 17
SOUND SPEED GRADIENT versus DEPTH FOR AN
EXPONENTIAL PROFILE WITH VARIOUS VALUES OF $C(0)/C(\infty)$

ARL - UT
AS-76-742
KEH - DR
7 - 5 - 76

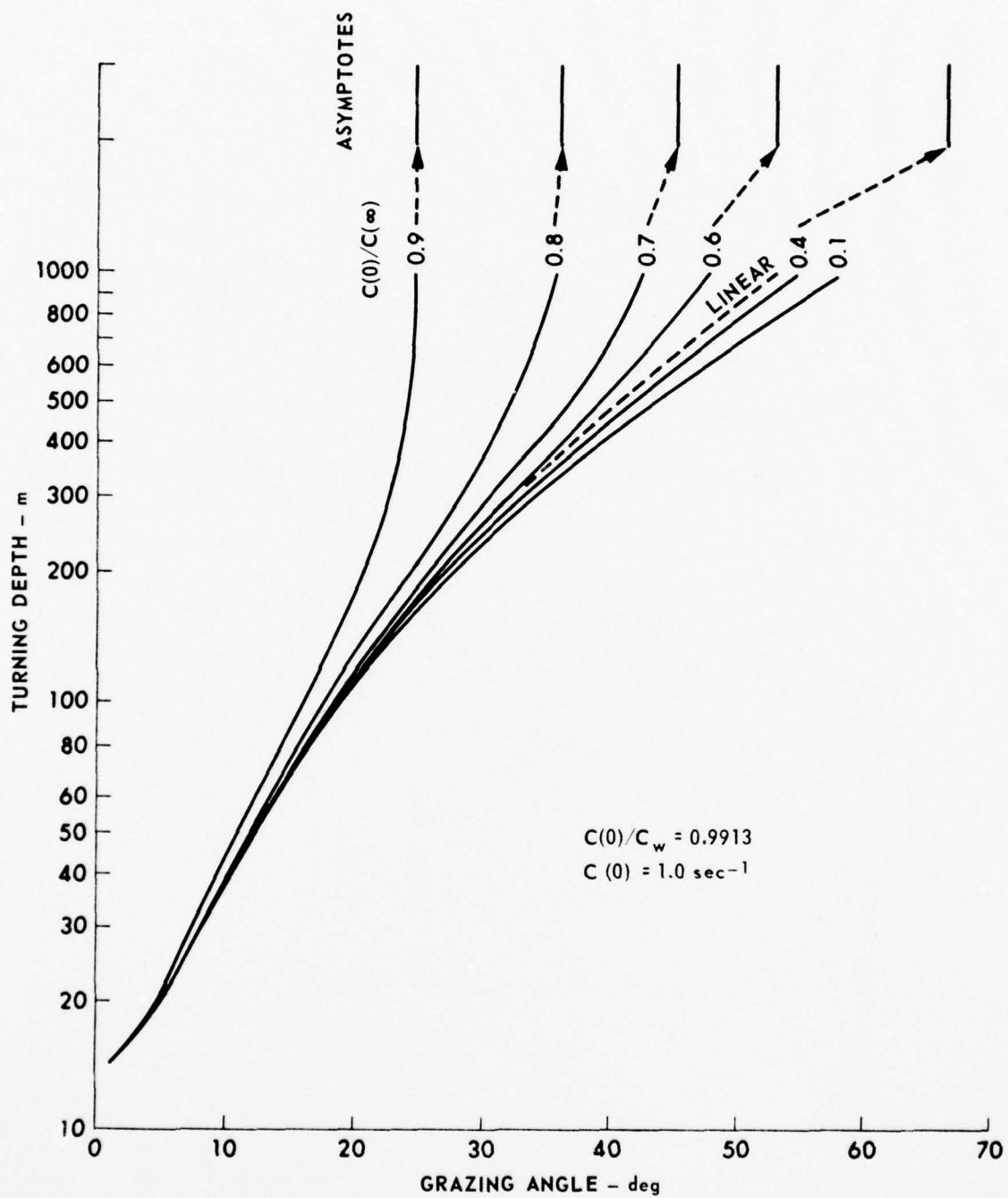


FIGURE III - 18
 TURNING DEPTH versus GRAZING ANGLE FOR AN
 EXPONENTIAL PROFILE WITH VARIOUS VALUES OF $C(0)/C(\infty)$

ARL - UT
 AS-76-741
 KEH - DR
 7 - 5 - 76

that for $\theta \leq 25^\circ$ and $0.8 \geq C(0)/C(\omega) \geq 2/3$, the maximum deviation from linear behavior is 45 m. For this range of $C(0)/C(\omega)$, the sound speed gradient at 200 m can range from 0.66 to 0.975. Thus, although a considerable variation of $C'(Z)$ can occur, the turning depth will range only over a comparatively narrow interval. Consequently, the hidden depth values which are previously determined in several cases using the linear profile will not be greatly altered by the introduction of such an exponential profile.

As a final problem in this hidden depth section, we shall briefly examine the question of the frequency dependence of the hidden depth. There are two ways in which frequency enters the problem: directly and through the variation of attenuation with frequency. The second of these is the subject of continuing investigation and will be discussed in a later report; we shall consider here only the direct frequency dependence.

An estimate of the direct frequency dependence can be carried out in the following way. First, we expand the linear sound speed profile wave number $k_1^2(Z) = \omega^2/c^2(Z)$ in a power series in $Z - Z_T$, $k_1^2(Z) = k_1^2 \{a + (Z - Z_T)b + 1/2(Z - Z_T)^2c + \dots\}$ with $a = (1 + \beta Z_T)^{-2}$ and $b = -2\beta(1 + \beta Z_T)^{-3}$ and where the linear profile is given by $C_1(Z) = C_1(1 + \beta Z)$. Hence, in the neighborhood of Z_T we have the differential equation

$$\frac{d^2 p_1}{dZ^2} + \left[k_1^2 a - k_0^2 \cos^2 \theta + k_1^2 b(Z - Z_T) \right] p_1 = 0 \quad , \quad (1)$$

the solution of which is given by

$$p_1(Z - Z_T) = a \text{Ai} \left[\left(\frac{2\beta u_0^3}{k_1} \right)^{1/3} (Z - Z_T) \right] + b \text{Bi} \left[\left(\frac{2\beta u_0^3}{k_1} \right)^{1/3} (Z - Z_T) \right] \quad , \quad (2)$$

where $\mu_0 = k_0 \cos \theta$ and (a) and (b) are constants. Upon introducing the phase velocity $v = c_0 / \cos \theta$ and the gradient $g = C_1 \beta$, we have

$$p_1(Z - Z_T) \cong a \operatorname{Ai} \left[\frac{\omega}{v} \left(\frac{2g}{\omega} \right)^{1/3} (Z - Z_T) \right] + b \operatorname{Bi} \left[\frac{\omega}{v} \left(\frac{2g}{\omega} \right)^{1/3} (Z - Z_T) \right] \quad (3)$$

Now, below the turning point we must have a decreasing pressure field, so we take $b=0$ and obtain

$$p_1(Z - Z_T) \cong a \operatorname{Ai} \left[\frac{\omega}{v} \left(\frac{2g}{\omega} \right)^{1/3} (Z - Z_T) \right] \quad (4)$$

Now consider two frequencies f_1 and f_2 and suppose that $p(Z - Z_T)$, for $Z > Z_T$, has the value ϵ at $f=f_1$ at $Z=Z_1$. That is,

$$p_1(Z_1 - Z_T; f_1) = \epsilon = a \operatorname{Ai} \left[\frac{\omega_1}{v} \left(\frac{2g}{\omega_1} \right)^{1/3} (Z_1 - Z_T) \right] \quad (5)$$

This equation determines the constant (a). We now require that, at the second frequency f_2 , the pressure $p(Z - Z_T; f_2)$ equals ϵ at some depth $Z=Z_2$. Furthermore, we suppose that $Z_1 = Z_T + n\lambda_1$, and we obtain

$$\operatorname{Ai} \left[\frac{\omega_2}{v} \left(\frac{2g}{\omega_2} \right)^{1/3} (Z_2 - Z_T) \right] = \operatorname{Ai} \left[\frac{n 2\pi c_1}{v} \left(\frac{2g}{\omega_1} \right)^{1/3} \right] \quad (6)$$

which, upon the introduction of $Z_2 = Z_T + n\delta\lambda_2$, reduces to

$$Ai \left[\delta \left(\frac{n2\pi c_1}{v} \right) \left(\frac{a_g}{\omega_2} \right)^{1/3} \right] = Ai \left[\left(\frac{n2\pi c_1}{v} \right) \left(\frac{a_g}{\omega_1} \right)^{1/3} \right] , \quad (7)$$

which yields directly $\delta = (f_2/f_1)^{1/3}$. This same one-third power law was obtained by Williams⁹ in his investigations.

To recapitulate these results, if at a frequency f_1 , the pressure is reduced to a factor ϵ at a depth Z_1 (which is n wavelengths below the turning depths), then, at $f=f_2$, the pressure will achieve this same value ϵ at a distance $n\delta$ wavelengths below the turning point. The factor δ is then given by $\delta = (f_2/f_1)^{1/3}$. This rather weak frequency dependency indicates, for example, that the previous results at 50 Hz would be altered by a factor of 1.23 at 100 Hz.

Having investigated the question of the hidden depths and some of its determining factors, we are now prepared to consider other sensitivity aspects which can occur above the hidden depth.

C. Bottom Loss Sensitivity Problems Above the Hidden Depth

This section deals with some bottom loss sensitivity problems in the region of sediment above the hidden depth. Unfortunately, although it is possible to ask, and to answer, quite specific questions in this domain, the very large number of relevant variables makes systematic study difficult. Moreover, it is to some extent physically unrealistic to consider independent variations in many of these parameters since the physical properties of real sediments couple them together.

It is useful to consider a subdivision into categories which, while not completely independent, reflect different physical processes and acoustical effects. The most useful such breakdown is in terms of the following problem areas:

(1) variation in sediment type (density, sound speed, and attenuation) with fixed layering, sound speed profile function, and substrate,

- (2) substrate effects, such as the importance of shear waves in the substrate,
- (3) sound speed profile and gradient effects, with other sediment parameters fixed,
- (4) effects of a continuously variable density gradient,
- (5) attenuation effects (singling out this important parameter that is difficult to measure to determine the required precision of for which detailed knowledge
- (6) frequency dependence of all the above, and
- (7) sediment shear wave effects, treating the sediments as solids rather than fluids.

Although it has been widely appreciated for some time that all these various effects are component parts of bottom reflection loss, very little has been done in the way of detailed quantitative and systematic studies of them. In large measure, this is due to the lack of adequate models incorporating the various processes, a deficiency which has only recently been remedied by the BOTLOSS model developed by ARL/UT and by a model developed at NUC by H. Buckner. Some work in the direction of a sensitivity study was carried out at SACLAN¹⁴ by Strangerup, although it was restricted to isovelocity, isodensity sediments.

In the remainder of this section we shall consider briefly the first four of the topics listed above. The remaining three will be considered in a subsequent report under this contract as will additional and more complete considerations on the first four. Investigation of the problems associated with the first four categories is not complete, but the results presented here do indicate trends and establish some qualitative bounds on the importance of these questions.

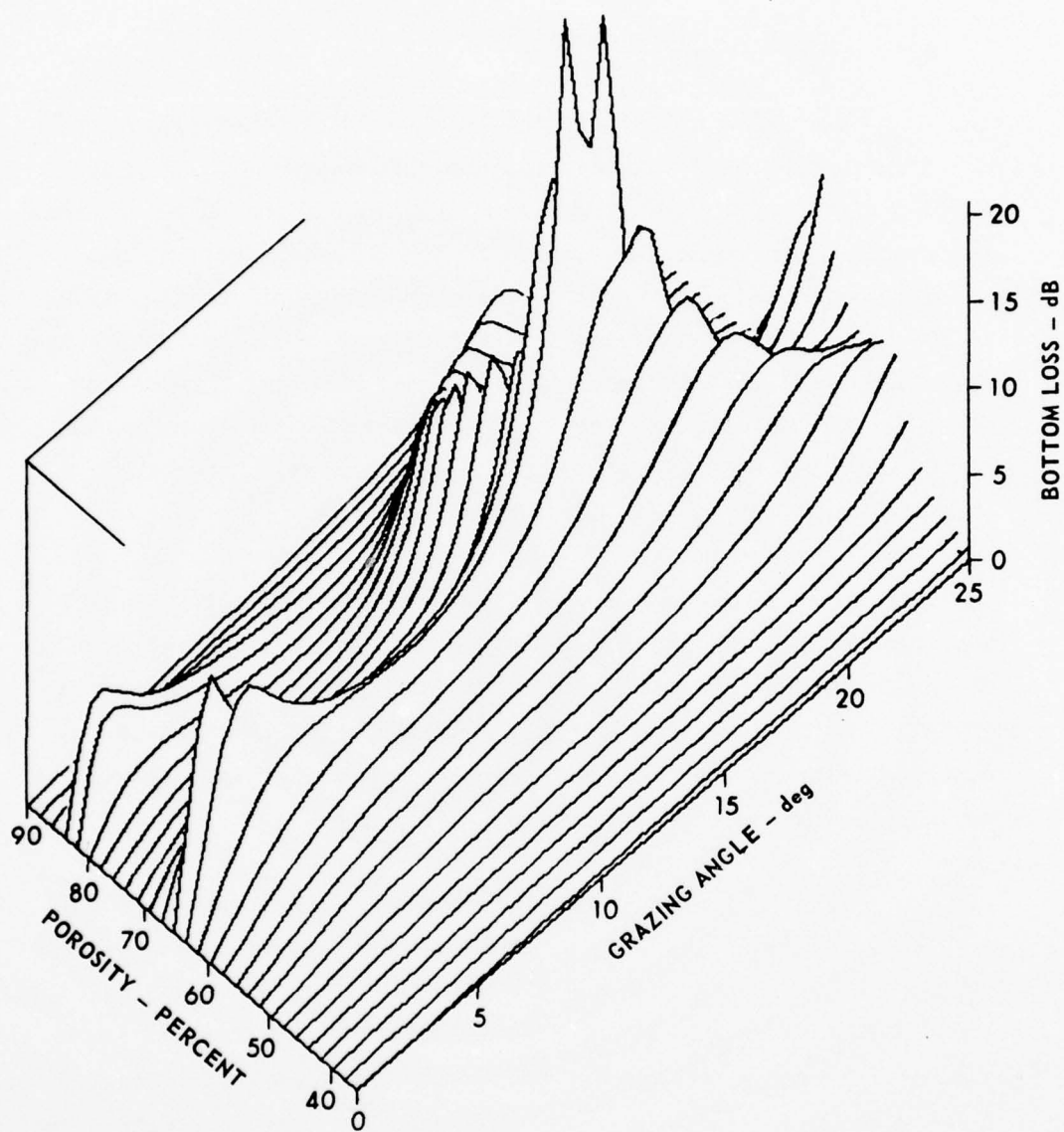
1. Variations in Sediment Type

Even with all other problem parameters fixed (layering, sound speed profile function, gradient, and substrate, etc.) the problem of the influence of sediment type variations on bottom loss involves, at a minimum, variations in sound speed, density, and attenuation. One possibility for circumventing this difficulty is to relate these three parameters to a single parameter such as porosity or mean grain size. The work of Akal¹¹ and Hamilton¹² has shown that, for a considerable variety of sediments, these three parameters can be usefully related to porosity. Furthermore, appropriate equations have been developed by these authors.

Upon fixing all other parameters in the problem, then it is possible to study sediment type variations by examining the behavior of bottom loss versus angle versus porosity. An empirical approach to this type of study was taken by Hall and Watson¹⁵ who used empirical fits to AMOS data and developed curves giving bottom loss versus grazing angle parameterized by porosity.

It is quite straightforward to employ the aforementioned results of Hamilton and Akal to generate appropriate parameter sets for use in our bottom loss model. This has been done and Figs. III-19 and III-20 show two resulting three-dimensional surfaces in the case of a linear sound speed profile with a gradient of 1.2 sec^{-1} in a 100 m layer and a 200 m layer, respectively. The substrate is a homogeneous solid.

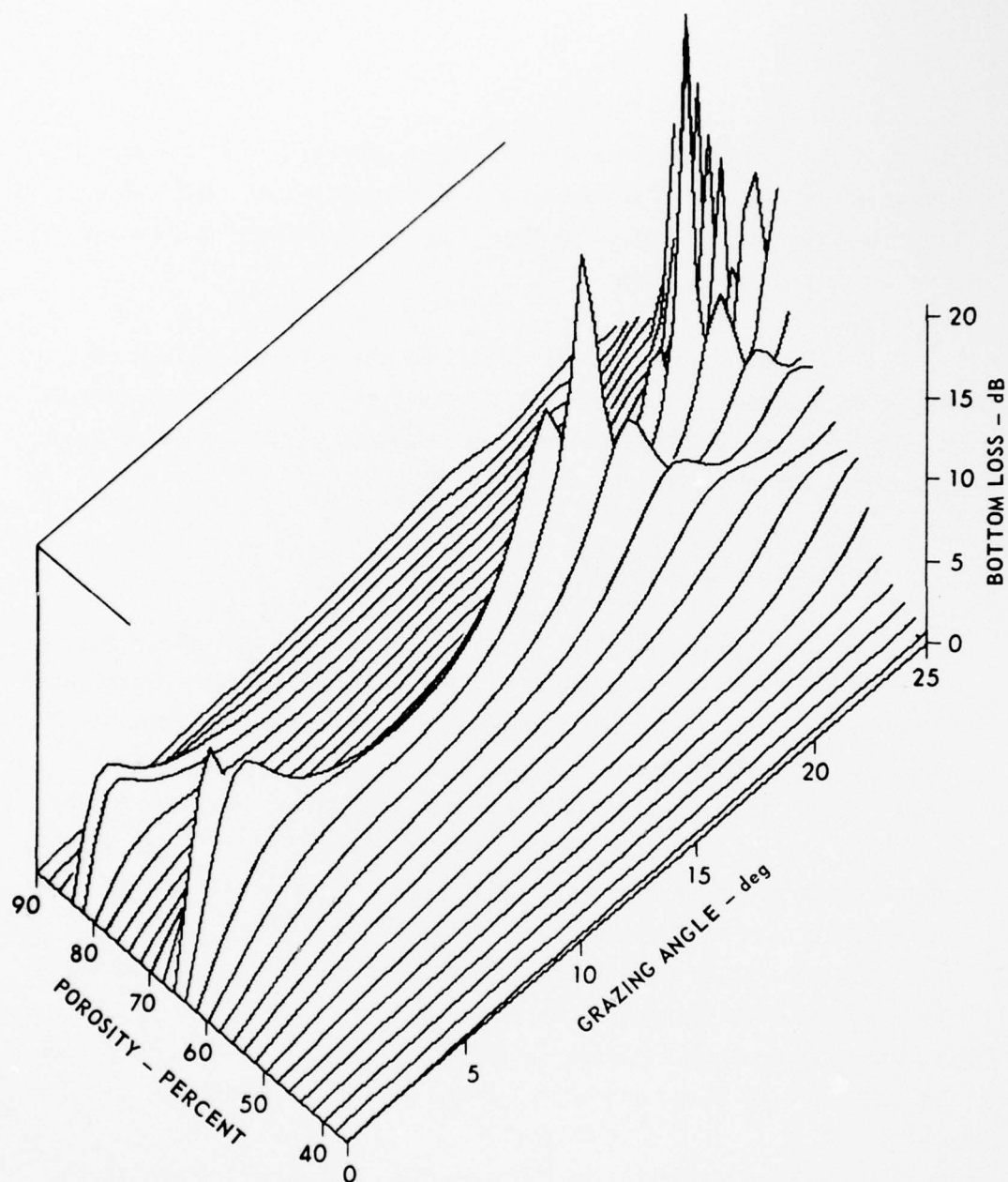
There are two striking features of these surfaces: the bladed structures at low angles and the curving ridge at higher angles. Interpretation of these curves is not yet complete, but it is certain that the prominent curving ridge is associated with Stoneley waves at the sediment-substrate interface, whereas the bladed structures seem



FREQUENCY: 50 Hz
 LAYER THICKNESS: 100 m
 SOUND SPEED GRADIENT: 1.2 sec^{-1}

FIGURE III - 19
 BOTTOM LOSS versus GRAZING ANGLE
 versus POROSITY FOR A 100 m LAYER
 OVERLYING A SOLID SUBSTRATE

ARL - UT
 AS-76-687
 KEH - RFO
 6 - 28 - 76



FREQUENCY: 50 Hz
 LAYER THICKNESS: 200 m
 SOUND SPEED GRADIENT: 1.2 sec^{-1}

FIGURE III - 20
 BOTTOM LOSS versus GRAZING ANGLE
 versus POROSITY FOR A 200 m LAYER
 OVERLYING A SOLID SUBSTRATE

ARL - UT
 AS-76-688
 KEH - RFO
 6 - 28 - 76

AD-A041 378

TEXAS UNIV AT AUSTIN APPLIED RESEARCH LABS
A SENSITIVITY STUDY OF UNDERWATER SOUND PROPAGATION LOSS AND BO--ETC(U)
FEB 77 K E HAWKER, K C FOCKE, A L ANDERSON N00039-77-C-0003
ARL-TR-77-17 NL

UNCLASSIFIED

2 OF 2
ADA
041378



to be a residue of an intromission angle effect. It is noteworthy that, since the bladed structures lie at angles such that the substrate is below the hidden depth, no change is seen in these structures between the 100 m and 200 m cases.

These curves show directly how the bottom loss can be expected to change with sediment type variations. Future work will include producing additional such curves with different sound speed gradients and at different frequencies.

2. Substrate Effects

The most obvious effects to be expected from the presence of a solid substrate located above the hidden depth would be associated with the critical angles of compressional and shear waves in the substrate. Such critical angle effects are indeed evident in Figs. III-21 through III-23, which show the bottom loss for a clay sediment having a constant gradient of 1.2 sec^{-1} and for the three frequencies 25 Hz, 50 Hz, and 100 Hz. The shear wave critical angle is at 55.2° and the compressional wave critical angle is at 74° . The dashed curves show the bottom loss for the same set of parameters except that the substrate shear wave speed has been set to 0. Figure III-23 shows an example, at 5° , of the bladed structure seen in the porosity plots discussed in the previous subsection.

In addition to the features just mentioned, these three figures display a very prominent peak in bottom loss at low angles, much below the shear wave critical angle. That they are associated not only with the substrate but also with its solid aspects is demonstrated by their disappearance in the fluid substrate case. These peaks are examples of the peaks comprising the curving ridge seen in Fig. III-19.

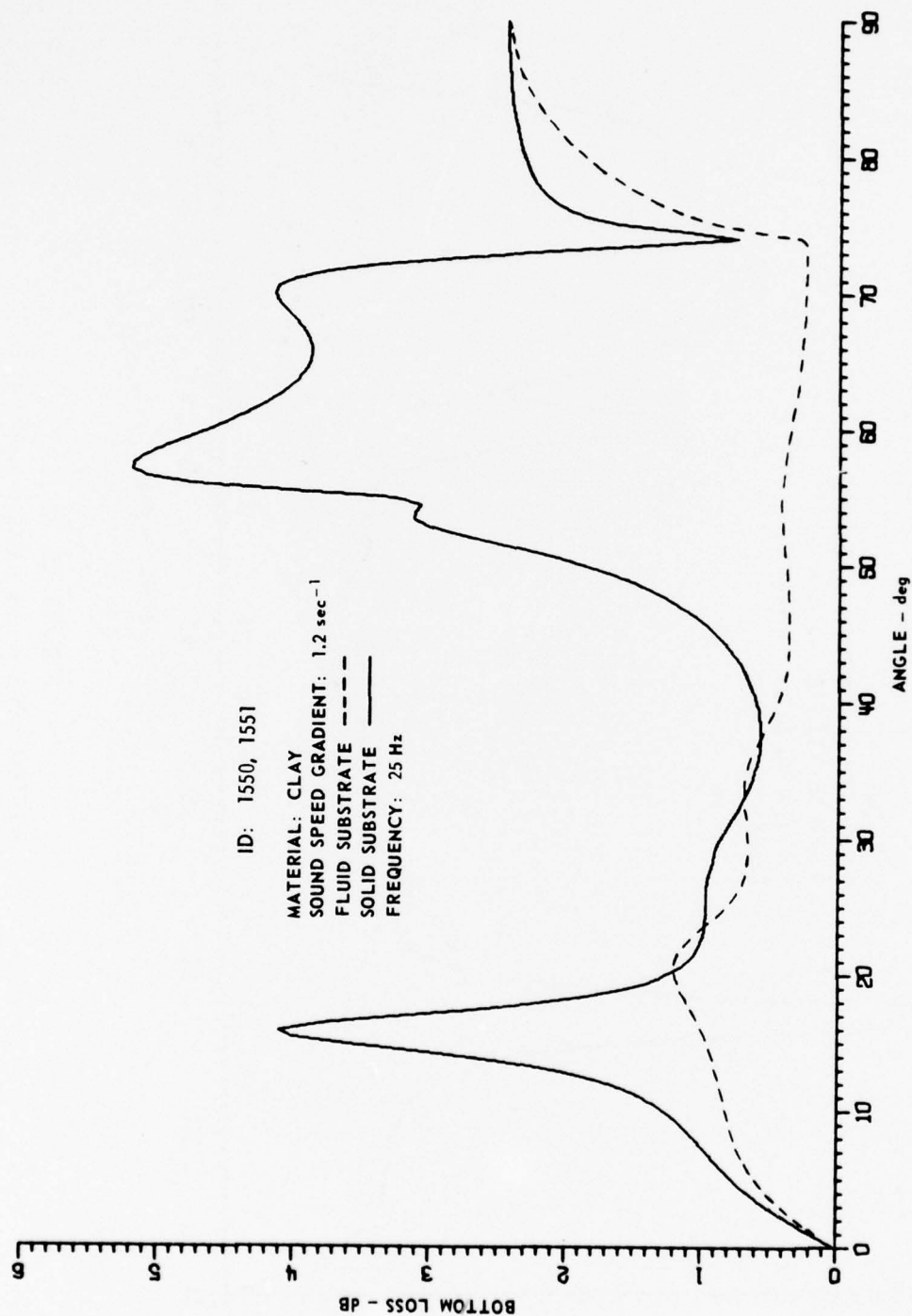


FIGURE III - 21
 BOTTOM LOSS VERSUS GRAZING ANGLE
 FOR A 100 m CLAY LAYER AT 25 Hz

ARL - UT
 AS-76-205
 KEH - DR
 2-27-76

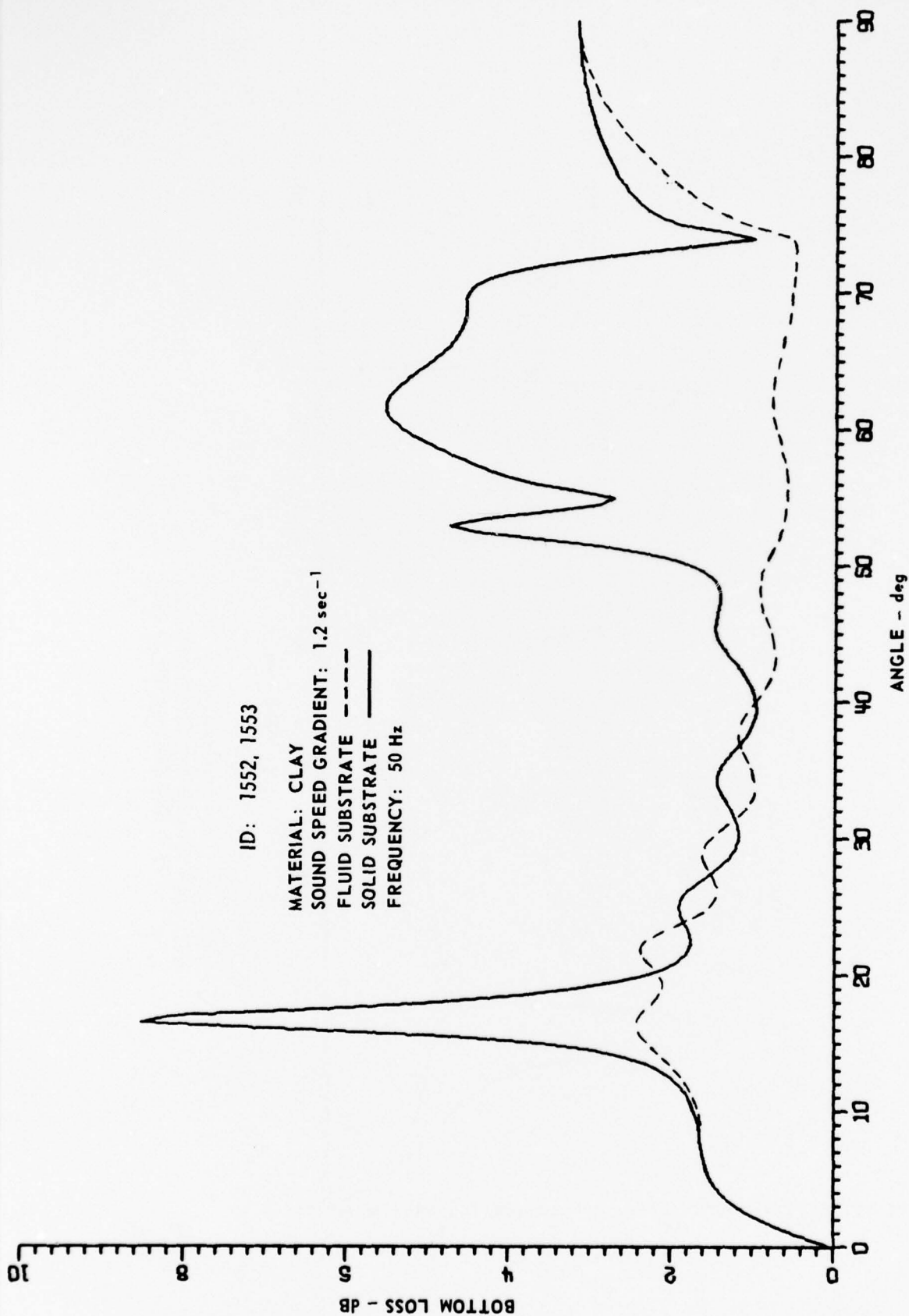


FIGURE III -22
 BOTTOM LOSS versus GRAZING ANGLE
 FOR A 100 m CLAY LAYER AT 50 Hz

ARL - UT
 AS-76-206
 KEH - DR
 2 - 27 - 76

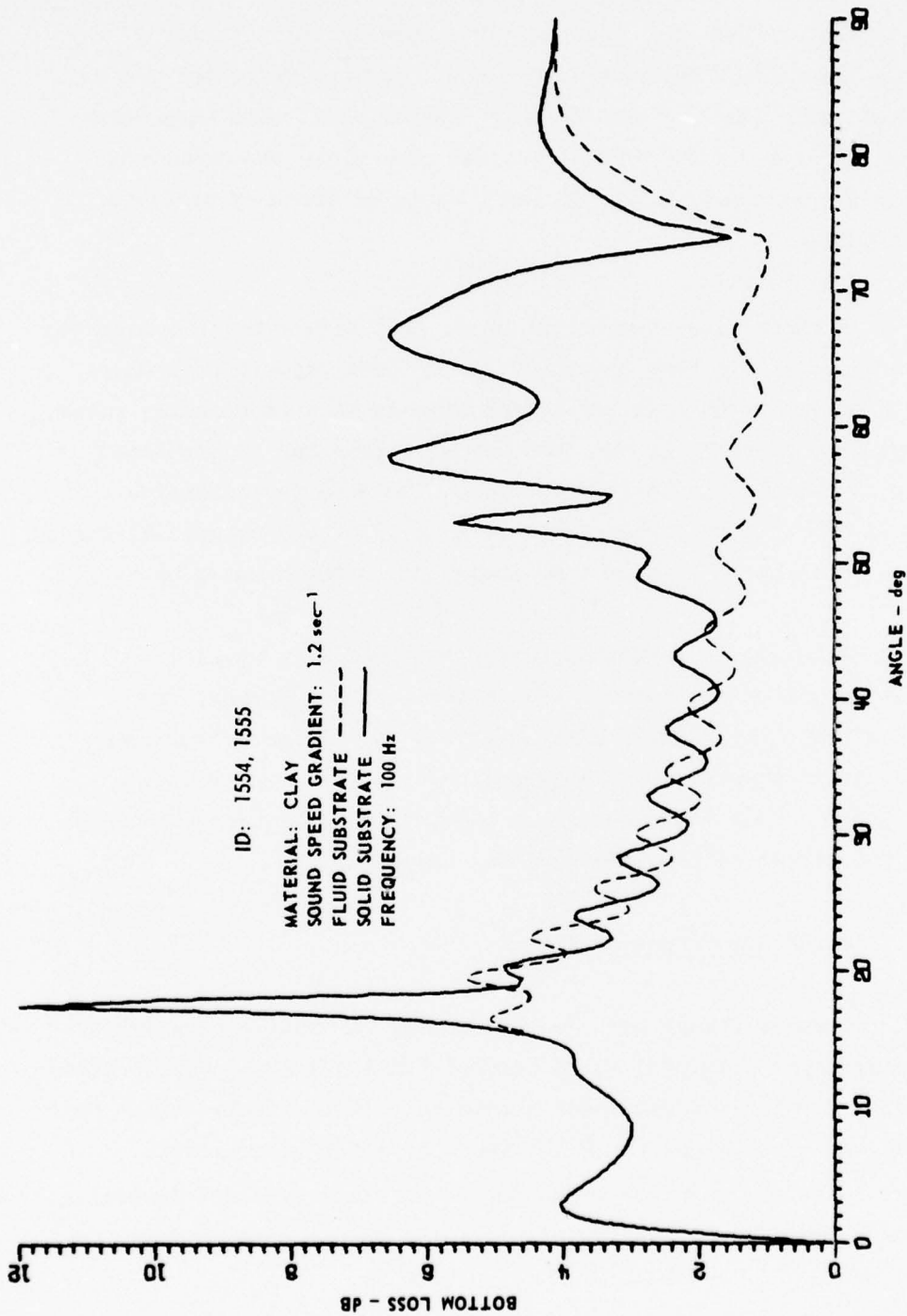


FIGURE III - 23
 BOTTOM LOSS VERSUS GRAZING ANGLE
 FOR A 100 m CLAY LAYER AT 100 Hz

ARL - UT
 AS-76-207
 KEH - DR
 2 - 27 - 76

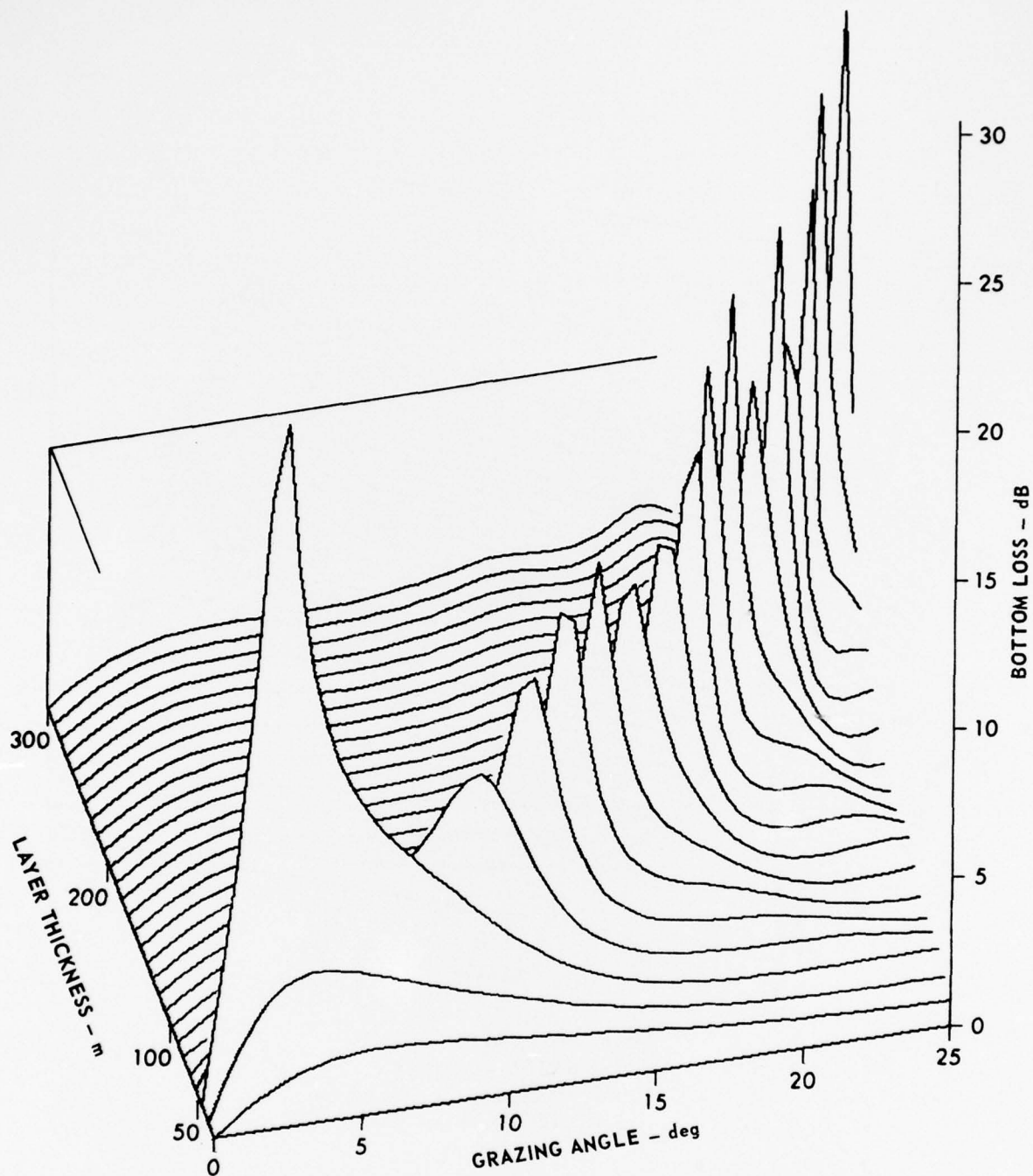
A more dramatic presentation of this effect is seen in Figs. III-24 and III-25. These figures show bottom loss for a variable thickness clay layer overlying a perfect reflector and a solid substrate (at the same depth), respectively. The very large increase in loss in the solid substrate case along the prominent ridge is yet another example of the effects of Stoneley waves at the interface.

A theoretical investigation of this effect has been carried out and results have been obtained showing conclusively that these large peaks in bottom loss are indeed associated with Stoneley waves. Moreover, the location of the Stoneley wave peak can be predicted using a relatively simple theory without the need for extensive numerical calculation. These matters as well as others were discussed in a previous paper¹⁶ and are the subject of a forthcoming paper.¹⁷

Finally, it is not suggested that Stoneley waves will appreciably modify the concept of a hidden depth. Rather, the effects of Stoneley waves are to lead to a very large bottom loss when the solid substrate is below the turning depth and near the hidden depth. That is, even though the interface is near the hidden depth, the effect of the interface may not be small.

3. Sound Speed Profile Effect

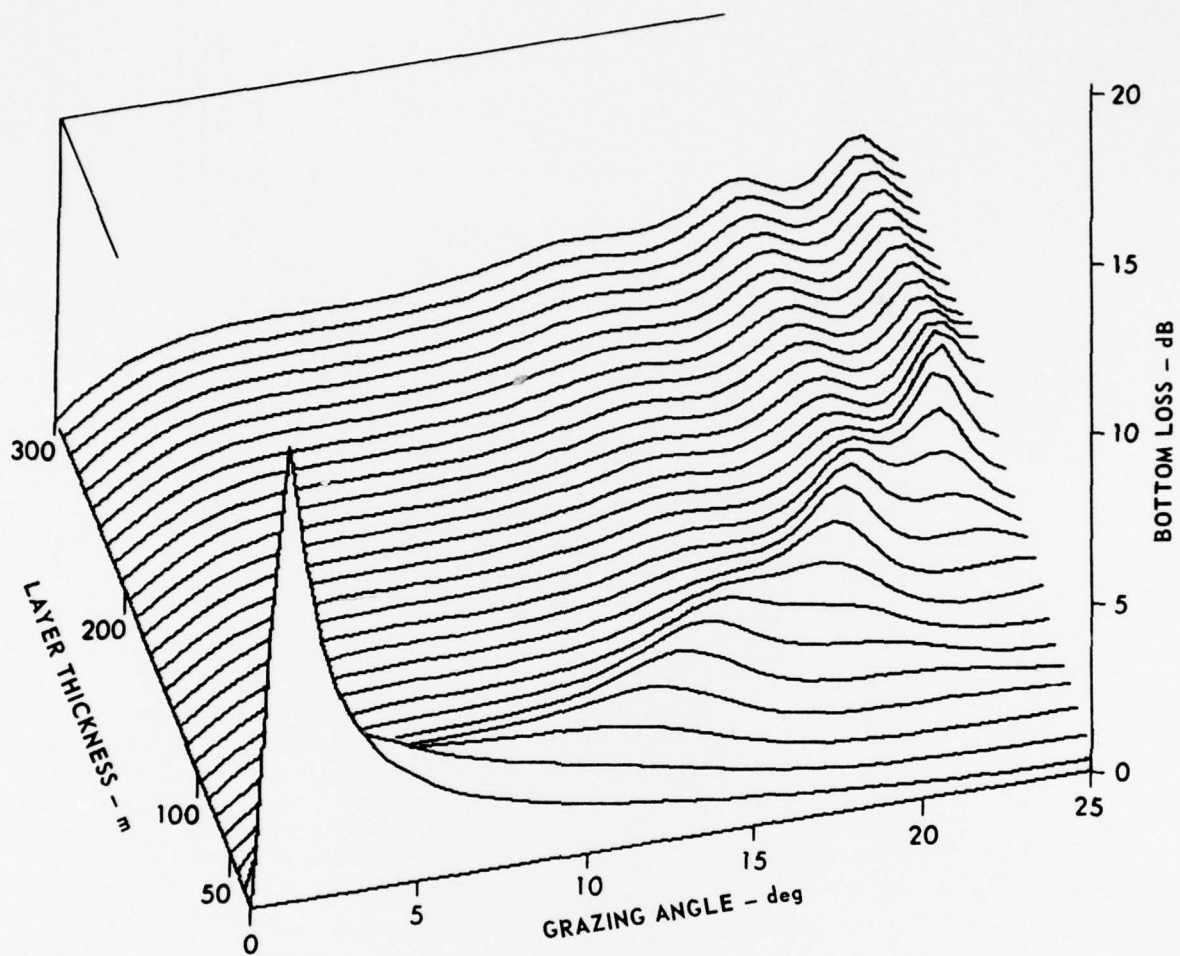
Figures III-26 through III-28 show the bottom loss for a 150 m clay layer overlying solid (dashed line) and fluid (solid line) substrates for three sound speed gradients. It is observed that there is always an angle below which the two curves are coincidental. Moreover, this angle increases as the sound speed gradient increases. This angle itself is a manifestation of the hidden depth effect.



FREQUENCY: 50 Hz
 LAYER MATERIAL: CLAY
 SOUND SPEED GRADIENT: 1.0 sec^{-1}
 SUBSTRATE: SOLID

FIGURE III-24
 BOTTOM LOSS versus GRAZING ANGLE
 versus LAYER THICKNESS FOR A CLAY LAYER
 OVERLYING A SOLID SUBSTRATE

ARL - UT
 AS-76-685
 KEH - RFO
 6 - 28 - 76



FREQUENCY: 50 Hz
 LAYER MATERIAL: CLAY
 SOUND SPEED GRADIENT: 1.0 sec^{-1}
 SUBSTRATE: PERFECT REFLECTOR

FIGURE III - 25
 BOTTOM LOSS versus GRAZING ANGLE
 versus LAYER THICKNESS FOR A CLAY LAYER
 OVERLYING A PERFECT REFLECTOR

ARL - UT
 AS-76-686
 KEH - RFO
 6 - 28 - 76

ID: 1537, 1541

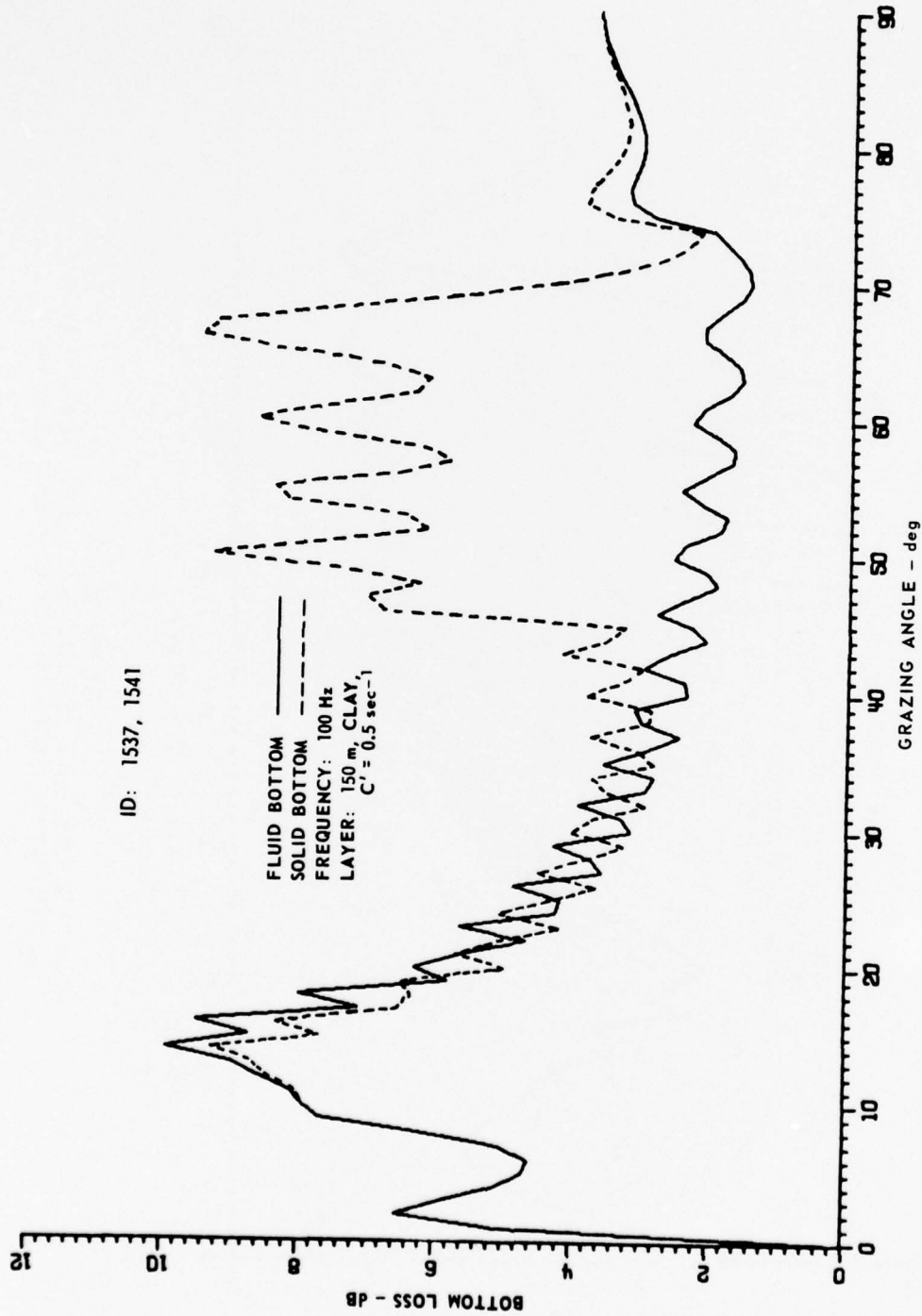


FIGURE III - 26
BOTTOM LOSS versus GRAZING ANGLE FOR A 150 m CLAY
LAYER HAVING A SOUND SPEED GRADIENT OF 0.5 sec^{-1}

ARL - UT
AS-76-151
KEH - DR
2 - 18 - 76

ID: 1538, 1542

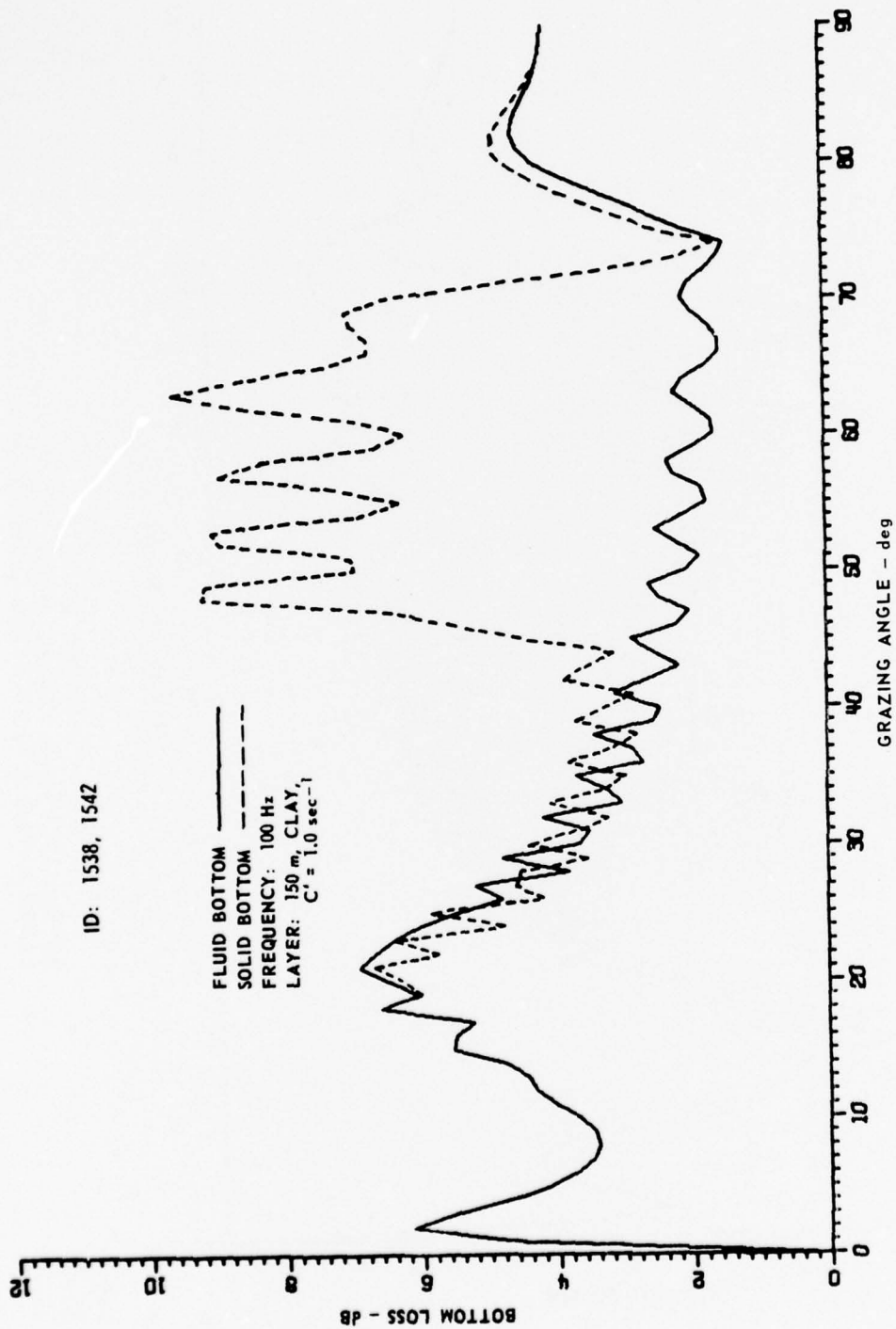
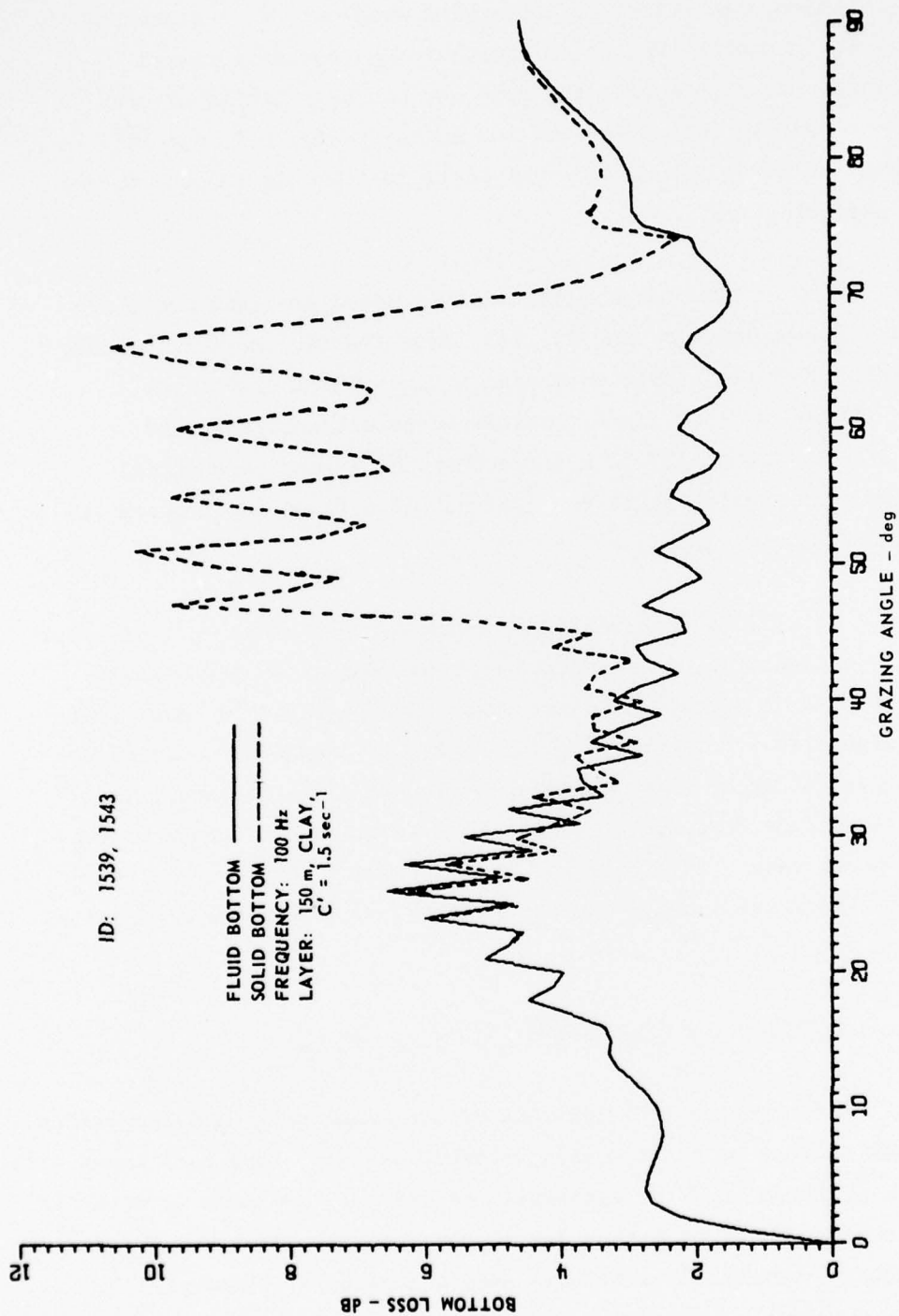


FIGURE III - 27
BOTTOM LOSS versus GRAZING ANGLE FOR A 150 m CLAY
LAYER HAVING A SOUND SPEED GRADIENT OF 1.0 sec^{-1}

ARL - UT
AS-76-152
KEH - DR
2 - 18 - 76

ID: 1539, 1543



ARL - UT
AS-76-153
KEH - DR
2 - 18 - 76

FIGURE III - 28
BOTTOM LOSS versus GRAZING ANGLE FOR A 150 m CLAY
LAYER HAVING A SOUND SPEED GRADIENT OF 1.5 sec^{-1}

Also, the effect of increasing gradient, at low grazing angles, is to reduce the bottom loss through increased upward refraction. At high angles the gradient has very little effect. The broad peak in bottom loss at low angles ($\approx 16^\circ$, 23° , and 28°) occurs at an angle for which a ray would just become tangent to the substrate interface.

The effects of a variable sound speed gradient are shown in Figs. III-29 through III-32. All these figures are for the case of a thin 4.5 m silt layer overlying a thick 500 m clay layer. Figure III-29 is for a linear profile (constant gradient) and Figs. III-30 through III-32 are for three different exponential profiles. At a given angle the gradient at a fixed depth increases with increasing $C(\infty)/C(0)$.

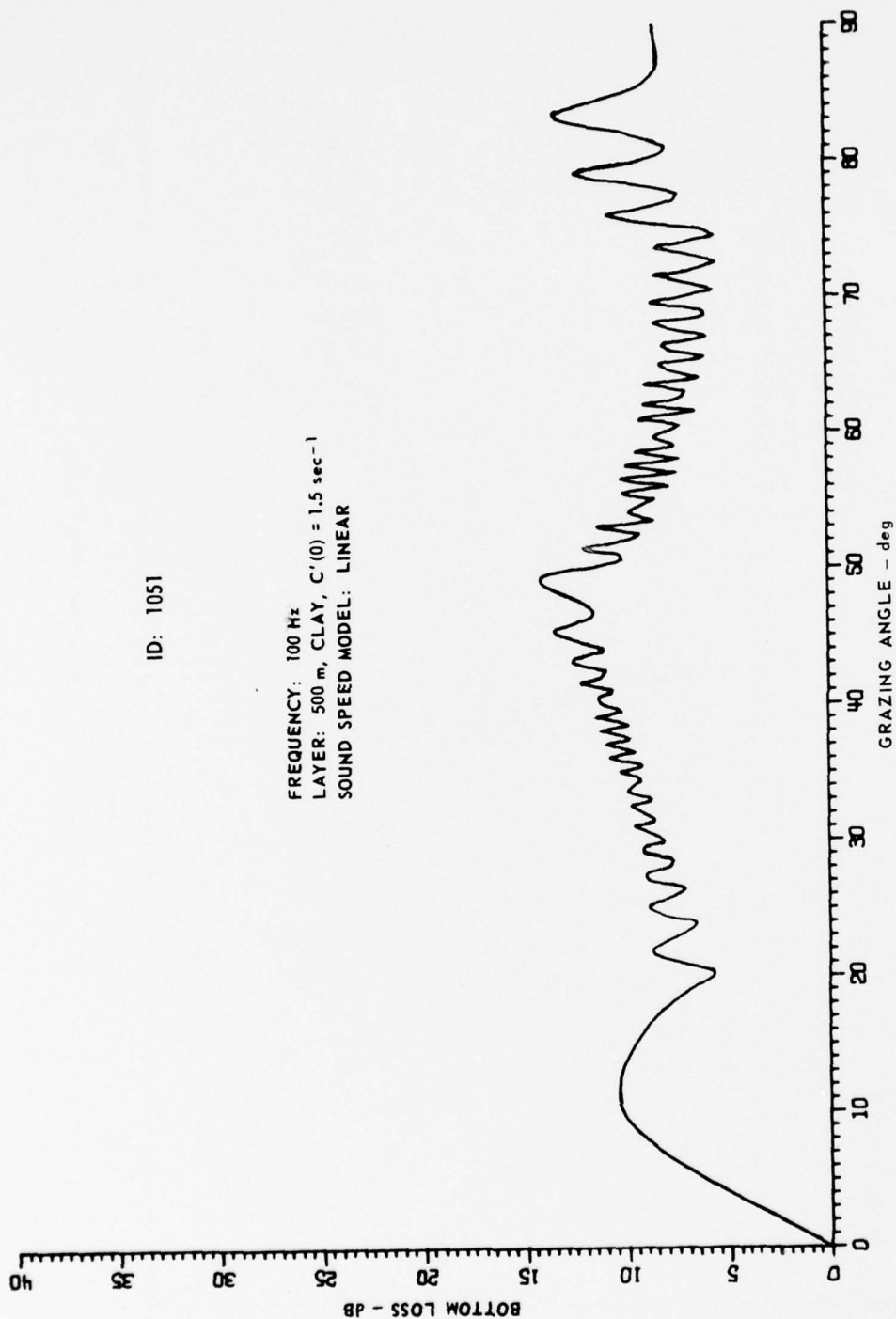
It will be observed that, below approximately 25° , all four curves are identical, thus indicating that changes in sound speed gradient have no effect on bottom loss. In the midangle range there is a large effect for $C(\infty)/C(0)=1.28$ and a progressively less effect for larger values of this parameter. As $C(\infty)/C(0)$ increases, the resulting bottom loss curve is seen to approach more closely to the linear model case. This behavior is consistent with the results given in the first section of this chapter concerning the exponential profile.

4. Effects of a Continuously Variable Density

Although the modifications of the usual wave equation (which were made because of continuously variable density) have been known since the work of Bergmann,¹⁸ no systematic effort has been made to determine the corresponding effect on bottom loss. Some general effects due to a continuously variable density have been discussed by Tolstoy^{12,13} although not in the context of this study.

ID: 1051

FREQUENCY: 100 Hz
LAYER: 500 m, CLAY, $C'(0) = 1.5 \text{ sec}^{-1}$
SOUND SPEED MODEL: LINEAR



ARL - UT
AS-76-154
KEH - DR
2 - 18 - 76

FIGURE III - 29
BOTTOM LOSS versus GRAZING ANGLE FOR A 500 m CLAY
LAYER HAVING A CONSTANT SOUND SPEED GRADIENT

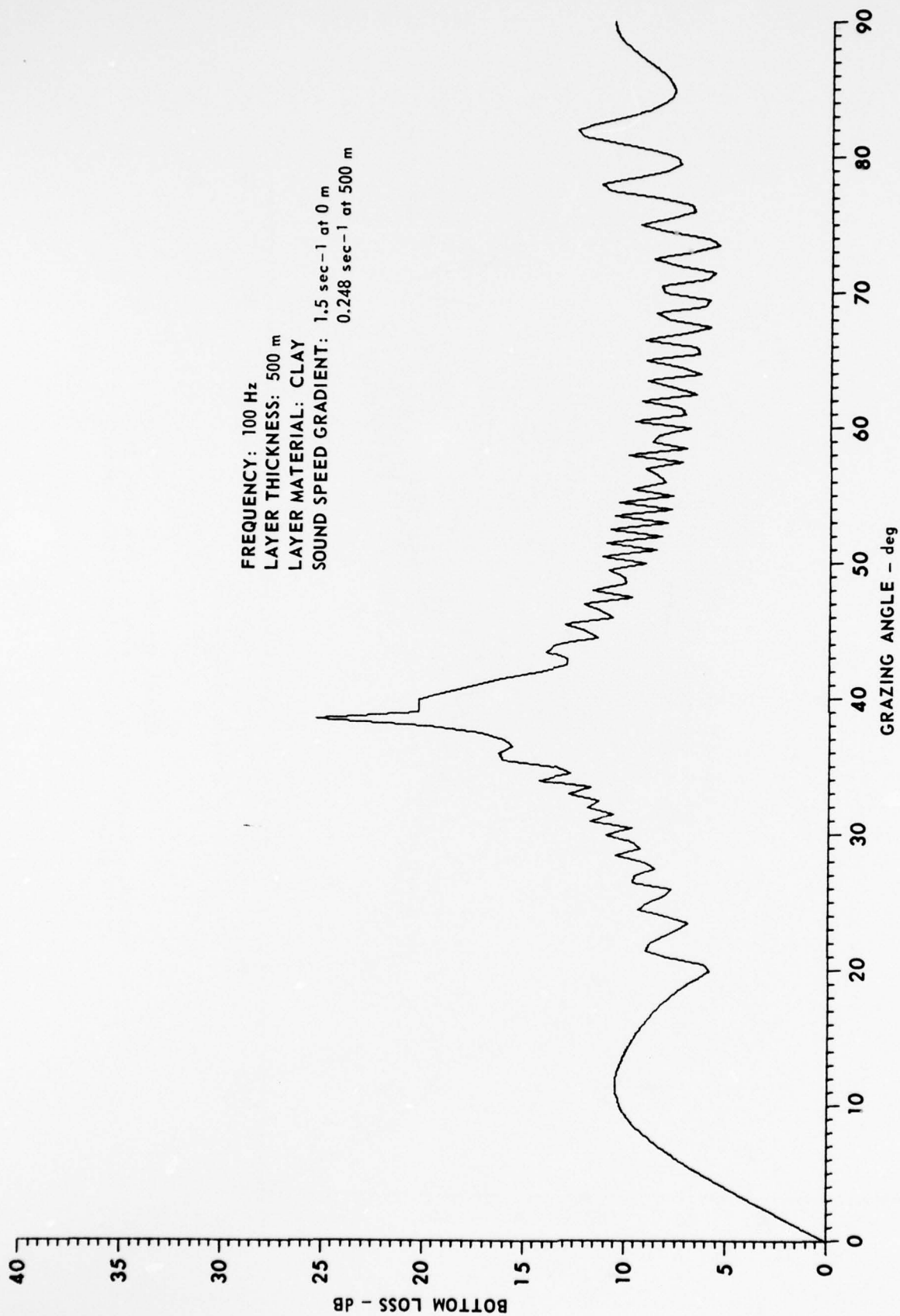


FIGURE III - 30
 BOTTOM LOSS versus GRAZING ANGLE FOR AN EXPONENTIAL PROFILE
 IN A 500 m LAYER WITH $C(\infty)/C(0) = 1.28$

ARL - UT
 AS-76-656
 KEH - DR
 6-15-76

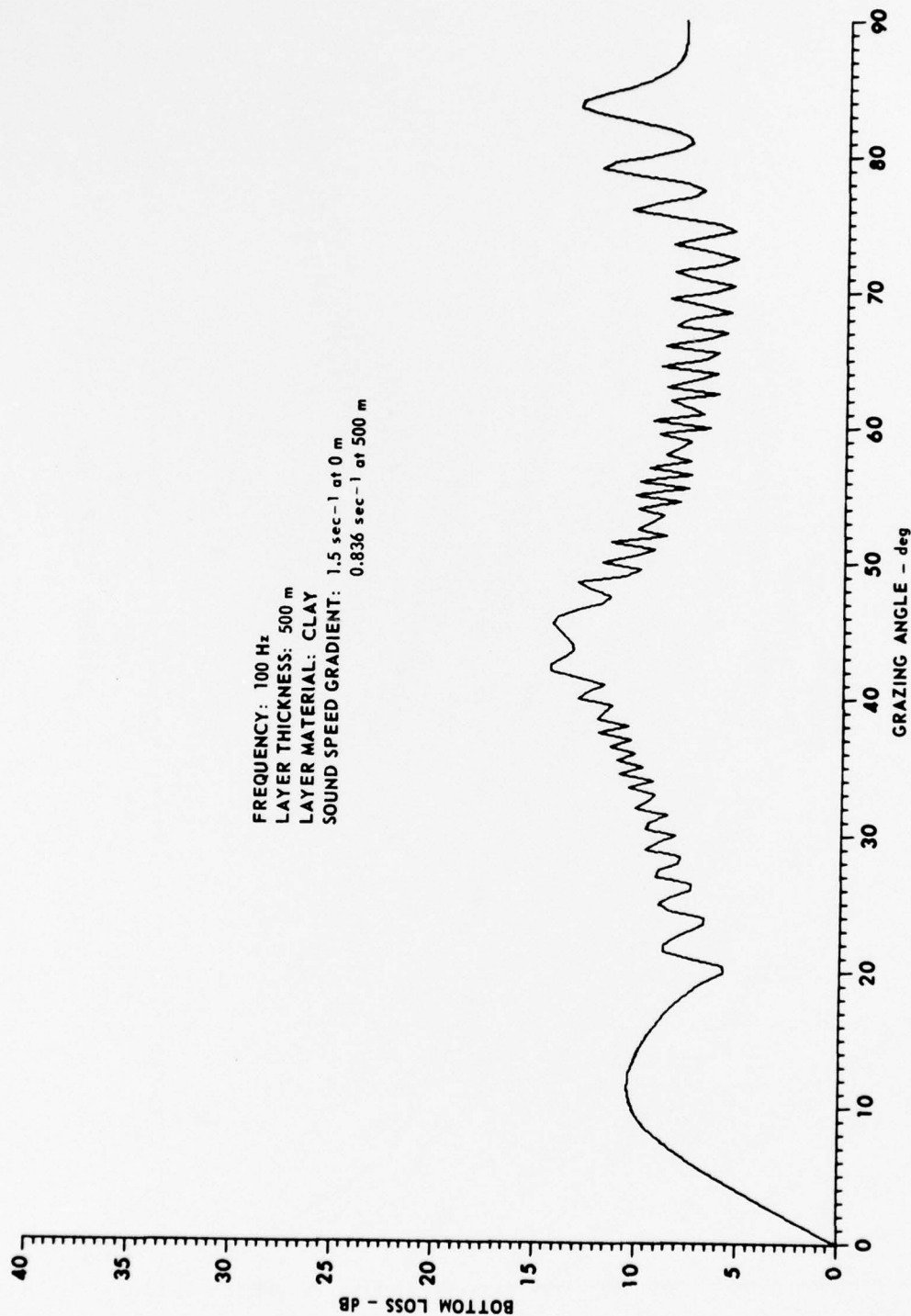


FIGURE III -31
 BOTTOM LOSS versus GRAZING ANGLE FOR AN EXPONENTIAL PROFILE
 IN A 500 m LAYER WITH $C(\infty)/C(0) = 1.60$

ARL - UT
 AS-76-657
 KEH - DR
 6 - 15 - 76

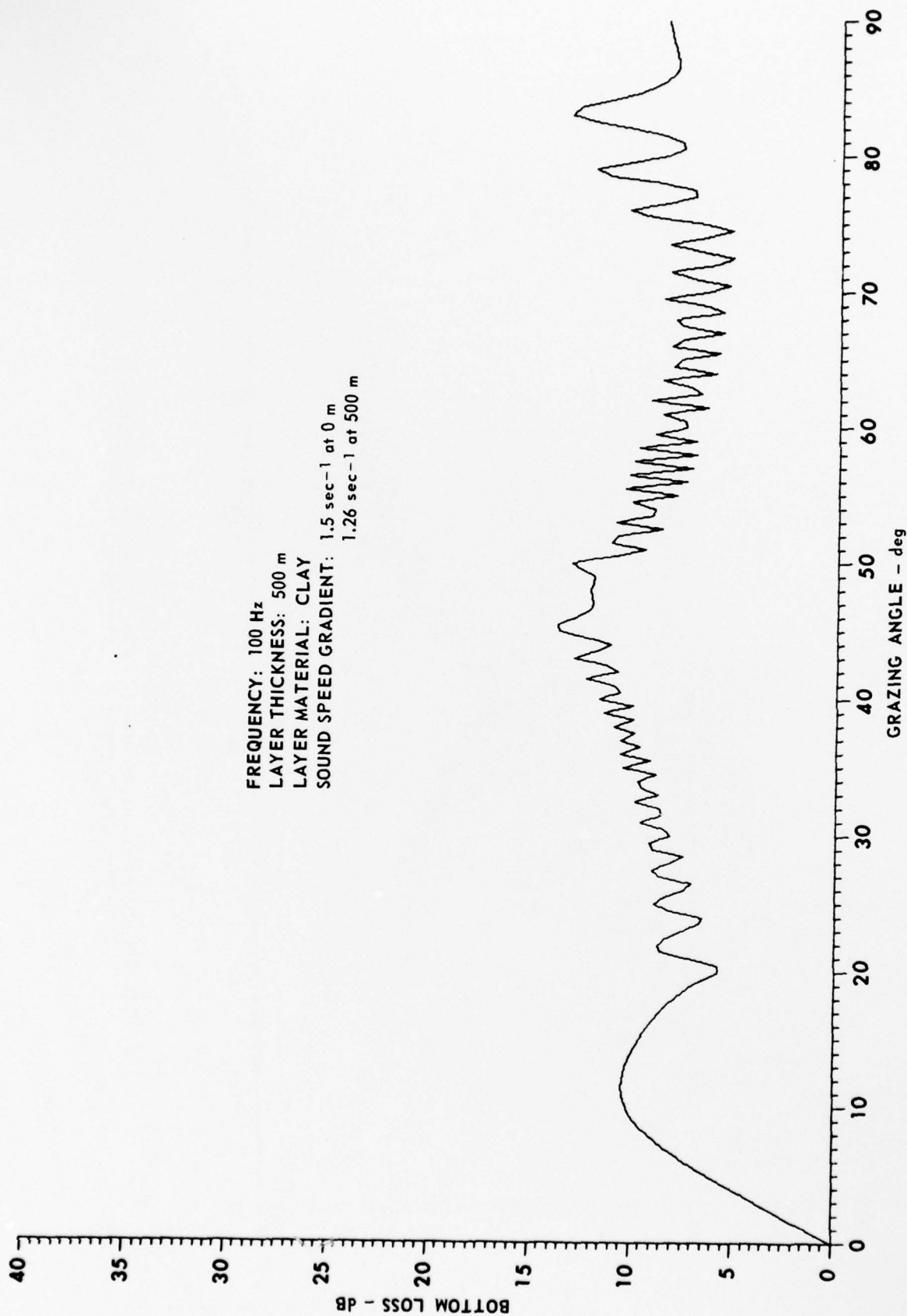


FIGURE III - 32
 BOTTOM LOSS versus GRAZING ANGLE FOR AN EXPONENTIAL PROFILE
 IN A 500 m LAYER WITH $C(\infty)/C(0) = 1.92$

ARL - UT
 AS-76-658
 KEH - DR
 6-15-76

The bottom loss model (BOTLOSS) includes the possibility of having a continuously variable density. Therefore the capability for investigating this question in detail now exists. Some work has been done in this direction and an indication of its nature will be given here.

By employing an appropriate transformation it can be shown (see Hawker and Foreman⁶) that the effects of a continuously variable density can be separated into three parts:

- (1) a refractive effect caused by a modification of the sound speed profile,
- (2) a change in pressure amplitude with depth as $\rho(Z)$, and
- (3) an interface effect.

That is, the solution to the modified wave equation

$$\frac{d^2 p}{dZ^2} - \frac{\rho^1(Z)}{\rho(Z)} \frac{dp}{dZ} + \left(\frac{u^2}{c^2(Z)} - k_o^2 \cos^2 \theta \right) p = 0 \quad (8)$$

can be written as

$$p(Z) = \sqrt{\rho(Z)/\rho(Z_o)} f(Z) \quad , \quad (9)$$

where Z_o is a reference depth and $f(Z)$ is the solution to the equation

$$\frac{d^2 p}{dZ^2} + \left(\frac{u^2}{c^2(Z)} - k_o^2 \cos^2 \theta \right) f = 0 \quad , \quad (10)$$

with

$$\begin{aligned} \tilde{C}(Z) = \omega \left[\frac{\omega^2}{c^2(Z)} - \frac{1}{4} \frac{d}{dZ} \left(\ln \rho(Z) \right)^2 \right. \\ \left. + \frac{1}{2} \frac{d^2}{dZ^2} \left(\ln \rho(Z) \right) \right]^{-1/2} . \end{aligned} \quad (11)$$

Furthermore, the density enters in the interface continuity conditions, so an increase in density with depth will result in a larger value of density being used in these conditions.

It is straightforward to show, using values of ρ'/ρ , that $\tilde{C}(Z) \cong C(Z)$. Hence the refractive effects are negligible. Moreover, examination of the structure of the reflection coefficient shows that generally the amplitude factor $\rho(Z)$ is also of little importance. The major effect due to density changes is therefore expected to be the interface effect. The results of current studies of Hamilton²¹ will make available actual data concerning the expected values of density gradients in various sediment types (in addition to other important parameters). It will therefore be appropriate in the near future to carry out extensive and realistic model studies on the effects of density gradients and to finally resolve this problem. This is not to imply that this effect is large. Figure III-33 shows the bottom loss for a 100 m clay layer with and without a density gradient. Although a large change can occur in the vicinity of the Stoneley wave peak, it is seen that generally, and especially at low angles, the density gradient is likely to be of small importance. Work on this problem is continuing and more definite results will be given in a future report.

ID: 1531, 1534

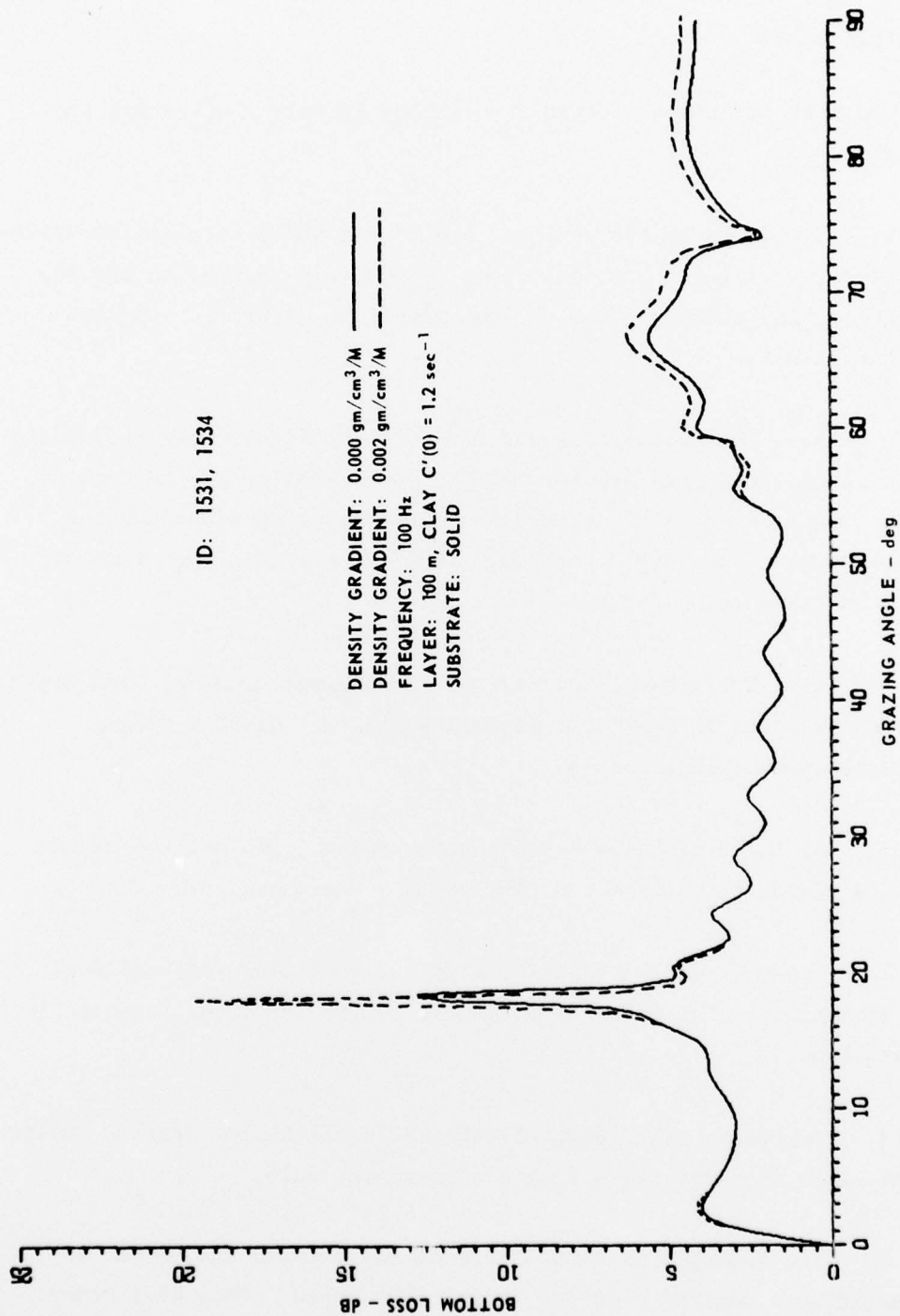


FIGURE III -33
BOTTOM LOSS versus GRAZING ANGLE FOR A 100 m CLAY
LAYER WITH AND WITHOUT A DENSITY GRADIENT

ARL - UT
AS-76-167
KEH - LR
2 - 18 - 76

D. Conclusions

The most important conclusions reached in this chapter are the following.

1. The depth in the sediment column for which detailed knowledge is necessary, called the hidden depth, is closely related to the ray turning depths, although they are not identical except in the high frequency limit.

- a. The location of the hidden depth is strongly influenced by the sound speed gradient through its determination of the turning depth. The gradient also affects the distance between the turning depth and the hidden depth, although this is less important than the effect on the turning depth.

- b. The gradual decrease in sound speed gradient with depth expected to occur in realistic sediments does not exert a strong influence on the hidden depth.

- c. The distance between the turning depth and the hidden depth is frequency dependent according to a one-third power law.

2. The most useful tool for studying sensitivity to sediment type variation is the porosity parameterization developed principally by Hamilton.

3. Substrate shear wave effects are small at low grazing angles except where Stoneley waves play a significant role.

4. The behavior of bottom loss at low grazing angles can be dominated by a peak in loss due to Stoneley waves. This will occur for sediment thickness up to several hundred meters and primarily for clay-silt type sediments.

5. Preliminary indications are that density gradients do not yield important effects although a much wider class of examples needs to be considered.

6. Apart from considerations involving Stoneley waves, the effects of a sound speed gradient above the hidden depth arise from an interplay between the upward refractive effects of the gradient and the effects of absorption.

ACKNOWLEDGMENTS

The authors wish to express appreciation for the material contributions of Terry Foreman, ARL/UT, who assisted in much of the computer programming used in this study.

Also, appreciation is extended to Professor A. O. Williams, Jr., of Brown University and ARL/UT and to Dr. Loyd Hampton, ARL/UT, for helpful discussion and advice.

REFERENCES

1. K. E. Hawker, A. L. Anderson, K. C. Focke, and T. L. Foreman, "Initial Phase of a Study of Bottom Interaction of Low Frequency Underwater Sound," Applied Research Laboratories Technical Report No. 76-14 (ARL-TR-76-14), Applied Research Laboratories, The University of Texas at Austin, April 1976.
2. C. W. Spofford, "The FACT Model," Vol. I, AESD Maury Center Report No. 109, November 1974.
3. C. L. Baker and C. W. Spofford, "The FACT Model," Vol. II, AESD, Maury Center Technical Note No. TN-74-04, December 1974.
4. H. K. Brock, "The AESD Parabolic Equation Model," AESD, Maury Center Technical Note No. TN-75-07, December 1975.
5. K. E. Hawker, T. L. Foreman, and K. C. Focke, "A Status Report on Propagation and Bottom Loss Models in Use at ARL/UT," Applied Research Laboratories Technical Memorandum No. 77-1 (ARL-TM-77-1), Applied Research Laboratories, The University of Texas at Austin, January 1977.
6. D. Gordon, "Theoretical Propagation of Low-Frequency Sound in the Deep Ocean and its Interaction with the Bottom" (U), Naval Undersea Center Report NUC TP 536, January 1977. CONFIDENTIAL
7. F. Tappert, Presentation at The International Workshop on Low-Frequency Propagation and Noise, unedited proceedings, Woods Hole, Massachusetts, October 1974. SECRET
8. K. E. Hawker and T. L. Foreman, "A Plane Wave Reflection Coefficient Model Based on Numerical Integration: Formulation, Implementation and Application," Applied Research Laboratories Technical Report No. 76-23 (ARL-TR-76-23), Applied Research Laboratories, The University of Texas at Austin, 21 June 1976.
9. A. O. Williams, "Hidden depths: acceptable ignorance about ocean bottoms," J. Acoust. Soc. Am. 59, 1175-1179 (May 1976).
10. E. L. Hamilton, "Compressional-Wave Attenuation in Marine Sediments," Geophysics 37, (620) 1972.
11. T. Akal, "The Relationship Between the Physical Properties of Underwater Sediments that Determine Bottom Reflection," Marine Geology 13, (251) 1972.

12. E. L. Hamilton, "Prediction of Deep-Sea Sediment Properties: State of the Art," in Deep-Sea Sediments, A. L. Inderbitzen (ed.) (Plenum Press, New York, 1974).
13. A. O. Williams, Jr., "Acoustic reflection from a structured sea bottom," J. Acoust. Soc. Am. 59, 62 (1976).
14. P. Strangerup, "A Detailed Study of Sound Reflections from a Layered Ocean Bottom," SACLANT Technical Report No. 42, SACLANT ASW Research Centre, La Spezia, Italy, 1963.
15. H. R. Hall and W. H. Watson, "An Empirical Bottom Reflection Loss Expression for Use in Sonar Range Prediction," Naval Undersea Warfare Center Report NUWC TN10, 1967.
16. K. E. Hawker, "The Influence of Surface Waves on Plane Wave Bottom Reflection Loss for Realistic Ocean Sediments," paper presented at the 92nd Meeting of the Acoustical Society of America, San Diego, California, November 1976.
17. K. E. Hawker, "The Influence of Stoneley Waves on Bottom Reflection Loss," in preparation for submission to J. Acoust. Soc. Am.
18. P. G. Bergmann, "The wave equation with a variable index of refraction," J. Acoust. Soc. Am. 17, 329 (1946).
19. I. Tolstoy, "The Theory of Waves in Stratified Fluids Including the Effects of Gravity and Rotation," Rev. Mod. Phys. 35, 207 (1963).
20. I. Tolstoy, "Effects of Density Stratification on Solid Waves," J. Geophys. Res. 20, 6009 (1965).
21. E. L. Hamilton, "Acoustic and Related Properties of the Sea Floor: Density and Porosity Profiles and Gradients," Naval Undersea Center Report NUC TP459 (1975).

28 February 1977

DISTRIBUTION LIST FOR
ARL-TR-77-17
UNDER CONTRACT N00039-77-C-0003
UNCLASSIFIED

Copy No.

1 - 5	Commanding Officer Naval Electronic Systems Command Department of the Navy Washington, DC 20360 Attn: Code 320
6	Commander Naval Sea Systems Command Department of the Navy Washington, DC 20362 Attn: A. P. Franceschetti
	Commanding Officer Naval Ocean Research and Development Activity National Space Technology Laboratories Bay St. Louis, MS 39520
7	Attn: Samuel Marshall (Code 340)
8	Herbert Eppert (Code 360)
9	Thomas Pyle (Code 430)
10	Hugo Bezdek (Code 460)
11	Roy Gaul (Code 600)
12	Aubrey L. Anderson (Code 320)
13	Commanding Officer Office of Naval Research Arlington, VA 22217 Attn: J. B. Hersey (Code 102-OS)
	Commander Naval Undersea Center Department of the Navy San Diego, CA 92132
14 - 16	Attn: Code 40
17	M. A. Pedersen (Code 307)
18	R. R. Gardner
19	Edwin L. Hamilton
20	Homer P. Bucker (Code 409)
21	H. Morris
22	D. Gordon

Distribution List for ARL-TR-77-17 under Contract N00039-77-C-0003 (Cont'd)

Copy No.

	Director Naval Research Laboratory Department of the Navy Washington, DC 20375
23 - 25	Attn: Code 8160
26	B. G. Hurdle
27	R. H. Ferris
28	Ronald Dicus (Code 8120)
	Naval Oceanographic Office Department of the Navy Washington, DC 20373
29	Attn: W. H. Geddes
30	K. V. Mackenzie
31	Commanding Officer Naval Ocean Research and Development Activity Liaison Office Arlington, VA 22217 Attn: R. S. Winokur
	Commander Naval Air Development Center Department of the Navy Warminster, PA 18974
32	Attn: C. L. Bartberger
33	P. Haas
	Commander New London Laboratory Naval Underwater Systems Center Department of the Navy New London, CT 06320
34	Attn: F. R. DiNapoli
35	S. R. Santaniello
36	R. L. Deavenport
37	P. Herstein
38	Commanding Officer Naval Coastal Systems Laboratory Panama City, FL 32401 Attn: E. G. McLeroy, Jr.

Distribution List for ARL-TR-77-17 under Contract N00039-77-C-0003 (Cont'd)

Copy No.

39	Chief of Naval Material Department of the Navy Washington, DC 20360 Attn: G. R. Spalding (Code 0345)
40 - 41	Superintendent Naval Postgraduate School Monterey, CA 93940
	Woods Hole Oceanographic Institution Woods Hole, MA 02543
42	Attn: John Ewing
43	Earl E. Hays
44	Morris Schulkin, Consultant 9325 Orchard Brook Drive Potomac, MD 20854
45	Bolt Beranek and Newman, Inc. 50 Moulton Street Cambridge, MA 02138 Attn: Preston W. Smith, Jr.
46	Science Applications, Inc. 1651 Old Meadow Road McLean, VA 22101 Attn: John Hanna
47	Applied Research Laboratory Pennsylvania State University P.O. Box 30 State College, PA 16801 Attn: D. C. Stickler
48	Underwater Systems, Inc. 3121 Georgia Avenue Silver Spring, MD 20910 Attn: Marvin S. Weinstein
49	Geophysics Laboratory Marine Science Institute The University of Texas 700 Strand Galveston, TX 77550 Attn: J. L. Worzel, Director

Distribution List for ARL-TR-77-17 under Contract N00039-77-C-0003 (Cont'd)

Copy No.

- 50 TRACOR, Inc.
1601 Research Boulevard
Rockville, MD 20850
Attn: R. J. Urick
- 51 National Oceanic and Atmospheric Administration
Atlantic Oceanographic and Meteorological Laboratory
15 Rickenbacker Causeway
Miami, FL 33149
Attn: Peter A. Rona
- 52 Geophysical and Polar Research Center
Department of Geology and Geophysics
The University of Wisconsin
Madison, WI 53700
Attn: C. S. Clay
- 53 The Catholic University of America
6220 Michigan Avenue, NE
Washington, DC 20017
Attn: H. M. Uberall
- Lamont-Doherty Geological Observatory
Palisades, NY 10964
- 54 Attn: Henry R. Kutschale
55 John E. Nafe
56 R. E. Houtz
57 George M. Bryan
- 58 Brown University
Providence, RI 02912
Attn: A. O. Williams, Jr.
- 59 Yale University
Department of Engineering and Applied Science
New Haven, CT 06320
Attn: Franz B. Tuteur
- University of Auckland
Physics Department
Auckland, New Zealand
- 60 Attn: Alick Kibblewhite
61 Kris Tindle

Distribution List for ARL-TR-77-17 under Contract N00039-77-C-0003 (Cont'd)

Page No.

	Defence Scientific Establishment HMNZ Dockyear Devonport, Auckland New Zealand
62	Attn: Michael Guthrie
63	R. N. Denham
64 - 75	Commanding Officer and Director Defense Documentation Center Defense Services Administration Cameron Station, Building 5 5010 Duke Street Alexandria, VA 22314
76	Office of Naval Research Resident Representative Room 582, Federal Building Austin, TX 78701
77 - 78	Environmental Sciences Division, ARL/UT
79	Glen E. Ellis, ARL/UT
80	Karl C. Focke, ARL/UT
81	Terry L. Foreman, ARL/UT
82	Ruth Gonzalez, ARL/UT
83	Loyd D. Hampton, ARL/UT
84	Kenneth E. Hawker, ARL/UT
85	Claude W. Horton, ARL/UT
86	Max K. Miller, ARL/UT
87	Stephen P. Mitchell, ARL/UT
88	Steven R. Rutherford, ARL/UT
89	Donald J. Shirley, ARL/UT
90	Jack A. Shooter, ARL/UT
91	Steven L. Watkins, ARL/UT

Distribution List for ARL-TR-77-17 under Contract N00039-77-C-0003 (Cont'd)

Copy No.

92	Winifred Williams, ARL/UT
93	Reuben H. Wallace, ARL/UT
94	Library, ARL/UT
95 -119	Reserve, ARL/UT